Development of novel mesoporous magnetic adsorbents from industrial waste and their application for removal of lead and efavirenz in aqueous solutions

By

Thabang Kgoedi (14798344)

submitted in accordance with the requirements for

the degree of

Master of Science

in Chemistry

at the

UNIVERSITY OF SOUTH AFRICA

Supervisor: Prof N Mketo

Co-supervisor: Dr TG Kebede

: Prof LM Madikizela

February 2024

DECLARATION

Name: Thabang Kgoedi

Student number: 14798344

Degree: Master of Science in Chemistry

Exact wording of the title of the dissertation as appearing on the electronic copy submitted for examination:

Development of novel mesoporous magnetic adsorbents derived from industrial waste and their application for adsorptive removal of lead and efavirenz in aqueous solutions

I declare that the above dissertation is my own work and that all the sources that I have used or quoted have been indicated and acknowledged by means of complete references.

I further declare that I submitted the dissertation to originality checking software and that it falls within the accepted requirements for originality.

I further declare that I have not previously submitted this work, or part of it, for examination at Unisa for another qualification or at any other higher education institution.

(The dissertation will not be examined unless this statement has been submitted.)

T.Kgoedi

SIGNATURE DATE: February 2024

UNIVERSITY OF SOUTH AFRICA

KEY TERMS DESCRIBING THE TOPIC OF A DISSERTATION/THESIS

The Executive Committee of Senate decided that in order to assist the library with retrieval of information, master's and doctoral students must list approximately ten key terms which describe the topic of the dissertation/thesis at the end of the summary of the dissertation/thesis.

If the dissertation/thesis is not written in English, the key terms in English must be listed at the end of the English summary.

The following is an example of key terms used for a thesis/dissertation:

Title of thesis/dissertation:

Development of novel mesoporous magnetic adsorbents derived from industrial waste and their application for adsorptive removal of lead and efavirenz in aqueous solutions

KEY TERMS:

Industrial waste; coal fly ash; petroleum coke; efavirenz; lead; wastewater; Fe_3O_4@ACF, Fe_3O_4@AFA, Fe_3O_4@ABA, Fe_3O_4@APC and magnetic mesoporous adsorbents

ACKNOWLEDGEMENTS

- I am humbled and grateful to have had the guidance, encouragement, and support of Prof Nomvano Mketo, Dr Tmesgen Girma Kebede, and Prof Lawrence Mzukisi Madikizela, throughout MSc journey. Their contributions were valuable for the success of the research project.
- The financial support from the University of South Africa, College of Science and Technology (CSET) was a critical component of the project's completion and I will be forever grateful.
- Department of Chemistry, University of South Africa (UNISA) for supporting this research by providing the required facilities.
- The Food and Environmental Analytical Chemistry Research Group's (Ms. Mussiwa Sengane, Mr. Njabulo Mdluli, Mr. Mxolisi Kiwanuka, Mr. Kgomotso Mabena, Mr. Divin Mukendi, Mr. Cyril Zuma, Mr. Samual Mgiba and precious brother Mr Oluseyi Salami and Dr. Masixole Sihlahla) unwavering support and positivity were instrumental in keeping me motivated, even during challenging times.
- I would like to express my utmost gratitude to Dr. S Mpelane for his invaluable assistance with TEM analysis, and to Ms Orienda Sebabi for her unmatched expertise in X-ray diffraction measurements. Moreover, I cannot fail to mention Ms Luleka Menzi's generous assistance with the SEM-EDS, provided by the esteemed UNISA Physics Department, Institute of Nanotechnology, and Water Sustainability and Chemical Engineering Department. Their exceptional contributions have been crucial to the success of our project, and I am truly grateful for their support.
- I am filled with deep gratitude towards my friends and family (my mother Tebogo Kgoedi, grandparents Oupa and Ntlhoile Kgoedi, awesome aunts Kamogelo and Musa Kgoedi lovely siblings Paris and Luna Kgoedi) for their unwavering support, encouragement, and guidance throughout my journey. Their presence has been a constant source of strength, motivating me to strive towards my goals and pursue my dreams with unwavering determination.
- Finally, I humbly thank the Almighty for granting me the strength and patience to persevere on this journey. His divine blessings have been my guiding light, and I am forever grateful.

PUBLICATION(S)

1. T. Kgoedi[a], T. G Kebede[b], L. M Madikizela[c], N Mketo[a]. *Adsorptive removal of Pb(II) ions from aqueous solutions using magnetic mesoporous pet coke and coal fly ash-based adsorbents* **(IN PREPARATION)**.
2. T. Kgoedi[a], T. G Kebede[b], L. M Madikizela[c], N Mketo[a]. *Adsorptive removal of efavirenz from aqueous solutions using magnetic mesoporous coal fly ash-based adsorbents* **(IN PREPARATION)**

CONFERENCES

1. T. Kgoedi[a], T. G Kebede[b], L. M Madikizela[c], N Mketo[a] *Adsorptive removal of efavirenz from aqueous solution using magnetic mesoporous adsorbent derived from coal fly ash,* (**Oral**), ChromSA conference, Pretoria, South Africa, September 2023.

2. T. Kgoedi[a], T. G Kebede[b], L. M Madikizela[c], N Mketo[a]. *Adsorptive removal of Pb(II) ions from aqueous solutions using magnetic mesoporous petroleum coke and coal fly ash-based adsorbents*, (**Oral**), ACC2023 conference, Thessaloniki, Greece, November 2023.

ABSTRACT

Industrial waste materials have garnered increased attention as viable adsorbents that could be used for the extraction of heavy metals and organic pollutants from wastewater. This is primarily due to their abundant availability in large quantities and economical cost-effectiveness. Coal fly ash, bottom ash, and fly ash are examples of industrial waste generated from coal combustion in power plants, while petroleum coke is derived from oil refineries. These waste materials contain diverse functional groups, including carbon, calcium oxide, silicon dioxide, aluminium oxide, and iron oxide, which makes them ideal for the remediation of wastewater. Previous research studies have indicated that modified industrial waste materials possess greater adsorption capabilities. As a result, this study sought to modify coal fly ash (RCFA), bottom ash (RBA), fly ash (RFA), and petroleum coke (RPC) by adding iron oxide (Fe_3O_4) nanoparticles. This modification enables easy separation with an external magnet and enhances their effectiveness in adsorbing lead and efavirenz.

The following adsorbents Fe_3O_4@APC, Fe_3O_4@ACFA, Fe_3O_4@AFA, and Fe_3O_4@ABA were prepared in a two-step method. The first step was activation of the RPC, RBA, RFA, and RCFA with NaOH then followed by incorporating Fe_3O_4 nanoparticle. These mesoporous magnetic materials were successfully prepared and characterized using various techniques such as thermogravimetric analysis (TGA), scanning electron microscopy coupled to energy dispersive X-ray spectroscopy (SEM-EDS), ultraviolet-visible spectroscopy (UV-Vis), Fourier transform infrared spectroscopy (FTIR), transmission electron microscopy (TEM) and Brunauer-Emmett-Teller analysis (BET).

The Langmuir, Temkin, and Freundlich isotherm models were applied to analyse the equilibrium data. The maximum adsorption capacities for obtained for lead were 48.8, 15.63, 12.16, and 270.27 mg/g for Fe_3O_4@ACFA, Fe_3O_4@AFA, Fe_3O_4@ABA, and Fe_3O_4@APC, respectively. The maximum adsorption capacities for efavirenz obtained were 25.38, 37.64, 13.07 and 76.54 mg/g Fe_3O_4@ACFA, Fe_3O_4@APC, Fe_3O_4@ABA, Fe_3O_4@AFA respectively. Based on the adsorption isotherms for lead ions, both Fe_3O_4@ACFA and Fe_3O_4@AFA, are best described by the Temkin isotherm while Fe_3O_4@ABA and Fe_3O_4@APC were best described by the Langmuir and Freundlich isotherm, respectively. Additionally, adsorption of efavirenz was best described by the Langmuir isotherm for all prepared adsorbents.

The kinetic data were also evaluated for the lead and efavirenz which revealed that the pseudo-second-order equation provided the best correlation for both lead and efavirenz. Thermodynamic parameters suggest that the adsorption process is endothermic and spontaneous for lead. However, for efavirenz it behaved differently on various adsorbents, revealing non-spontaneous adsorption. The adsorption process for lead was endothermic for all adsorbents, whereas for efavirenz it was found to be endothermic for Fe_3O_4@APC and Fe_3O_4@ACFA adsorbents, while exothermic for Fe_3O_4@ABA and Fe_3O_4@AFA adsorbents. The findings demonstrate that Fe_3O_4@ACFA, Fe_3O_4@APC, Fe_3O_4@ABA, and Fe_3O_4@AFA possesses the potential to effectively remove lead ions and efavirenz from aqueous solutions.

TABLE OF CONTENTS

LIST OF FIGURES

LIST OF TABLES

LIST OF EQUATIONS

LIST OF ABBREVIATIONS AND ACRONYMS

ABA - Activate Bottom Ash
AC - Activated Carbon
ACFA - Activated Coal Fly
AFA - Activated Fly Ash
APC - Petroleum Coke
ARM - Activated Red Mud
Al_2O_3 - Aluminium Oxide
NH - Ammonium Ion
ANOVA - Analysis Of Variance
ARVs - Antiretroviral Dr
As - Arsenic
<LOQ - Below Method Quantitation Limi
BFS - Blast Furnace Slag
RBA - Bottom Ash
BBD - Box–Behnken design
Cd^{2+} - Cadnium
Ca - Calcium
$CaCl_2$ - Calcium chloride
CaO - Calcium oxide
CO_2 - Carbon dioxide
CO_3 - Carbon trioxide
CEC - Cation Exchange Capacity
CCD - Central Composite Design
CCD - Charge Coupled Device
Cr - Chromium
CFA - Coal fly ash
CFAPG - Coal fly ash-based porous geopolymer
Co^{2+} - Cobalt
Cu^{2+} - Copper
$CuSO_4$ - Copper(II) Sulfate
EDS - Energy Dispersive Spectroscopy
$\Delta H°$ - Enthalpy Change
$\Delta S°$ - Entropy Change
EDTA - Ethylenediamine Tetraacetic Acid
FA - Formic Acid
FTIR - Fourier-Transformed Infrared
FFD - Full Factorial Design
$\Delta G°$ - Gibbs Free Energy Change
HPLC - High-Pressure Liquid Chromatography
HIV/AIDS - Human Immunodeficiency Virus/ Acquired Immunodeficiency Syndrome
HCl - Hydrochloric Acid
H - Hydrogen
$HCrO^{4-}$ - hydrogenchromate
OH - Hydroxide
ICP-OES - Inductively Coupled Plasma Optical- Emission spectroscopy
Fe_2O_3 - Iron (II) Oxide
Fe_3O_4 - Iron Oxide
MNPs - Iron Oxide Magnetic Nanoparticles
R_L - Langmuir dimensionless equilibrium constant
Pb^{2+} - lead
LTA - Linde Type A
γ-Fe_2O_3 - Maghemite

m-SPE - Magnetic Solid Phase Extraction

Mn^{2+} - Manganese

Hg(II) - Mercury

MOF - Metal-Organic Frameworks

MCFA - Modification Of Coal Fly Ash

MIP - Molecularly Imprinted Polymer

Ni^{2} - Nickel

HNO_3 - Nitric Acid

RPC - Raw Petroleum Coke

PC - Petroleum coke

PPCPs - Pharmaceuticals and Personal Care Products

pHpzc - Point of Zero Charge

RCFA - Raw coal fly ash

RM - Red Mud

RM/CS - Red Mud Modified By Chitosan

SEM - Scanning Electron Microscope

SED - Secondary Electron Detector

SAD - Selected Area Diffraction

Si - Silicon

SiO_2 - Silicon Dioxide

NaOH - Sodium Hydroxide

BET - Brunauer-Emmett teller

TGA - Thermogravimetric analysis

Th - Thorium

TiO_2 - Titanium Dioxide

TEM - Transmission Electron Microscope instrument

Uv - Ultraviolet

USEPA - United States Environmental Protection Agency

U - Uranium

WWTP - Wastewater Treatment Plants

WCBFS - Water-Cooled Blast Furnace Slag

WHO - World Health Organization

Y - Yttrium

ZFA - Zeolites Fly ash

Zn - Zinc

Zr - Zirconium

CHAPTER 1: INTRODUCTION

PREAMBLE

In this chapter, a brief background of heavy metals, pharmaceuticals as emerging pollutants, industrial waste materials, iron oxide nanoparticles and mesoporous materials as suitable adsorbent materials is discussed. The chapter also focuses on describing problem statement, aim and objective, hypothesis, and justification of the study. Lastly, the outline of the entire dissertation which explains the content of each chapter of the dissertation is summarized.

1.1. Background of the study

Aquatic environments are ecosystems that comprise of various forms of water bodies that are essential to life. The importance of these environments' matrices cannot be overstated, as they provide various benefits to all living things. They play critical roles in flood control, nutrient cycling, carbon sequestration, water supply, food provision, and recreation purposes among other vital roles. Four primary types of aquatic environments that are mostly essential are oceans, rivers, lakes, and wetlands, each characterized by its unique characteristics and organisms found in them [1]. Pollution is a major threat to water bodies, which results in the generation of water pollution [2,3].

Wastewater is water that has undergone physical, chemical, or biological changes because of the introduction of certain pollutant compounds, thus making it unfit for human and animal consumption and irrigation purposes [4]. There are various forms of wastewater, and these include domestic, storm, and industrial wastewater. A wide range of organic and inorganic pollutants are found to contaminate water resources. Some of these contaminants include heavy metals, dyes, pharmaceuticals, surfactants, pesticides, personal care products, among others. [5,6]. These contaminants are normally found in groundwater, surface water, municipal wastewater and drinking water [7]. There is a wide range of technologies available for water remediation, and these including membrane separation [8,9], coagulation-flocculation [10], and ion-exchange among others. While these methods are certainly efficient in the removal of pollutants, they can also be costly and generate sludge and other by-products waste materials that require careful disposal. Additionally, the use of chemicals for water treatment can lead to secondary pollution [11]. Biological treatment is another option, but it is important to be aware

that it can produce nutrient-rich biosolids that may contribute to eutrophication and negatively impact aquatic life and ecosystem [12].

1.2. Heavy metals

Heavy metals are naturally occurring metallic elements that have high densities (>5 g/cm^3). They are known for their toxic properties even when present in low concentration levels (≥ 0.001 ppb) [13]. The most common and toxic heavy metals include lead, mercury, arsenic, and cadmium among others. These metals can be deposited into the environment through various activities such as anthropogenic (industrial, agricultural, mining and urban) and natural processes (volcanic activities and rock weathering) [14]. They can enter the human body via different mechanisms such as dermal, inhalation and oral ingestion of contaminated food chain products thus causing damage to vital organs as shown in **Figure 1.1,** which ultimately results in various adverse health effects and even in fatalities [15]. The World Health Organization (WHO) has reported that heavy metals like cadmium, lead, mercury, and copper can contaminate drinking water due to impurities in galvanized pipes and plumbing systems, and contamination of ground water. The maximum permissible levels for some targeted heavy metals ranged between 0.001 and 0.01 µg/L for domestic purposes [16].

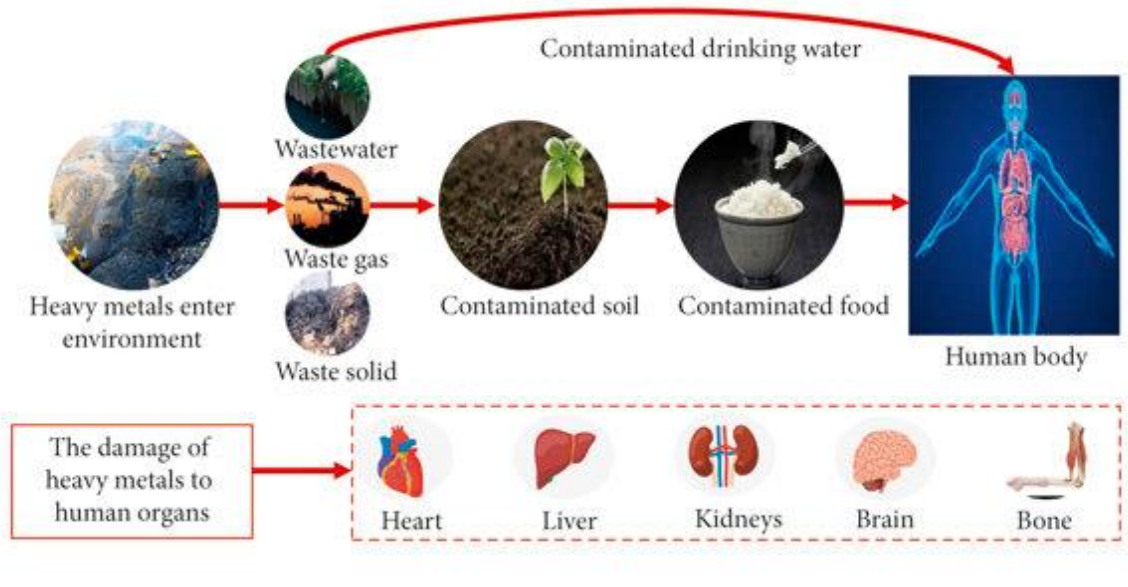

Figure 1.1: Schematic illustration of how heavy metals enter the human body [15].

1.3. Emerging pollutants

Emerging pollutants such as pharmaceuticals are substances detected in the environment but not routinely monitored or subject to environmental regulation. They are commonly used in daily life and can accumulate in various environmental compartments[17].

Pharmaceutical active chemicals have been detected in drinking water, sediments, groundwater, oceans, and surface waters for over 50 years [18]. The rapid growth of the pharmaceutical industry has led to the discharge of untreated waste from various sources, resulting in the detection of harmful substances in aquatic ecosystems. Various types of pharmaceuticals, such as beta-blockers, blood lipid regulators, analgesics, anti-inflammatory drugs, hormones and antiepileptics, have been found in aquatic environments in concentrations ranging from ng/L to μg/L [15]. Humans may be exposed to toxic compounds that contaminate the aquatic environment through drinking water or eating aquatic species. Therefore, potential health concerns due to exposure to pharmaceuticals are worrisome, particularly for nations where surface water is the primary supply of drinking water and there is a lack of regulations for the presence of these compounds. The present study focuses on efavirenz which is known as an anti-retroviral drug. This pharmaceutical drug has been detected in South African waters with its highest concentration of 140 μg/L found in the WWTP influent [51]. Due to constant detection in South African waters, this study investigated the application industrial waste for removal of lead and efavirenz in water contaminated water.

1.4. Adsorbents

Adsorbents are materials that attract and keep molecules of gases or solutions on their surface [19]. They have a large surface area, contain various functional groups resulting to specific physical and chemical interactions, thus making them selective and effective at capturing and concentrating target pollutant. Different adsorbents materials have varying affinities for specific contaminants, allowing their targeted removal [20]. Some adsorbents can be regenerated and reused over several cycles, making them a cost-effective solution. However, adsorbent materials have a finite capacity and require replacement or regeneration once they become saturated [21]. They can also be limited in applicability and suffer from reduced efficiency in removing pollutants in complex mixtures [22]. There are different types of adsorbents available, such as polymeric adsorbents, natural mineral adsorbents, industrial by-product adsorbents, and carbon-based nanomaterial adsorbents. Waste materials derived from

agricultural, animal, and industrial sources present an efficient and economical solution for eliminating heavy metals and organic pollutants from wastewater[19].

1.4.1. Coal fly ash

Coal fly ash is a by-product of coal power plants and was found to be alkaline in nature [24]. Depending on the amount of unburned carbon during its application and the type of combustion technology used, the physical appearance of CFA can be light or dark grey in colour. The primary constituents of CFA are oxides such as silicon dioxide (SiO_2), aluminium oxide (Al_2O_3), iron (III) oxide(Fe_2O_3), titanium dioxide (TiO_2) and calcium oxide (CaO). There are two categories of CFA, and these are Class F and Class C. The CFA with low CaO (<8%) content is classified as Class F, while CFA with high CaO (>8%) content is classified as Class C [25]. Currently, CFA is utilized mainly in mine backfilling, paving, cement concrete and low-end building materials [26]. CFA was recommended as the best alternative adsorbent to replace activated carbon for the application of water treatment. This is mainly because of the low cost, environmental benefit (waste usage) and possibility of regeneration[27].

1.4.2. Petroleum coke

Petroleum coke (PC) is a by-product of the petroleum refining process, produced from all types of oils (light/heavy crudes) during the refinery process. There two forms of PC namely, green PC and calcined PC. Green PC serves as fuel, while calcined PC is utilized by manufacturers as a feedstock for various products, such as aluminium, paints, coatings, and colorants [28]. PC is a non-porous solid, which is commonly activated before being used in various applications. The PC's structure (**Figure 1.2**) is still a mystery in scientific circles, as it is a complex combination of carbon, hydrogen, nitrogen, oxygen, sulphur, and other metallic impurities [29].

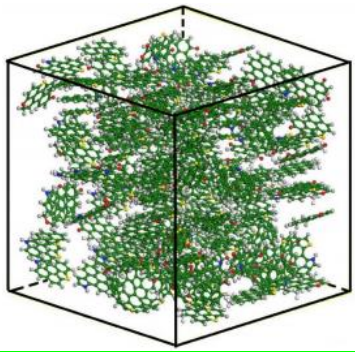

Figure 1.2: Proposed structural illustration of petroleum coke. Green for carbon, red for oxygen, yellow for sulphur [29].

According to an economic study of decreasing activated carbon (AC) manufacturing costs, PC is the most promising raw material among other carbonaceous resources such as wood, used tires, carbon black, charcoal, and lignite. This is because PC contains high fixed carbon content (over 90%) and high surface area [30].

1.4.3. Mesoporous materials

Mesoporous materials are arranged structures with pore sizes ranging from 2 to 50 nanometres (**Figure 1.3**). These materials have garnered attention from researchers recently due to their unique mechanical, electrical, and optical characteristics, as well as the combination of bulk and surface properties to their overall behaviour [31]. The pore structure of these porous materials gives an extraordinarily large surface area inside a comparatively small volume of material, making them ideal for catalysis, molecule separation and selective behaviour towards some elements [32].

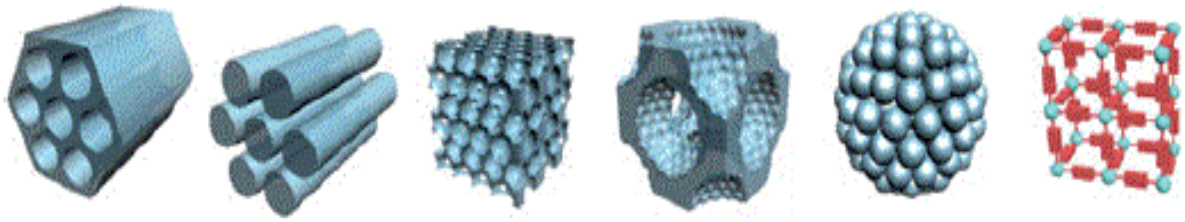

Figure 1.3: Various types of mesoporous materials [31].

1.5. Iron oxide nanoparticles.

The use of magnetism for water purification is a notion that has been around for a long time [33]. Magnetism has been used in a variety of water treatment procedures, including anti-scaling techniques in boilers, factory pipes, coagulation, and biological processes. The application of magnetism in an adsorption process is a relatively recent notion that is gaining attention among scientists [34]. Magnetic adsorbents are a novel type of adsorbent in which magnetic particles, which are oxides of metals including iron, cobalt, nickel, and copper among others, are embedded in a base adsorbent. Due to the presence of a metal component in the adsorbent, the magnetic adsorbent may be quickly and readily separated from water when an external magnetic field is applied [35,36]. The Fe_3O_4 NPs are easy to prepare as indicated in **Figure 1. 4**, and provide several advantages such as biocompatibility, superparamagnetic properties, low toxicity, and high chemical stability [37].

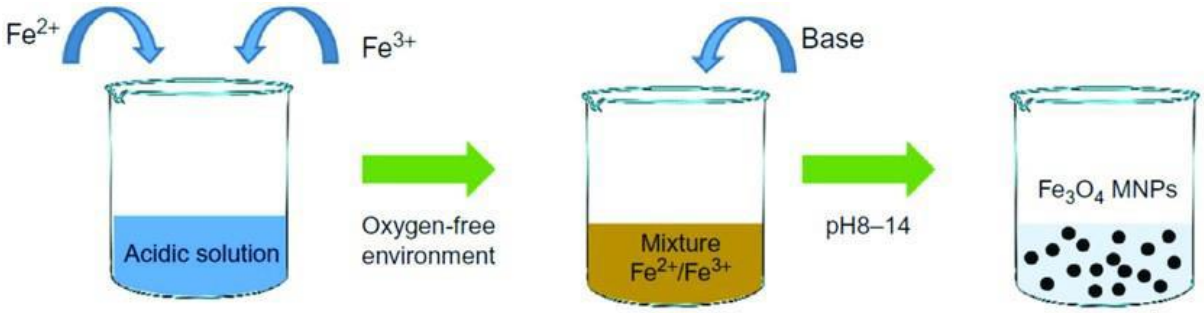

Figure 1.4: Schematic illustration for the preparation of the iron oxide NPs [38]

Among iron oxide magnetic nanoparticles (MNPs), magnetite (Fe_3O_4), maghemite (γ-Fe_2O_3) and hematite (α-Fe_2O_3) are considered ideal oxide supports because they can be prepared easily, have a high surface area, and can be separated via magnetic fields after the reaction. However, pure MNPs are poorly dispersed in an aqueous medium due to their hydrophobic surface. To enhance their dispersity in the aqueous medium, MNPs must be coated with inorganic shells or hydrophilic polymer [39,40]. Hence, they have been utilized in various applications such as biomedicine [41–43], food analysis [44], water treatment [45] and biological separation[46] . Although there is no significant knowledge of magnetic mesoporous CFA or PC, it is evident that for the proposed research project, the above-mentioned factors can be used as a point of reference.

1.6. Problem statement

The shortcomings of existing wastewater treatment techniques have been reported, particularly in the case of the chemical precipitation method for the removal of heavy metals.[47]. The main drawback during chemical precipitation is that there is a generation of large sludge containing minor heavy metals. Membrane filtration can remove heavy metals, but it is an expensive procedure [24]. Despite being effective for metal ion adsorption, conventional adsorbents materials such as activated carbon, metal-organic framework, alumina and zeolites all have certain limitations such as sludge generation, high preparation cost, poor chemical stability, challenging recyclability, inefficient selectivity etc. [36,48]. These adsorbents have been studied for the removal of heavy metals and other emerging contaminants, and the most used adsorbents were activated carbon. However, the predominantly non-polar surface of activated carbon often limits its effectiveness [49]. Conversely, the occurrence of efavirenz in wastewater and its transfer to surface water bodies resulting in contamination of the aquatic environment was reported in various studies [50]. There is evidence that this pharmaceutical drug compound is not entirely removed by conventional wastewater treatment plant

mechanisms [51]. Most concerning is the lack of research which has been conducted on the removal of efavirenz from surface waters and wastewater [52]. Some of the research studies reported in literature involved the application of molecularly imprinted polymers [53–55], graphene wool [56], nanofibers [57] and Biochar from olive residue, tomato residue, rice husks and African palm tree [55] for adsorption of efavirenz in water. The disadvantages of such adsorbent materials included low surface area, resulting in lower desorption capacities. Therefore, this study attempts to address the aforementioned challenges through the application of coal fly ash and petroleum coke coated with iron oxide nanoparticle for efficient removal of lead and efavirenz in water.

1.7. Aim and objectives of the study

1.7.1. Aim

The aim of the study was to prepare, characterize and apply mesoporous magnetic adsorbents derived from coal fly ash and pet-coke for adsorptive removal of lead and efavirenz in aqueous solutions.

1.7.2. Specific objectives were to:

1. Prepare and characterize coal fly ash and pet-coke-derived magnetic mesoporous adsorbents.
2. Determine the optimum conditions (i.e., pH, initial solution concentration, contact time, adsorbent dosage, temperature, etc) for efficient adsorption by using multivariate optimization tools.
3. Conduct the kinetic and thermodynamic studies using the optimum conditions.
4. Perform adsorptive removal of Pb and efavirenz from aqueous solutions using magnetic mesoporous adsorbents.
5. Compare the performance of pet-coke and coal fly ash-based adsorbents for efficient removal of Pb and efavirenz in aqueous solutions.

1.8. Research questions

1. What is the possibility that the synthesized magnetic mesoporous adsorbents may not be effective in removing both Pb and efavirenz.

2. What are the factors that might affect the adsorptive removal of Pb and efavirenz using magnetic mesoporous adsorbent?
3. How will the introduction of magnetic nanoparticles and the pore size enhancement affect adsorbent's efficacy for the adsorptive removal of Pb and efavirenz?
4. How many times can the synthesised magnetic mesoporous adsorbent be reused?
5. Between coal fly ash and pet coke-based adsorbents, which one will be more effective for the removal of Pb and efavirenz?

1.9. Rationale/motivation/justification of the study

The scientific research for the development of more suitable and low-cost adsorbents for the removal of heavy metals, pharmaceuticals and personal care products (PPCPs) from aqueous solutions is still an ongoing progress. For this study, the development of magnetic mesoporous adsorbents for the removal of lead and efavirenz were considered. The alkaline nature of CFA imparts the neutralizing property of the material, while the oxides such as alumina, silica, calcium oxide, and iron oxides present in both materials were expected to act as adsorption sites for the lead ions and efavirenz protons [58,59].

As CFA and PC have electron-conducting properties and are strong alkali substances, it was anticipated that they can be used to remove lead ions and efavirenz from aqueous solutions by precipitation or electrostatic adsorption [60]. Therefore, the developed adsorbents have superior adsorption capabilities due to their high surface area and easy separation caused by the presence of magnetic iron nanoparticles [61]. Additionally, the present research project is expected to improve industrial waste management and provide cost-effective adsorbents for the removal of lead and efavirenz in aqueous solutions.

The modification of PC and CFA with magnetic nanoparticles and adsorption mechanisms was expected to bring new scientific knowledge to the field of Analytical Chemistry. South African research scientific community will benefit from the proposed study because waste generated from coal-fired power stations and oil refineries will be recycled and used as adsorbent for the removal of heavy metals and pharmaceuticals in wastewater. Therefore, this study will decrease the costs associated with the disposal of industrial waste by reusing these materials as adsorbents for water treatment. Furthermore, it will improve water quality and reduce water scarcity and environmental pollution in our country.

1.10. Hypothesis

- Coal fly ash has strong alkalinity and a negatively charged surface at high pH, making it effective for removing lead ions and efavirenz from water through precipitation or electrostatic adsorption.
- The surface area of coal fly ash plays a significant role in its capacity to adsorb metal ions and organic pollutants.
- Petroleum coke has a porous structure and various functional groups like oxygen, sulphur, and nitrogen, providing abundant adsorption sites for ions.
- Lead ions are expected to primarily interact with petroleum coke through ion exchange, electrostatic attractions, and a substantial surface area.
- Efavirenz interacts with pet coke through π-π stacking, hydrophobic interactions, and Van der Waals forces.
- The alignment of efavirenz's aromatic system with electron-rich regions on pet coke enhances adsorption.
- Efavirenz's hydrophobic properties and Van der Waals forces also contribute to the adsorption process.
- These interactions collectively impact the adsorption capacity and efficiency of efavirenz onto pet coke.

1.11. Dissertation/Thesis outline

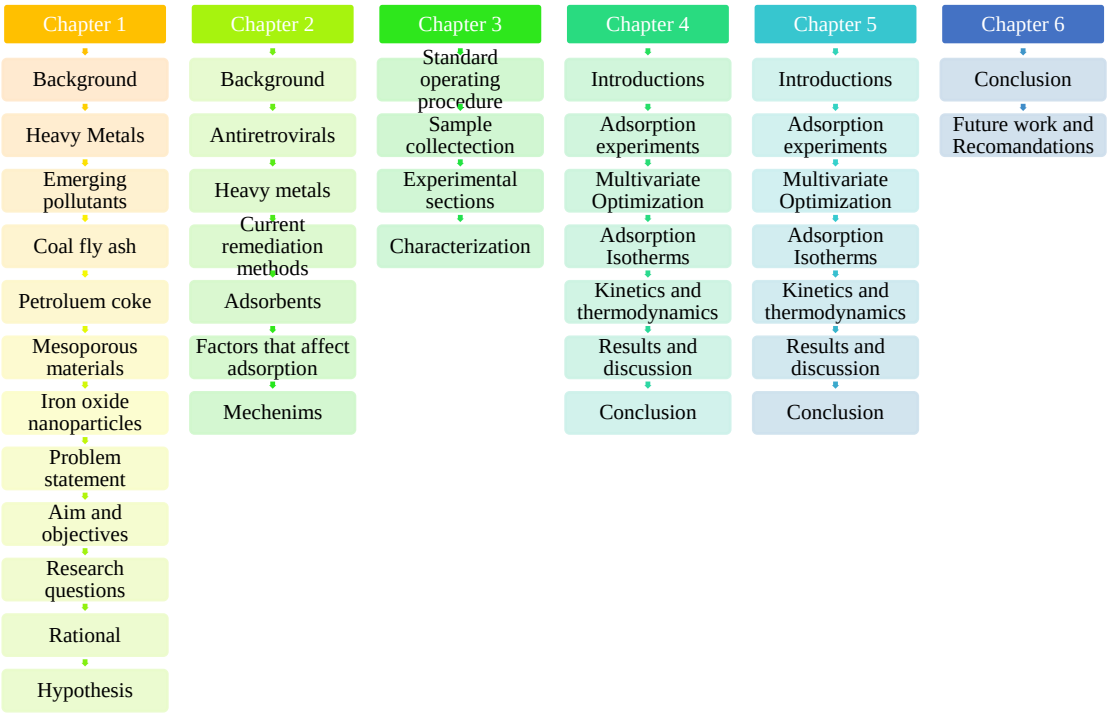

Chapter one (Introduction), This chapter discuss the background information on heavy metals, adsorption technique, coal fly ash (CFA), petroleum coke (PC) and mesoporous material. It further explains the effects of heavy metals on humans that are present in wastewater. A brief introduction to coal fly ash, petroleum coke and mesoporous materials is also discussed.

Chapter two (Literature review) reviews in detail the studies that have been reported on the use of industrial waste material as adsorbents for heavy metals and antiretrovirals. It further evaluates the factors affecting adsorptions as well as the mechanisms involved in the adsorption of heavy metals and antiretrovirals.

Chapter three (Methodology) outlines the general procedures and methodologies that were followed to generate data for this study. This includes all the general laboratory techniques and characterization techniques used to confirm the synthesised adsorbents. A detailed description of multivariate optimization methods is also outlined in this chapter.

Chapter four (Quantitative analysis) outlines the data acquired from the adsorptive studies for lead (Pb). The adsorption mechanism and other influencing factors and favourable

conditions in the adsorption process have also been discussed in this chapter. Furthermore, discusses the adsorptive capacity, the kinetic and thermodynamic studies in detail.

Chapter five (Quantitative analysis) outlines the data acquired from the adsorptive studies for efavirenz from the adsorbent samples. The adsorption mechanism and other influencing factors and favourable conditions in the adsorption process have also been discussed in this chapter. Furthermore, discusses the adsorptive capacity, and the kinetic and thermodynamic studies in detail.

Chapter Six (Conclusion and future recommendations), This chapter summarizes the overall findings regarding the study's goal. In addition, recommendations and work that may be done in the future are offered in this chapter.

REFERENCE

[1] A. Balasubramanian, Aquatic Ecosystems- freshwater types, (2011) 24.

[2] I. Bashir, F.A. Lone, R.A. Bhat, S.A. Mir, Z.A. Dar, S.A. Dar, Concerns and threats of contamination on aquatic ecosystems, Bioremediation and Biotechnology: Sustainable Approaches to Pollution Degradation (2020) 1–26. https://doi.org/10.1007/978-3-030-35691-0_1/TABLES/4

[3] O.I. Ogidi, U.M. Akpan, Aquatic Biodiversity Loss: Impacts of Pollution and Anthropogenic Activities and Strategies for Conservation, (2022) 421–448. https://doi.org/10.1007/978-981-19-3326-4_16.

[4] J. Dissanayake, P; Tennakoon, M; Burmeister, Guide to on-site wastewater management for industrial and commercial establishments and other institutions guide for vehicle service station owners and managers, (2008).

[5] S.D. Richardson, S.Y. Kimura, Water analysis: Emerging contaminants and current issues, (2020) 473–505. https://doi.org/10.1021/acs.analchem.9b05269.

[6] A. Ali, M. Rashid, M. Irfan, N. Ekmi, M. Zul, Z. Man, J. Siame, K. Azizi, A review on geopolymers as emerging materials for the adsorption of heavy metals and dyes, 224 (2018) 327–339. https://doi.org/10.1016/j.jenvman.2018.07.046.

[7] J.K. Ahmed, M. Ahmaruzzaman, A review on potential usage of industrial waste materials for binding heavy metal ions from aqueous solutions, 10 (2016) 39–41.

[8] F. Fu, Q. Wang, Removal of heavy metal ions from wastewaters: A review, (2010). https://doi.org/10.1016/j.jenvman.2010.11.011.

[9] E. Da'na, Adsorption of heavy metals on functionalized-mesoporous silica: A review, (2017). https://doi.org/10.1016/j.micromeso.2017.03.050.

[10] W. Konicki, I. Pełech, E. Mijowska, I. Jasin´ska, J. Jasin´ska, Adsorption of anionic dye Direct Red 23 onto magnetic multi-walled carbon nanotubes-Fe 3 C nanocomposite: Kinetics, equilibrium and thermodynamics, (2012). https://doi.org/10.1016/j.cej.2012.08.025.

[11] U. Shamraiz, R.A. Hussain, A. Badshah, B. Raza, S. Saba, Functional metal sulfides and selenides for the removal of hazardous dyes from Water, (2016) 33–41. https://doi.org/10.1016/J.JPHOTOBIOL.2016.03.013.

[12] Y.A. Rahman, M.H. Nachabe, S.J. Ergas, Biochar amendment of stormwater bioretention systems for nitrogen and Escherichia coli removal: Effect of hydraulic loading rates and antecedent dry periods, (2020). https://doi.org/10.1016/j.biortech.2020.123428.

[13] C. Rees, P. Devi, Heavy Mwtal 3Rd, 23 (2001) 163–167.

[14] K.B.L. Borchert, R. Boughanmi, B. Reis, P. Zimmermann, C. Steinbach, P. Graichen, A. Svirepa, J. Schwarz, R. Boldt, S. Schwarz, M. Mertig, D. Schwarz, Removal of Lead , Cadmium , and Aluminum Sulfate from Simulated and Real Water with Native and Oxidized Starches, (2021) 429–453.

[15] Y.J. Hong, Y.J. Hong, W. Liao, W. Liao, Z.F. Yan, Y.C. Bai, C.L. Feng, Z.X. Xu, D.Y. Xu, Progress in the Research of the Toxicity Effect Mechanisms of Heavy Metals on Freshwater Organisms and Their Water Quality Criteria in China, (2020). https://doi.org/10.1155/2020/9010348.

[16] S.J. Cobbina, A.B. Duwiejuah, R. Quansah, S. Obiri, Comparative Assessment of Heavy Metals in Drinking Water Sources in Two Small-Scale Mining Communities in, 064 (2015) 10620–10634. https://doi.org/10.3390/ijerph120910620.

[17] C.R. Ohoro, A.O. Adeniji, L. Semerjian, O.O. Okoh, A.I. Okoh, Occurrence and distribution of pharmaceuticals in surface water and sediment of Buffalo and Sundays River estuaries, South Africa and their ecological risk assessment, (2021) 187–195. https://doi.org/10.1016/j.emcon.2021.09.002.

[18] S. González Alonso, M. Catalá, R.R. Maroto, J.L.R. Gil, Á.G. de Miguel, Y. Valcárcel, Pollution by psychoactive pharmaceuticals in the Rivers of Madrid metropolitan area (Spain), (2010) 195–201. https://doi.org/10.1016/j.envint.2009.11.004.

[19] K.S. Knaebel, Adsorbent Selection, (N.D.).

[20] S. Michael Abegunde, K. Solomon Idowu, O. Morayo Adejuwon, T. Adeyemi-Adejolu, A review on the influence of chemical modification on the performance of adsorbents,

Resources, Environment and Sustainability 1 (2020) 100001. https://doi.org/10.1016/j.resenv.2020.100001.

[21] T.S. Anirudhan, C.D. Bringle, P.G. Radhakrishnan, Heavy metal interactions with phosphatic clay: Kinetic and equilibrium studies, (2012) 149–157. https://doi.org/10.1016/J.CEJ.2012.06.024.

[22] R. Chakraborty, R. Verma, A. Asthana, S.S. Vidya, A.K. Singh, Adsorption of hazardous chromium (VI) ions from aqueous solutions using modified sawdust: kinetics, isotherm and thermodynamic modelling, (2021) 911–928. https://doi.org/10.1080/03067319.2019.1673743.

[23] Y. Li, Q. Du, T. Liu, J. Sun, Y. Jiao, Y. Xia, L. Xia, Z. Wang, W. Zhang, K. Wang, H. Zhu, D. Wu, Equilibrium, kinetic and thermodynamic studies on the adsorption of phenol onto graphene, (n.d.). https://doi.org/10.1016/j.materresbull.2012.04.021.

[24] M. Ahmaruzzaman, Industrial wastes as low-cost potential adsorbents for the treatment of wastewater laden with heavy metals, (2011) 36–59. https://doi.org/10.1016/j.cis.2011.04.005.

[25] M.L.D. Jayaranjan, E.D. van Hullebusch, A.P. Annachhatre, Reuse options for coal fired power plant bottom ash and fly ash, (2014) 467–486. https://doi.org/10.1007/s11157-014-9336-4.

[26] I.J. Alinnor, Adsorption of heavy metal ions from aqueous solution by fly ash, (2007) 853–857. https://doi.org/10.1016/j.fuel.2006.08.019.

[27] V. Gadore, M. Ahmaruzzaman, Tailored fly ash materials: A recent progress of their properties and applications for remediation of organic and inorganic contaminants from water, (2021) 101910. https://doi.org/10.1016/j.jwpe.2020.101910.

[28] National Association of Manufacturers, Petroleum Coke: Essential to Manufacturing, National Association of Manufacturers (n.d.) 2.

[29] Wu, Conversion of Petroleum Coke to Porous Materials, (2019).

[30] M. Yuan, S. Tong, S. Zhao, C.Q. Jia, Adsorption of polycyclic aromatic hydrocarbons from water using petroleum coke-derived porous carbon, (2010) 1115–1120. https://doi.org/10.1016/j.jhazmat.2010.05.130.

[31] J. V Vaghasiya, Innovations in Engineered Mesoporous Material for Energy Conversion and Storage Applications, 1 (2017) 1–2.

[32] A.M. Holban, A.M. Grumezescu, E. Andronescu, Inorganic nanoarchitectonics designed for drug delivery and anti-infective surfaces, 2016. https://doi.org/10.1016/B978-0-323-42861-3.00010-8.

[33] R.D. Ambashta, M. Sillanpää, Water purification using magnetic assistance: A review, 180 (2010) 38–49. https://doi.org/10.1016/j.jhazmat.2010.04.105.

[34] N. Ivanova, V. Gugleva, M. Dobreva, I. Pehlivanov, S. Stefanov, V. Andonova, We are IntechOpen , the world ' s leading publisher of Open Access books Built by scientists , for scientists TOP 1 %, Intech i (2016) 13.

[35] A.M. Atta, Y.M. Moustafa, A.O. Ezzat, A.I. Hashem, Novel magnetic silica-ionic liquid nanocomposites for wastewater treatment, (2020). https://doi.org/10.3390/nano10010071.

[36] D. Mehta, S. Mazumdar, S.K. Singh, Magnetic adsorbents for the treatment of water/wastewater-A review, (2015) 244–265. https://doi.org/10.1016/j.jwpe.2015.07.001.

[37] A. Ali, H. Zafar, M. Zia, I. ul Haq, A.R. Phull, J.S. Ali, A. Hussain, Synthesis, characterization, applications, and challenges of iron oxide nanoparticles, (2016) 49–67. https://doi.org/10.2147/NSA.S99986.

[38] M.R.Z. Kouhpanji, B.J.H. Stadler, A guideline for effectively synthesizing and characterizing magnetic nanoparticles for advancing nanobiotechnology: A review, (2020) 1–37. https://doi.org/10.3390/s20092554.

[39] Y. Fang, W. Xue, R. Zhao, S. Bao, W. Wang, L. Sun, L. Chen, G. Sun, B. Chen, Effect of nanoporosity on the electromagnetic wave absorption performance in a biomass-templated Fe3O4/C composite: A small-angle neutron scattering study (2019) 319–327. https://doi.org/10.1039/c9tc04569d.

[40] R. Xiong, Y. Wang, X. Zhang, C. Lu, L. Lan, In situ growth of gold nanoparticles on magnetic γ-Fe 2O3@cellulose nanocomposites: A highly active and recyclable catalyst for reduction of 4-nitrophenol, (2014) 6454–6462. https://doi.org/10.1039/c3ra46761a.

[41] A. Akbarzadeh, M. Samiei, S. Davaran, Magnetic nanoparticles: Preparation, physical properties, and applications in biomedicine, (2012). https://doi.org/10.1186/1556-276X-7-144.

[42] J.R. McCarthy, K.A. Kelly, E.Y. Sun, R. Weissleder, Targeted delivery of multifunctional magnetic nanoparticles, (2007) 153–167. https://doi.org/10.2217/17435889.2.2.153.

[43] M.L. Bruschi, L. de A.S. de Toledo, Pharmaceutical Applications of Iron-Oxide Magnetic Nanoparticles, 2019, Vol. 5, Page 50 5 (2019) 50. https://doi.org/10.3390/MAGNETOCHEMISTRY5030050.

[44] M. Cao, Z. Li, J. Wang, W. Ge, T. Yue, R. Li, V.L. Colvin, W.W. Yu, Food related applications of magnetic iron oxide nanoparticles: Enzyme immobilization, protein purification, and food analysis, (2012) 47–56. https://doi.org/10.1016/J.TIFS.2012.04.003.

[45] P. Xu, G.M. Zeng, D.L. Huang, C.L. Feng, S. Hu, M.H. Zhao, C. Lai, Z. Wei, C. Huang, G.X. Xie, Z.F. Liu, Use of iron oxide nanomaterials in wastewater treatment: A review, (2012) 1–10. https://doi.org/10.1016/J.SCITOTENV.2012.02.023.

[46] M.G.M. Schneider, M.J. Martín, J. Otarola, E. Vakarelska, V. Simeonov, V. Lassalle, M. Nedyalkova, Biomedical Applications of Iron Oxide Nanoparticles: Current Insights Progress and Perspectives, (2022) 204. https://doi.org/10.3390/PHARMACEUTICS14010204.

[47] R. Kumar, M.A.L.I.F. Hewaidy, Modified Adsorbents for Removal of Heavy Metals from Aqueous Environment : A Review, (2019) 83–93. https://doi.org/10.1007/s41748-018-0085-3.

[48] J. Mo, Q. Yang, N. Zhang, W. Zhang, Y. Zheng, Z. Zhang, A review on agro-industrial waste (AIW) derived adsorbents for water and wastewater treatment, (2018) 395–405. https://doi.org/10.1016/j.jenvman.2018.08.069.

[49] X. Wu, H. Ma, L. Zhang, F. Wang, Applied Surface Science Adsorption properties and mechanism of mesoporous adsorbents prepared with fly ash for removal of Cu (II) in aqueous solution, (2012) 902–907. https://doi.org/10.1016/j.apsusc.2012.08.122.

[50] A. Nikolaou, S. Meric, D. Fatta, Occurrence patterns of pharmaceuticals in water and wastewater environments, (2007) 1225–1234. https://doi.org/10.1007/s00216-006-1035-8.

[51] V. Mhuka, S. Dube, M.M. Nindi, Occurrence of pharmaceutical and personal care products (PPCPs) in wastewater and receiving waters in South Africa using LC-Orbitrap™ MS, (2020) 250–258. https://doi.org/10.1016/j.emcon.2020.07.002.

[52] A.O. Adeola, J. de Lange, P.B.C. Forbes, Adsorption of antiretroviral drugs, efavirenz and nevirapine from aqueous solution by graphene wool: Kinetic, equilibrium, thermodynamic and computational studies, (2021) 100157. https://doi.org/10.1016/j.apsadv.2021.100157.

[53] P.S.M. and L.M.M. Sharlott N. Qwane, Synthesis, Characterization and Application of a Molecularly Imprinted Polymer in Selective Adsorption of Abacavir from Polluted Water, (2020) 84–91. https://doi.org/https://doi.org/10.17159/0379-4350/2020/v73a13.

[54] I. Chianella, K. Karim, E. V. Piletska, C. Preston, S.A. Piletsky, Computational design and synthesis of molecularly imprinted polymers with high binding capacity for pharmaceutical applications-model case: Adsorbent for abacavir, (2006) 73–78. https://doi.org/10.1016/j.aca.2005.11.068.

[55] Z. Terzopoulou, M. Papageorgiou, G.Z. Kyzas, D.N. Bikiaris, D.A. Lambropoulou, Preparation of molecularly imprinted solid-phase microextraction fiber for the selective removal and extraction of the antiviral drug abacavir in environmental and biological matrices, (2016) 63–75. https://doi.org/10.1016/j.aca.2016.01.059.

[56] A.O. Adeola, J. de Lange, P.B.C. Forbes, Adsorption of antiretroviral drugs, efavirenz and nevirapine from aqueous solution by graphene wool: Kinetic, equilibrium, thermodynamic and computational studies, (2021) 100157. https://doi.org/10.1016/j.apsadv.2021.100157.

[57] T.G. Kebede, M.B. Seroto, R.C. Chokwe, S. Dube, M.M. Nindi, Adsorption of antiretroviral (ARVs) and related drugs from environmental wastewaters using nanofibers, (2020) 104049. https://doi.org/10.1016/j.jece.2020.104049.

[58] W.O. Gordon, B.M. Tissue, J.R. Morris, Adsorption and decomposition of dimethyl methylphosphonate on Y 2O3 nanoparticles, (2007) 3233–3240. https://doi.org/10.1021/jp0650376.

[59] S.A.S. Ahmed, R.M.M.A. El-Enin, Th. El-Nabarawy, Adsorption properties of activated carbon prepared from pre-carbonized petroleum coke in the removal of organic pollutants from aqueous solution, (2011) 152–161. https://doi.org/10.5714/cl.2011.12.3.152.

[60] M. Ghaedi, N. Mosallanejad, Removal of Heavy Metal Ions from Polluted Waters by Using of Low Cost Adsorbents : Review, (2013) 7–22.

[61] M. Harja, G. Buema, N. Lupu, H. Chiriac, D.D. Herea, G. Ciobanu, Fly ash coated with magnetic materials: Improved adsorbent for cu (ii) removal from wastewater, (2021) 1–18. https://doi.org/10.3390/ma14010063.

CHAPTER 2: LITERATURE REVIEW

PREAMBLE

This chapter reviews recent studies conducted on the adsorptive removal of antiretroviral and heavy metals in aqueous solutions using various industrial waste-based adsorbents such as coal fly ash, blast furnace slag, lignin, red mud, and petroleum coke. Additionally, the chapter also elaborates on the factors that affect the adsorption process when using industrial waste-based adsorbents.

2.1. Background

2.1.1. Antiretroviral drugs (ARVs) in wastewater

In African countries, conventional wastewater treatment plants (WWTP) processes are only designed to remove suspended solids, nutrients, and microbes, and are not efficient in removing new emerging contaminants such as pharmaceuticals from water bodies [1]. This has been demonstrated by reports of high detection of pharmaceuticals in the effluents of WWTPs. Globally, WWTPs employ primary, secondary, and tertiary treatment processes, which have shown limited efficiency for the removal of pharmaceuticals such as antiretroviral drugs (ARVs) in wastewater [2]. The inefficient removal of ARVs in WWTPs is likely influenced by environmental factors and WWTP capabilities, operation conditions, as well as the physiochemical properties of ARVs. ARVs are used to manage human immunodeficiency virus/ acquired immunodeficiency syndrome (HIV/AIDS) [3]. However, they are not fully metabolized by the body and are excreted via urine or faecal processes into the wastewater. WWTPs are the main entry point for ARVs to water sources, and other sources of ARVs include improper disposal of hospital waste, pharmaceutical manufacturing waste, expired drugs, and poor sewage transport systems [4]. Moreover, due to the contamination of the ARVs in the WWTPs therefore the possibility of HIV resistance has sparked serious concerns [4]. It is imperative that we pay attention to this threat and take action to mitigate it. The sources of ARVs in the environment are illustrated in **Figure 2.1**.

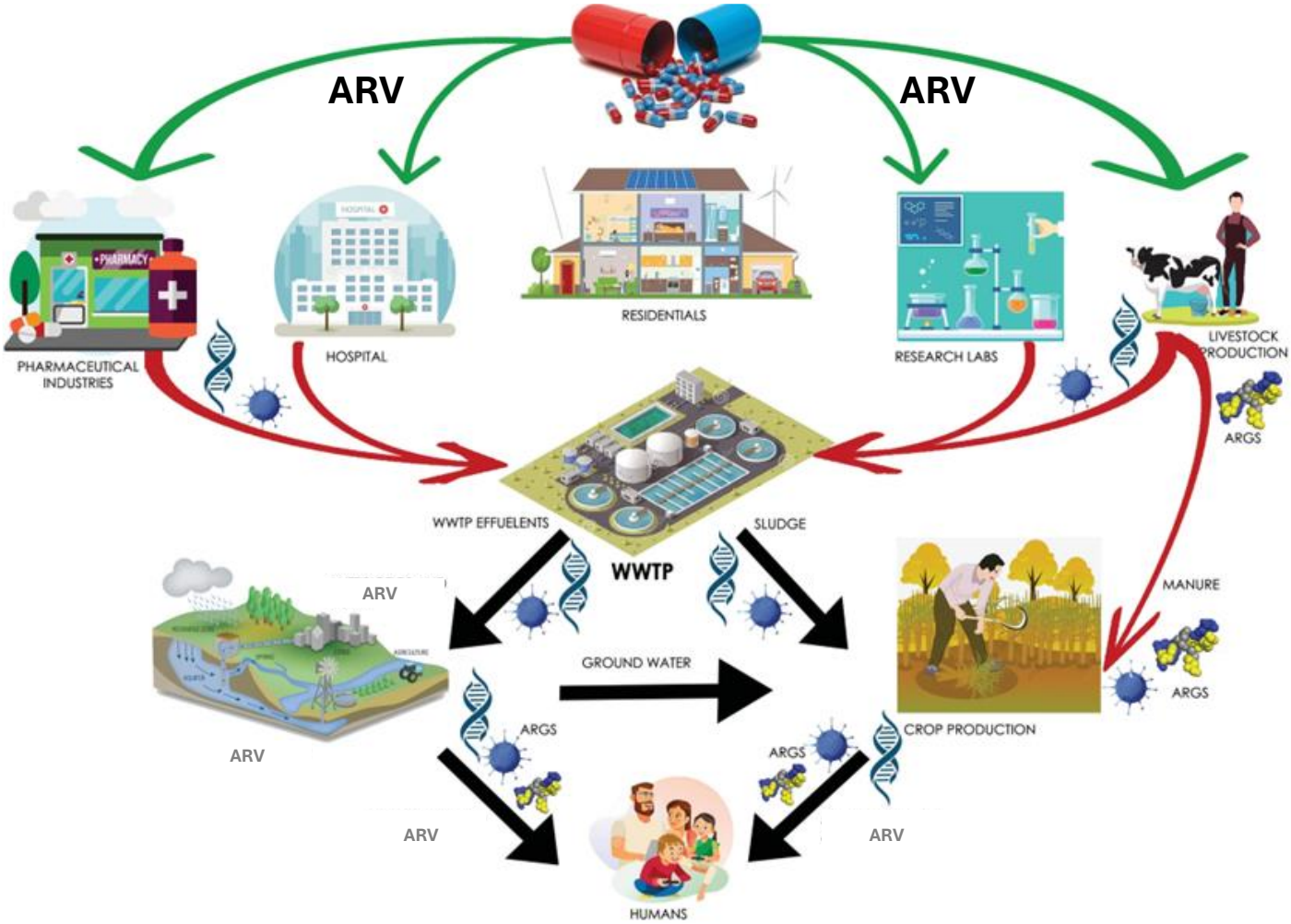

Figure 2.1: Schematic diagram showing various pathways through which pharmaceuticals enter the environment [5]

Countries with high prevalence of HIV/AIDS cases include South Africa, Mozambique, Nigeria, Kenya, and Uganda among other African countries. **Table 2.1** shows the detected concentrations in different waters South Africa. South Africa has the highest number of people living with HIV and the largest ARV rollout program globally, Kenya only appears as the fifth country in terms of the number of people living with HIV [6]. It was reported as indicated in **Table 2.1** that effluent water contained higher concentrations of different ARVs including emtricitabine, efavirenz, and lamivudine. However, efavirenz was also found to be higher in effluent water. This further reinforces that the presence of such ARVs can pose a problem to society.

Table 2.1: Concentrations of ARVDs in South African water bodies [7].

ARV	Measured concentration (µg/L)		
	Effluent	**Influent**	**Surface water**
Abacavir	Not detected	Not detected – 14a	
Maraviroc	Not detected - 0.039[a]	0.082 – 0.32[a]	
Zidovudine	0.087–0.5[a], not detected[a]	6.9 – 53[a], not detected	
Nevirapine	0.54–1.9[a], <LOQ-0.658[b]	0.67–2.8[a], <LOQ-0.681[b]	Not detected - 0.071[d]
Raltegravir	Not detected - 3.5[a]	0.061–17[a]	
Darunavir	0.13–17[a]	Not detected - 0.18[a]	
Saquinavir	Not detected[a]	Not detected -0.18[a]	
Atazanavir	0.078–0.74[a]	0.064–1.4[a]	
Indinavir	0.025–0.042[a]	0.26–0.59[a]	
Ritonavir	0.46–1.5[a], <LOQ[b]	1.6–3.2[a], <LOQ[b]	
Lopinavir	1.9–3.8[a]	1.2–2.5[a]	
Lamivudine	Not detected -0.13[a], <LOQ[b]	0.84–2.2[a], 3.67–20.9[b]	Not detected[d]
Efavirenz	20-34[a], 0.982–9.15[b], 2.79–93.1[c]	24-34[a], 1.42–15.4[b], 9.63–140[c], 5.5–14[e]	<LOQ-2.45c, 0.002–0.354d
Emtricitabine	<LOQ-41.7[b]	31.3–172[b]	Not detected - 0.013[d]
Tenofovir disoproxil			Not detected[d]

<LOQ – below method quantitation limit, a – KwaZulu-Natal [8]. b – Western Cape [9]. c – KwaZulu-Natal [10]. d – KwaZulu-Natal [11]. e – Gauteng [12]

2.1.2. Heavy metals

Heavy metals are released into the environment either by anthropogenic activities (industrialization, mining etc) or as natural deposits (in the Earth's crust) such as rock weathering or volcanic activities. As shown in **Figure 2.2,** industrial activities such as mining, metal finishing, plating, and semiconductors are the major sources of heavy metals present in wastewater. These activities release harmful heavy metals into the water sources, which then

end up in the food chain, posing a danger to both humans and animals. Highly stable and water-soluble heavy metals are harmful to humans, animals, and environmental health when their levels exceed the permissible limit shown in **Table 2.2**. Heavy metal toxicity can result in various adverse health effects such as damage or reduced mental and central nervous function, lower energy levels, and damage to the blood composition, lungs, kidneys, liver, and other vital organs [13].

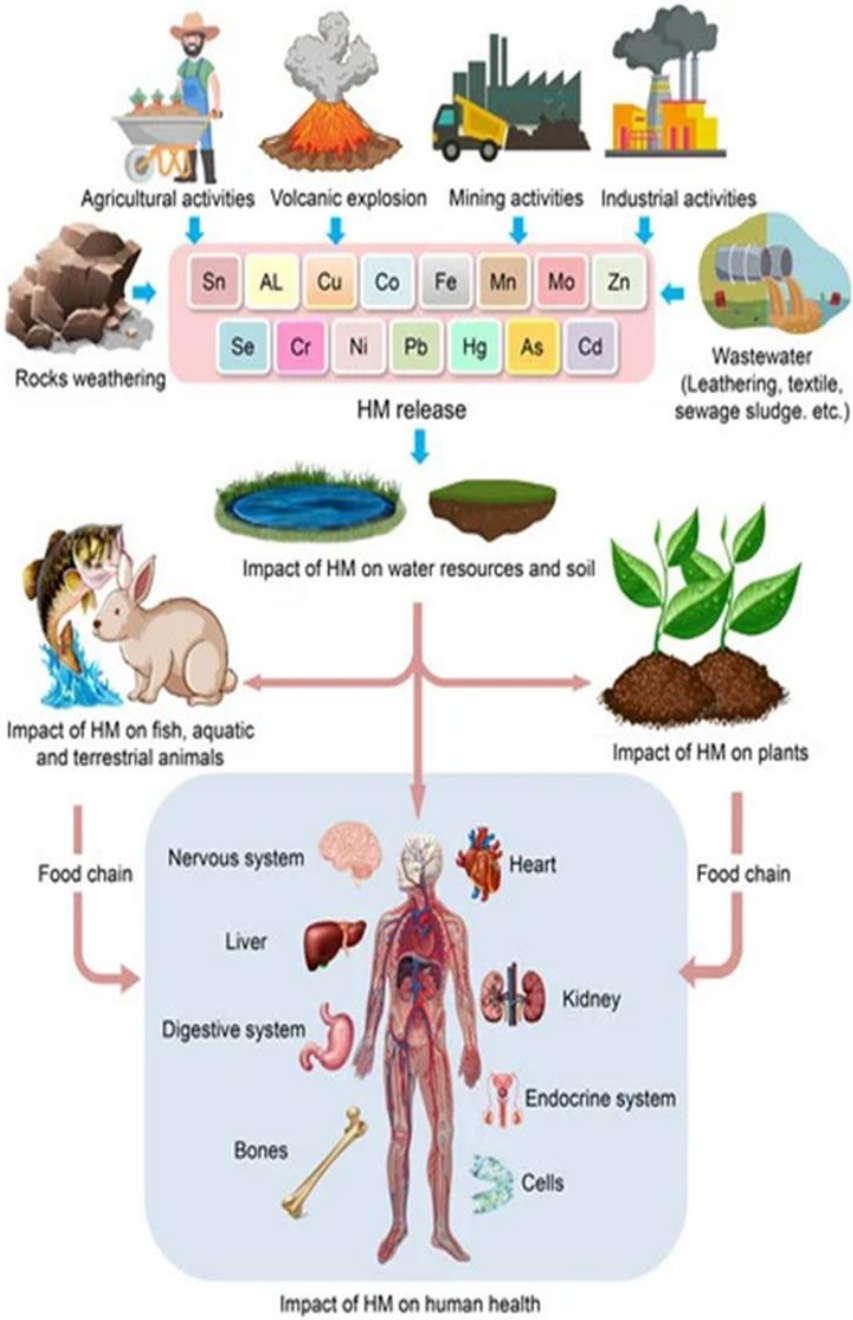

Figure 2.2: Sources of heavy metals in the aqueous ecosystem and health effects [14].

Table 2.2: Permissible limits and health effects of various toxic heavy metals in potable water [15].

Heavy metal	**Permissible limits for potable water (mg/L)**			Health hazard
	WHO	**EU standard**	**USEPA**	
Vanadium	1.4	Not reported	Not reported	Very toxic, and may cause paralysis
Iron	0.2	0.2	0.3	Excess amounts cause rapid pulse rates, congestion of blood vessels, hypertension
Manganese	0.05	0.05	0.05	Excess amounts are toxic and cause growth retardation, fever, sexual impotence, muscle fatigue, and eye blindness.
Mercury	0.001	0.001	0.002	The excess dose may cause headache, abdominal pain, diarrhoea, paralysis, gum inflammation, loosening of teeth, loss of appetite, etc.
Asernic	0.01	0.01	0.01	Carcinogenic, producing liver tumours, and gastrointestinal effects
Chromium	0.05	0.05	0.1	Suspected human carcinogen, producing lung tumours
Copper	2.0	1.3	2.0	Long-term exposure causes stomach-ache, irritation of nose, mouth, eyes, headache
Lead	0.01	0.01	0.015	Suspected carcinogen, anaemia, muscle and joint pains, kidney problems and high blood pressure

Cadmium	0.003	0.005	0.005	Carcinogenic, cause lung fibrosis, dyspnoea
Nickel	0.02	0.1	0.02	Causes chronic bronchitis, reduced lung function, and cancer of the lungs.
Zinc	3.0	Not reported	5.0	Causes short-term illness called “metal fume fever” and restlessness

2.2. Remediation methods for heavy metals and antiretrovirals in aqueous solutions

There are various treatment processes available for contaminated water streams, such as chemical precipitation, coagulation, solvent extraction, ultrafiltration, biological systems, electrolytic processes, reverse osmosis, oxidation with ozone/hydrogen peroxide, membrane filtration, ion exchange, photocatalytic degradation, and adsorption [15, 16]. Because of the high cost and disposal problems associated with the aforementioned treatment processes, many of these conventional methods have not been widely applied at large scale treatment of wastewater [18]. In accordance with abundant literature data, adsorption is one of the most popular methods for the removal of toxic pollutants from wastewater since the proper design of the adsorption process will produce a high-quality treated effluent and is specific to the targeted analyte(s) species. This process provides an attractive alternative to convention techniques for the treatment of contaminated water, especially if the adsorbent is inexpensive and does not require an additional pre-treatment step before its application. Adsorption is superior compared to the other techniques for water re-use in terms of initial cost, flexibility and simplicity of design, ease of operation and no usage toxic pollutants and waste generation [19]. **Table 2.3** shows the limitations of various processes used for the removal of toxic pollutants from wastewater.

Table 2.3: Treatment technologies for heavy metals and pharmaceuticals in aqueous solutions[20].

Method	Limitation
Ion exchange	Absorbent requires regeneration or disposal
Oxidation	High energy cost and production of by-products
Membrane filtration technologies	Concentrated sludge production, expensive
Coagulation & flocculation	High sludge production and formation of large particles
Electrochemical treatment	High energy cost and production of by-products
Photochemical	Formation of by-products
Biological treatment	Technology yet to be established and commercialized

2.3. Adsorption

Adsorption is a phenomenon in which molecules or particles in a medium, such as a liquid or gas, bind to the surface of a solid material, commonly referred to as the adsorbent material. Adsorption is mainly classified into two types (**Figure 2.3**): physical adsorption (physisorption) and chemical adsorption (chemisorption) which is also known as activated adsorption). Physical adsorption occurs when an adsorbate adheres to the surface of an adsorbent through nonspecific van der Waals forces. On the other hand, chemisorption occurs when chemical bonding creates strong attractive forces, such as ionic or covalent bonds, through chemical reactions. In chemisorption, the adsorbent and adsorbate molecules are bonded together through chemical reactions, resulting in stronger adhesion compared to physical adsorption. Physical adsorption is a reversible process but less specific, whereas chemisorption is irreversible [20, 21].

The adsorption capacity and efficiency of an adsorbent are significantly affected by its surface characteristics. Adsorbents typically possess a high surface area, which results in many adsorption sites. Moreover, the presence of functional groups on the surface increases the affinity of the adsorbent for specific contaminants compounds [23].

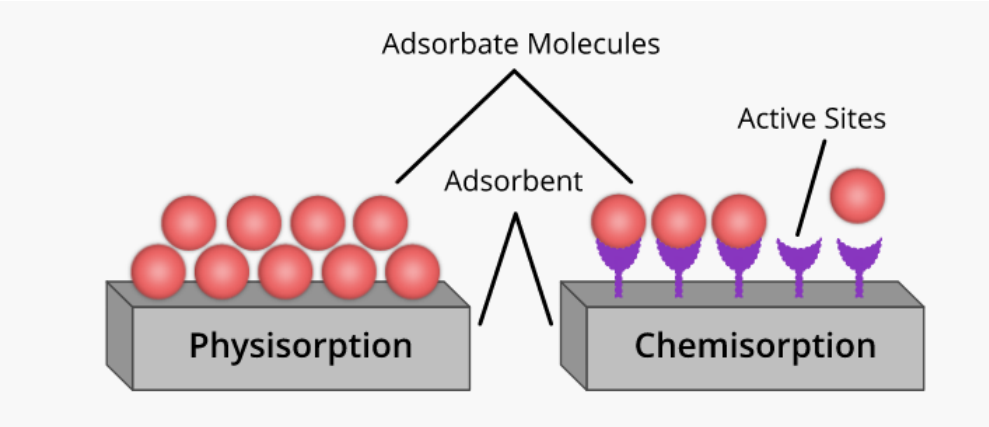

Figure 2.3: Types of adsorption processes [24]

Figure 2.4 shows the different adsorption mechanisms involved in the adsorption of metal ions, and organic pollutants onto different industrial wastes derived adsorbent materials. These including hydrogen bonding, ion exchange, electrostatic attraction, and chemical interactions between the metal ions, organic pollutants and the surface functional groups of the different industrial adsorbents. Most researchers translate the main adsorption process to the chemical interaction between the metal ions and the surface functional groups of different industrial wastes [25–29]. Organic molecules have bulky molecular structures that frequently result in

several conflicting interactions. Additional non-covalent bonding interactions might involve binding processes such as hydrophobic bonding, van der Waals, and π-π stacking, which have been shown to regulate the adsorption of various chemical contaminants [30].

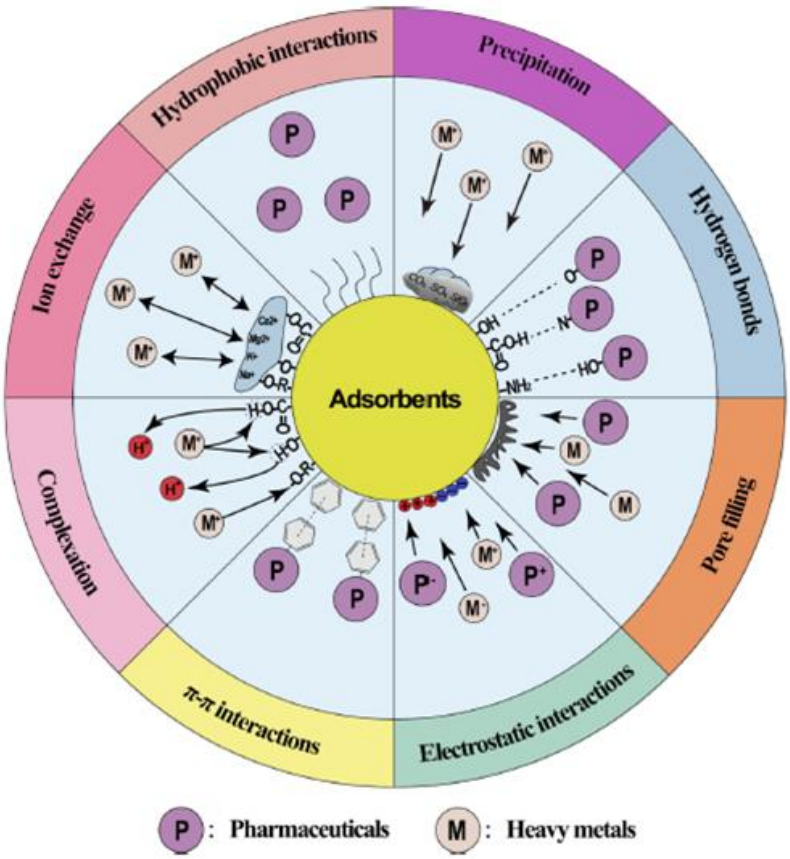

Figure 2.4: Different surface interactions occurring between pollutants (pharmaceuticals & heavy metals) and adsorbents [31].

Adsorption of these heavy/ trace metals ions and pharmaceuticals compounds can further be described by using the kinetic models and thermodynamic parameters. The common kinetic models are pseudo-first order, pseudo-second order and intra-particle diffusion kinetic [32]. Kinetic models determine the rate of biosorption during the removal of heavy/ trace metals ions and pharmaceuticals compounds from wastewater. Thermodynamic studies offer insights into the minimum kinetic energy necessary for the adsorbate to become bound to the adsorption site. The nature of adsorption is determined by whether it is spontaneous, random, endothermic, or exothermic [33].

2.3.1. Industrial waste-based adsorbents for antiretrovirals

The first African study published on the monitoring of ARVs in water was conducted in Nairobi, Kenya in 2012 [34]. They reported the occurrence of three ARVs, lamivudine, nevirapine, and zidovudine, in surface water at the highest concentrations of 1.2, 2, and 9 ng/L, respectively. Their work sparked more interest in other African researchers to investigate the occurrence of ARVs in water bodies, with South Africans following it up with 2 articles in 2015 [35]. Schoeman *et al* [36] reported the presence of efavirenz (17.4 ng/L) and nevirapine (2.1 ng/L) in influent and effluent water samples collected in a WWTP located in Gauteng Province, South Africa. Since then, more research has been published on these drugs, reporting their presence and removal from water bodies.

To date, no studies have reported adsorption removal of ARVs using industrial waste materials. However, there have been reports of the use of nanomaterials, as shown in **Table 2.4**. Kebede *et al*. [37] investigated the use of nanofibers from Mondia White for ARV drug (didanosine, ritonavir and efavirenz) elimination. The results showed a decrease in drug removal when the adsorbent dose was changed from 10 to 60 mg, which was attributed to adsorption active site aggregation or overlap. Chemisorption was reported to be the rate-limiting step in ARV adsorption. The nanofiber surfaces decreased the percentage removal due to electrostatic repulsive forces. The maximum percentage removal at the optimal pH was 75.1 - 92.8% [38].

A study by Qwane *et al* [39] presented the synthesis, characterization, and application of a molecularly imprinted polymer (MIP) for the selective adsorption of abacavir from polluted water. The MIP was synthesized using abacavir as the template molecule, Aliquat 336 as the functional monomer, and ethylene glycol dimethacrylate as the cross-linking agent. The study found that MIP selectively adsorbed abacavir from water in the presence of other antiretroviral drugs, with a maximum adsorption capacity of 5.98 mg/g. The adsorption mechanism was best described by the Freundlich isotherm and pseudo-second-order kinetic model, indicating multilayer coverage and chemisorption influenced by electrostatic attraction, respectively. The synthesized MIP selectively adsorbed abacavir from wastewater influent, effluent, and estuarine water with extraction efficiencies of 67%, 74%, and 76%, respectively. Moreover, MIP demonstrated reusability for at least 10 consecutive times without losing its extraction efficiency. This study is the first to report the application of Aliquat 336 as the functional monomer in the synthesis of MIP for the selective extraction of abacavir from water. These findings demonstrate the potential of MIPs as selective sorbents for the removal of

pharmaceuticals from water, with implications for environmental remediation and water treatment.

Additionally, other researchers have investigated the use of graphene wool as an adsorbent for the removal of efavirenz and nevirapine from water [19]. The study found that graphene wool demonstrated a high adsorption capacity for both drug compounds, with efavirenz showing a higher affinity for the adsorbent than nevirapine. The adsorption process was found to follow Langmuir and Freundlich isotherm models, where the maximum adsorption capacities for efavirenz and nevirapine were found to be 344.83 and 222.23 mg/g, respectively. The mechanism of adsorption was attributed to π–π interactions, hydrogen bonding, and van der Waals forces between the drugs and the graphene wool. The experimental results indicated that the adsorption process was favourable, spontaneous, and endothermic for both drugs. Computational studies further supported these findings, revealing the structural and energetic aspects of the adsorption process. This research provided valuable insights into the potential use of graphene wool as an effective adsorbent for the removal of pharmaceutical compounds from water [40].

Table 2.4: Absorbents reported for the removal of ARVDs from different water matrices.

Adsorbent	ARV	Optimum condition			Adsorption capacity (mg/g)	Adsorption mechanism	Detection technique	REF
		pH	Temperature (˚C)	Contact time (min)				
Graphene wool	Nevirapine	5	45	Not reported	48.31	Chemisorption	Spectrophotometer	[40]
	Efavirenz				4.41			
Nanofibres (Mondia White roots)	Nevirapine	7	35	120	(200.5[d], 189[e], 174[i])	Chemisorption	HPLC	[41]
	Didanosine				75.9[d], 72.5[e], 64.9[i]			
	Ritonavir				86.9[d], 72,8[e], 69.4[i]			
	Efavirenz				152.1[d], 138.4[e], 111.6[i]			
	Stavudine				160[i], 150.2[e], 136.4			
MIPs	Abacavir	5	Not reported	60	5.98	Chemisorption	UPLC – MS/MS	[39]
		Not reported			158	Chemisorption	LC-DAD-ES/MS	[42]

		8	45	Not reported	167	Chemisorption	LC – MS/MS	[43]
Biochar from olive residue, tomato residue, rice husks and African palm tree	Abacavir Atazanavir Darunavir Lamivudine Nevirapine Raltegravir	Parameters not reported			Optimum values not reported exhibited poor removal efficiencies	Chemisorption	HPLC – DAD	[44]
Alginate, polyvinylpyrro-lidone and activated carbon	Nevirapine Zidovudine	6.5			44.4 42.2	Physisorption	HPLC – DAD	[45]

e – effluent., i – influent, d – deionized water.

2.3.2. Industrial waste-based adsorbents for adsorption of heavy metals

Industrial waste has been identified as a low-cost adsorbent for the removal of both organic and inorganic pollutants from wastewater. However, functionalization process is required to increase its adsorption capacity. Generally, industrial waste is generated as a by-product, and these materials are locally available in large quantities, they are inexpensive. Various types of industrial wastes materials are readily available such as fly ash, blast furnace sludge, waste slurry, lignin, iron (III) hydroxide, and red mud, and all have been explored for their technical feasibility in removing toxic pollutants from contaminated water bodies [46]. Various types of industrial waste, including coffee husks, Areca waste, tea factory waste, sugar beet pulp, olive oil factory waste pomace, battery industry waste, biogas residual slurry waste, sea nodule residue, and grape stalk waste, have been used as inexpensive adsorbents for eliminating harmful heavy metals from wastewater [47].

Coal Fly ash

Coal fly ash (CFA) is a solid industrial waste generated by the combustion of coal from power plants. Coal fly ash consists of two forms, fly ash and bottom ash. Fly ash is made of fine particles that rise with flue gases during coal combustion, whereas bottom ash is ash that does not rise and remains at the bottom of the furnace. Fly ash is collected using particle filtration equipment, which prevent it from entering chimneys. The bottom ash is collected from the bottom of the furnace [48]. The geological location and type of coal usually determine the chemical composition of coal fly ash. It consists mainly of crystalline and amorphous silicon dioxide (SiO_2), calcium oxide (CaO), and aluminium oxide (Al_2O_3). They also contain a variety of toxic trace elements, which depend on the specific composition of the coal bed. The fly ash material solidifies while suspended in exhaust gases, resulting in a spherical particle shape and size ranging from 0.5 to 300 µm [49].

Based on the quantities of silica, aluminium, and iron coal fly ash can be classified into two types: Class C and Class F. The calcium, silica, alumina, and iron contents of the ash are the main defining characteristics of these classes. The chemical composition of burned coal (anthracite, bituminous, and lignite) significantly affects the physical and chemical characteristics of fly ash. With a pH range of 10–13, coal fly ash is a strong alkali material that develops a negatively charged surface at high pH. Therefore, it is logical to expect that

precipitation or electrostatic adsorption can remove metal ions and organic pollutants from aqueous solutions [50].

The physical properties of fly ash play a crucial role in its effectiveness as an adsorbent for the removal of heavy metals, as shown in **Table 2.5**. Fly ash exhibits a range of physical characteristics including morphology, particle size distribution, and surface area. The morphology of fly ash particles can vary from spherical to irregular, and the particle size distribution can range from fine to coarse. The appearance of CFA can range from dark brown to light grey, and this is influenced by the amount of unburned carbon present after the coal combustion process. Generally, the lighter the colour, the lower the carbon content, and vice versa. Lignite or sub-bituminous CFA typically has a lower carbon content and traces of calcium or lime, resulting in a greyish colour. However, bituminous and anthracite CFAs have higher carbon residues, making them appear darker in colour. In addition to colour, other important physical characteristics of CFA include the distribution of the particle size and surface area. Studies have shown that the particle sizes of CFA from bituminous and anthracite coals are like those of silt (less than 0.075 mm), whereas the CFA particles of sub-bituminous and lignite are larger (greater than 0.075 mm) [51]. For water remediation, the surface area of CFA, particle size distribution, porosity, and hydrophilicity are crucial. These physical properties directly affect the adsorption capacity and efficiency of fly ash. Larger surface areas and finer particle size distributions generally result in higher adsorption capacity and efficiency. Understanding the physical properties of fly ash is essential to optimise its use as an effective adsorbent for the removal of pollutants in air and water systems [52,53].

Table 2.5: Physiochemical properties of coal fly ash [51].

Characteristics	**Value**
pH	6 – 8
Bulk density (kg/m^3)	900 – 1300
Specific gravity	1.6 – 2.6
Porosity (%)	30 – 65
Particle size (nm)	0.001 – 0.1
Surface area (m^2/g)	5
Lime reactivity (MPa)	1 – 8

The chemical composition of the fly ash is a key factor in its adsorption performance**.** Modifying the chemical properties of fly ash through treatment or modification can enhance its adsorption performance [54].

As demonstrated in **Table 2.8,** there are numerous studies that have been conducted to investigate the removal of heavy metals using coal fly ash-based adsorbents. Hussain *et al.* [55] investigated the use of waste CFA for production of new innovated flocculants porous particles by modification of coal fly ash (CFA) using a multi-step base–acid–base (NaOH) modification method. Results showed that the surface area of the flocculant particles of MCFA was increased from 5.241 to 32.011 m^2/g, which increased the adsorption process of heavy metals (Mn^2, Cu^{2+}, Ni^{2+} and Pb^{2+}. The maximum removal efficiencies of MCFA for Mn^{2+}, Cu^{2+}, Ni^{2+}, and Pb^{2+} were recorded at 94.26%, 95.88%, 71.04%, and 99.91%, respectively. The Freundlich isotherm model was fitted for the adsorption process, and the maximum adsorption amounts of MCFA for Mn^{2+}, Cu^{2+}, Ni^{2+}, and Pb^{2+} were 558.9219, 0.4341, 210.9737, and 12.1957 mg/g, respectively. Moreover, the kinetic model indicated that physicochemical adsorption occurred between the adsorbate materials and the adsorbent.

Attari *et al.* [56] proposed a synthesis of zeolite Linde Type A (LTA) from coal fly ash (CFA-ZA) for the adsorptive removal of simulated Hg(II) solution made using an industrial wastewater matrix. The average removal efficiency of the CFA-ZA for Hg(II) was 94% with 10 mg/L initial concentration that is comparable with activated carbon. It was observed that CFA-ZA has strong affinity towards Hg(II) in all examined adsorbent/solution ratios. The mercury adsorption process was best described by Freundlich isothermal model. All adsorption processes reached equilibrium within approximately 120 min.

Tang *et al.* [57] used coal fly ash-based porous geopolymer (CFAPG) for the removal of Zn and found the optimal parameters were best described by the Bi_Langmuir model. This indicated that the two different sorption site classes on the surface of CFAPG with a total maximum Zn adsorption capacity of 13.42 mg/g. These results provided key parameters for the application of geopolymers as heavy metal adsorbents. Shyam *et al.* [58] studied the adsorption of Pb^{2+}, Ni^{2+} and Cr^{6+} from single metal solutions. The Pb^{2+} and Ni^{2+} removal was observed to be almost the same. The significant difference observed between single and binary metal adsorption is in the initial metal removal rate. Slightly lower initial metal removal rate observed in the case of binary adsorption was probably due to the presence of competing metal

ions in the solution. Fly ash-based adsorbents prepared in the laboratory exhibited comparatively more adsorption capacity than that of the parent material, fly ash.

Wang *et al.* [59] synthesised zeolite based on coal fly ash adsorption of lead. The results showed that synthesized zeolite has high adsorption capacity of 99.082 mg of Pb^{2+}per gram of adsorbent. Coal fly ash zeolite synthesized by wet milling had good Pb^{2+} adsorption performance when the initial pH of the solution was above 5. The adsorption kinetic results demonstrated that removal of Pb^{2+}via the synthesized zeolite followed pseudo-second-order kinetic model. Zhao *et al.* [60] conducted a study on the effects of modified fly ash and mechanisms of modified fly ash synthesis conditions on its cadmium adsorption capacity. The optimal result was achieved with an ash to base ratio of 5:5, a calcination temperature of 200 °C, and a calcination time of 3 hours, which resulted in adsorbing 90.27 mg/g of Cd^{2+} during the adsorption experiments.

Siahaan [61] prepared novel zeolite (K-type zeolite) for the adsorption of Pb^{2+} .Six types of zeolites (FA1, FA3, FA6, FA12, FA24, and FA48) were prepared, and their physicochemical properties, such as surface functional groups, cation exchange capacity, pHzpc, specific surface area, and pore volume, were evaluated. The quantity of Pb^{2+}adsorbed by the prepared zeolites followed the order FA < FA1 < FA3 < FA6 < FA12 < FA24 < FA48. Results indicated that the level of Pb^{2+} adsorbed was strongly related to the surface characteristics of the adsorbent. Low-cost adsorbents synthesised by Harja and colleagues [62] displayed a good capacity to remove copper, nickel, and lead ions (29.97 mg of Cu^{2+}per g of sorbent, 303 mg/g of sorbent, and 1111 mg/g of sorbent) from aqueous solutions.

According to Javadian *et al.* [63] , the zeolites have demonstrated their maximum efficiency when utilized under optimal sorption conditions. This included a dose of 0.08 g of ZFA in 25 mL of Cd (II) with a contact time of 7 hours and a pH of 5. The kinetic data showed that pseudo-second order equations controlled the adsorption process. According to adsorption isotherm studies, the Langmuir isotherm was proved to be the best fit for the experimental data, in comparison to Freundlich, D–R and Tempkin models. Thermodynamic parameters showed that the adsorption of Cd^{2+} onto ZFA was feasible, spontaneous and endothermic under studied conditions.

Blast furnace slag

Another low-cost adsorbent material showing the capability to adsorb heavy metals is blast furnace slag (BFS), an industrial by-product generated in steel plants [64]. Steel plants generate a large volume of granular blast furnace slag which is also being used as filler or in the production of slag cement. Blast furnace flue dust is a waste material from steel industries and can used to remove heavy metal ions from aqueous solutions. In recent years, numerous researchers have explored the possibility that using slag as an alternative adsorbent for the removal of heavy metals from wastewater [65,66]. The removal characteristics of different metal ions using different slags have been investigated in terms of adsorption isotherms/kinetics, and various removal mechanisms [67,68]. **Table 2.6** demonstrate the reported studies and findings using blast furnace slag for removal of several metal ions in water.

The results of a study revealed that the cation exchange capacity (CEC) of granulated blast furnace slag (BFS) is 89.21 ± 0.04 cmol/kg, which demonstrated a remarkable adsorption capacity for copper, zinc, and nickel. Due to the presence of alkali components and a negatively charged surface at high pH, it is believed that BFS removed metal ions primarily through precipitation or electrostatic adsorption. When compared to other materials, such as biochar and metal-organic frameworks (MOF), BFS has a higher specific surface area. Furthermore, BFS has an inherent self-alkalinity that facilitates the precipitation of Cr^{3+}. While the preparation of MOF materials is more complex, BFS is an easily obtained industrial waste. As a result, BFS is a more promising candidate for waste reuse in practical applications [69].

Sabah *et al*. [70] investigated the removal of $Pb^{2+}$and $Co^{2+}$from aqueous solutions using blast furnace slag, and their findings indicated that the adsorption process followed the Freundlich isotherm, suggesting physisorption. The inner layer sorption of metal ions on BFS may be attributed to the formation of metal-Sicomplexes between the Pb^{2+} ions and the Si of the slag via the exchange of H^{+} ions in the vicinity. Additionally, the negatively charged BFS surface at pH 6 favours electrostatic interactions with positive metal ions. Consequently, the electrostatic interactions between Pb^{2+}/Co^{2+} ions and the groups (-CO_3 and -OH) on the sorbent lead to multilayer adsorption of metal ions. The formation of metal-sulphur complexes via ion exchange and electrostatic interactions was considered a viable mechanism for metal-ion adsorption on BFS [71]. Considering the nature and composition of the BFS, an exchange interaction of the slag with the effluent may be described as follows [72]:

$$-SiO(Ca) + 2H-OH \rightarrow -Si - O - H_2 + Ca^{2+} + 2(-OH-)$$

In an acidic environment with a high concentration of hydrogen ions, it is expected that the above reaction will shift to the left. The basic slags provided a neutralizing effect, and the interaction between the Ca^{2+} ions and the freed H^+ ions from the slag was confirmed when the solution pH rose. This reaction was supported by the equation when the BFS came into contact with the solutions. The BFS slag demonstrated a remarkable ion exchange capacity, which was consistent with the sorption equilibrium. For divalent metal ions (M^{2+}) in solutions, the aforementioned reaction may be expressed as [67]:

$$(Si - O-)_2Ca^{2+} + H_3O^+ \rightarrow 2(Si\text{-}OH) + Ca^{2+} + OH^-$$

The lone pair of electrons in the oxygen atoms of OH^- groups play an important role in the complexation between metal ions and these OH^- groups [73] as illustrated in the schematic diagram shown in **Figure 2.5** which summarises the different BFS adsorbents used for removal of heavy metals in aqueous environments highlighting the condition, mechanisms, maximum adsorbent capacity, and percentage removal.

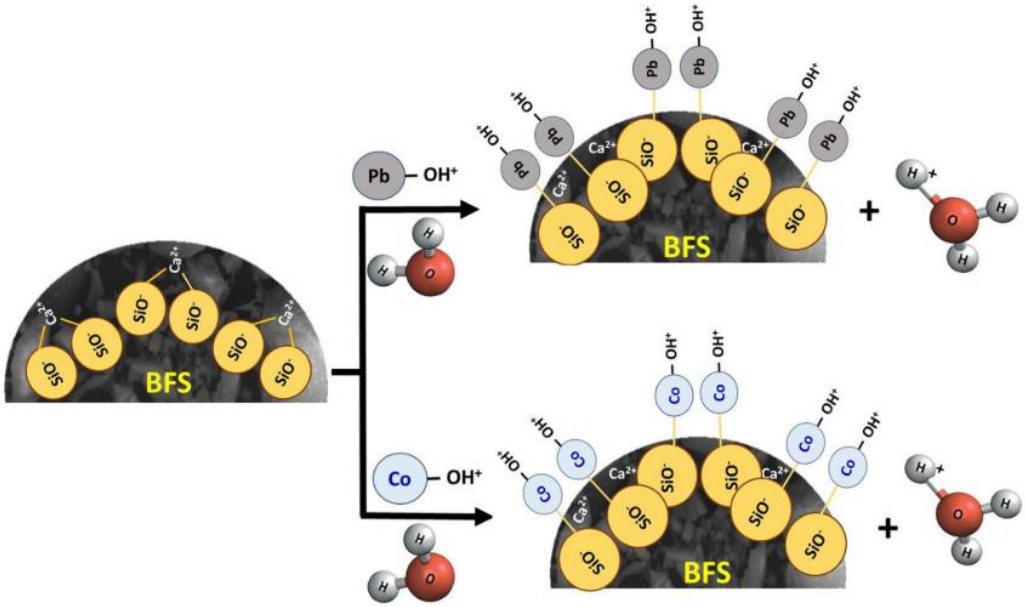

Figure 2.5: Schematic illustration of Pb and Co metal ions adsorption process by BFS [70].

The removal of lead by sorption on granulated blast-furnace slag was investigated by Dimitrova *et al* [72]. It was established that the sorption process occurs with increasing pH from 2 to 9. Maximum Pb^{2+} removal (97±98%) is achieved at pH value approximately 6.0±7.0. The equilibrium in the slag/lead solution system was described by the Freundlich adsorption isotherm. The constants in the Freundlich equation were calculated for different slag particle

sizes at pH 5.0±5.1. The percentage of lead removal at equilibrium increased with increasing slag amount but the sorption capacity decreased.

Water-quenched blast furnace slag (WBFS) was assessed by Want *et al* [74] for its capacity to remove Cu^{2+}, Cd^{2+}, and Zn^{2+} from aqueous solutions. The results showed that the removal efficiency increased with increasing adsorbent dosage and the optimum conditions for the removal of Cu^{2+}, Cd^{2+}, and Zn^{2+} were obtained in the dosage of 12, 16, and 16 g/L, respectively. The removal efficiency and adsorption amount of Cu^{2+}, Cd^{2+}, and Zn^{2+} onto WBFS increased on increasing the solution pH from 1 to 9, while the values decreased slightly as the pH further increased above 9. The adsorption process fitted the pseudo-second-order kinetic and Langmuir isotherm models. WBFS was feasible and endothermic in nature.

BFS was exploited as an adsorbent for the removal of Cr^{3+}, Pb^{2+}, and Cr-Pb by Chauchabe *et al.* [75]. The physicochemical tests indicated that the BFS was formed from a mixture composed mainly of silicates, aluminates, lime, and magnesium oxide. The specific surface area was found to be 325.6 m^2/g and the pHzpc value corresponded to 3.8. Equilibrium was obtained after 60, 50, and 80 min for Cr^{3+}, Pb^{2+}, and the Cr-Pb mixture, respectively. Under the experimental conditions (pH 4.8, agitate: 150 rpm, T: 20 °C), the adsorption capacities of Cr^{3+}, Pb^{2+}, Cr-Pb, Cr^{3+} in the mixture, and Pb^{2+} in the mixture were 43.16, 50.12, 39.91, 17.05, and 22.66 mg/g, respectively. Moreover, the adsorption isotherms revealed that the Langmuir model was the best fit for the metal ion adsorption processes examined ($R^2 = 0.99$). The kinetics indicated that the adsorption of the metal ions studied followed the pseudo-second-order model and that their transfers from the solution to the adsorbent are controlled by external and intraparticle diffusion. The thermodynamic study has shown that all the processes applied are spontaneous, exothermic, and less entropic. The desorption of the binary mixture revealed that saturated BFS can be efficiently exploited over four cycles.

Based on the affinity between oxalate and heavy metal, Le *et al* [76]synthesized a novel calcium oxalate/calcium silicate hydrate (Ca-Ox/C-S-H) adsorbent from blast furnace slag (BFS) by a facile oxalic acid/NaOH treatment. The BFS-derived CaOx/C-S-H exhibited superior maximum uptake capacities for Pb^{2+} (2117 mg/g) and Cd^{2+} (1083 mg/g). The removal mechanism involves ion exchange, and adsorption kinetics showed an equilibration time of 10 min for Pb^{2+} at a solid-to-liquid ratio of 1.0 g/L, in agreement with both the pseudo-first- and pseudo-second-order reaction kinetics models. The adsorption isotherms of Ca-Ox/C-S-H for both metal ions also fitted the Sips model well. CaOx/C-S-H showed high selectivity toward

Pb^{2+} among various heavy metals and coexisting ions in water, and demonstrated high retention of adsorption capacity after being recycled up to four times

El-Dars *et al* [77] investigated the adsorption of nickel (II) from aqueous solution onto different particle sizes of water-cooled blast furnace slag (WCBFS). The results showed that the Langmuir model better fitted the data obtained for the large-sized particles, while that for the finer-sized particles followed the Freundlich model best. Overall, the process was considered a second-order reaction which involved some degree of intraparticle diffusion.

The BFS was used as an adsorbent material for the removal of Pb^{2+} ions in solution by Chauchabe *et al* [78]. The physicochemical analysis assessed indicated that the BFS is essentially composed of silica, lime, and alumina. Its specific surface area was 275.8 m^2/g and its PZC was around 3.8. The adsorption study indicated that the maximum amount of Pb^{2+} adsorbed under optimum conditions (agitation speed: 150 rpm; pH: 5.4; particle size (Øs): 300 µm, T: 20°C) was 34.26 mg/g after 50 minutes of agitation, and adsorption yield was best for feeble initial concentrations. Langmuir gave the best fit for the adsorption isotherms, and the adsorption kinetics was better characterized by the pseudo-second order kinetic model. The adsorption mechanism study revealed that internal diffusion is not the only mechanism that controls the adsorption process and there is also an external diffusion, which contributes enormously to the transfer of $Pb^{2+}$from solution to adsorbent. Thermodynamic studies indicated that the Pb^{2+}adsorption on the blast furnace slag (BFS) was spontaneous, exothermic, and that the adsorbed Pb^{2+} is more ordered at the surface of the adsorbent.

Lignin

Lignin **(Figure 2.7)** is one of the natural polymers, which is abundantly present in the cell walls of terrestrial plants and acts as a binding agent for various fibrous materials. Lignin treated as a waste product in return poses severe environmental problems; especially their presence in the wastewater produces detrimental effects such as lead to high pH, biochemical oxygen demand (BOD), total suspended solids, dark colour, and toxicity. Based on its structural analysis, studies showed that it has a high molecular weight and surface area of 180 m^2/g, making its three-dimensional polymer structure (which involves different functional groups hydroxyl, methoxyl and phenolic groups) more favourable for the removal of heavy metals from wastewater. It is composed of propyl-phenolic subunits with various functional groups that depend on the source of biomass from which the lignin is extracted. These functional groups

act as active sites for binding pollutant species, such as dyes and Cr^{6+} [79,80]. Lignin materials offer several advantages over synthetic materials due to their biodegradability, carbon neutrality, cost-effectiveness, and their antimicrobial, stabilizing, and antioxidant properties. **Table 2.6** shows the reported finding for the removal of heavy metals using lignin-based adsorbents.

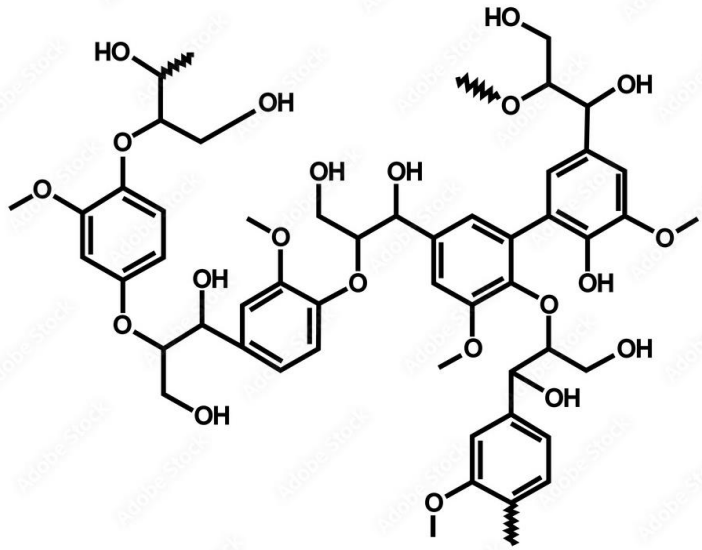

Figure 2.6: Structure of lignin [81]

According to Nair *et al*. [80], lignin, which is a solid waste product of the paper and cellulosic bioethanol industries, was impregnated with chitosan, a biopolymer derived from chitin. The two components were held together by weak bonding between the 1,4-glycosidic linkage, amide, and hydroxyl groups of chitosan and the ether and hydroxyl groups of lignin. The composite with an equal ratio of its two components showed optimal removal of organic dyes and Cr^{6+}. In acidic conditions (pH 5.9), the dye and Cr^{6+} were retained due to the electrostatic/chemical interaction between the constituents' protonated – NH and – OH groups and the carbonyl/sulphate and $HCrO^{4-}$ of the dye and Cr^{6+}, respectively. The authors reported that the protonated hydroxyl groups selectively attracted the $HCrO^{4-}$anion, electrostatically.

Zhou *et al*. [82] reported the development of a 3D nanocomposite of graphene, lignin, and sodium alginate using a hydrothermal method in an aqueous solution for the removal of Cd^{2+} and Pb^{2+}ions. The adsorption capacity of this composite was higher than that of graphene, achieving an optimum uptake capacity of 79.88 and 225.24 mg/g for Cd^{2+} and Pb^{2+}, respectively. Furthermore, the composite demonstrated almost 100% scavenging for both metal

ions in a real sample collected from a local smelter. In contrast, Vecino *et al*. [83] synthesized an alginate-vineyard pruning waste composite using the batch adsorption method to remove various nutrients and micronutrients from winery wastewater. The authors observed that a mixture of 5% sodium alginate and 0.5% vineyard pruning waste with 0.05 M $CaCl_2$ provided the best adsorption results, achieving a removal efficiency of 5.9 mg/g for Mg^{2+} and 0.3 mg/g for Zn^{2+}. More recently, Bustos *et al*. [84] used bio-oxidized grape marc from the winery industry as an adsorbent by encapsulating it with calcium alginate to remove $CuSO_4$. The adsorbent exhibited fast removal, with approximately 97.2% of $CuSO_4$ removed within 5 minutes, and a maximum removal efficiency of 2785 mg/g. The authors also noted that sulphate ions were removed through precipitation as calcium sulphate.

Red mud

The by-product known as red mud is generated during the caustic leaching of bauxite in the alumina industry. It is comprised of Fe_2O_3, Al_2O_3, SiO_2, Na_2O, CaO, trace amounts of Zr, Y, Th, and U elements, as well as rare earth elements. Red mud has a reddish-brown colour and is composed of fine particles of silica, aluminium, iron, calcium, titanium oxides and hydroxides, which gives it high surface reactivity. Due to its unique properties, red mud has been the subject of numerous studies in, including those on the removal of toxic heavy metals from wastewater from aqueous solutions.

Lyu *et al* [85] employed a hydrothermal method for the modification of red mud using colloidal silica and sodium hydroxide under mild conditions and applied it to adsorb Pb^{2+} ions in aqueous solutions. Highlighted two pathways for Pb^{2+} removal from solutions as shown in **Figure 2.8**. Two pathways were highlighted for the removal of b bas shown pathway I: Firstly, Na and Ca ions in the modified red mud dissolve into the solution in the experimental conditions; then as exchange, the Pb ions in the solution adsorb on the surface of the modified red mud and interact with that carbonate to form $PbCO_3$ and $Pb_3(CO_3)_2(OH)_2$. Pathway II: Some carbonate ions are released into the solution when calcite in modified red mud dissolves; then $PbCO_3$ and $Pb_3(CO_3)_2(OH)_2$ precipitates are formed by the liquid phase reaction between Pb ions and CO_3^{2-} ions in the solution. These precipitates are subsequently adsorbed on the surfaces of the modified red mud and grow gradually.

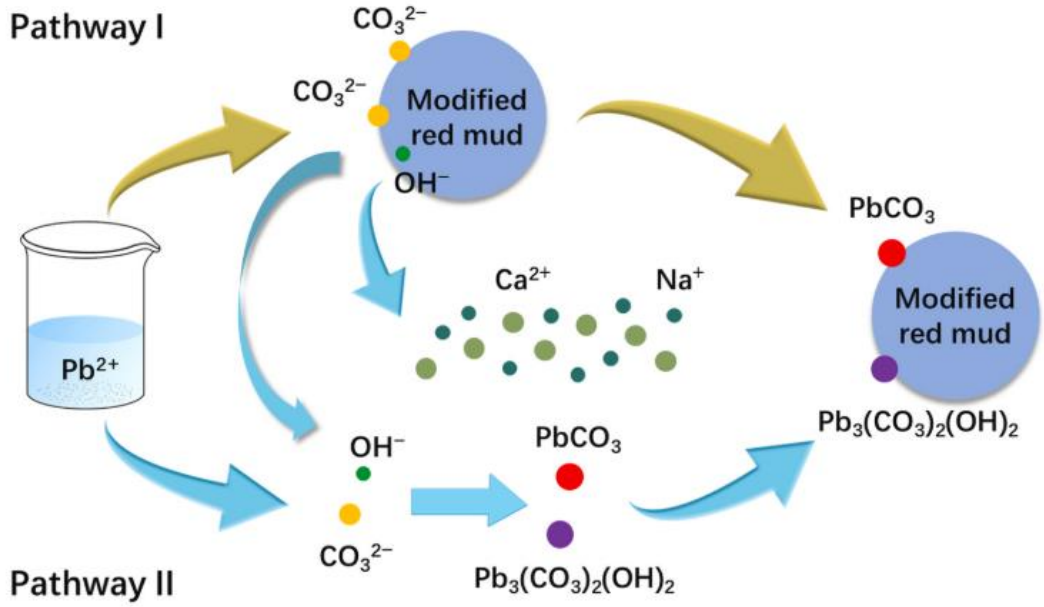

Figure 2.7: Schematic mechanism of the modified red mud to remove Pb^{2+}ions in aqueous solutions [85].

Red mud has been proposed as a potential solution for decontaminating acid mine drainage and mining sites and other contaminated areas that generate acidic leachates and high concentrations of hazardous heavy metal ions. Its physiochemical properties make it a promising precursor material for adsorbent material synthesis. Using red mud to remove lead ions from wastewater could have significant environmental benefits, as it offers a double advantage. However, due to its low adsorption capacity and strength structure, red mud typically requires modification before it can be used as an adsorbent [86]. There are several common methods for modifying materials, including acidification, neutralization, thermal treatment, organic modification, and composite material synthesis [87]. These modifications have been shown to improve adsorption efficiency for heavy metal ions.

The utilization of iron oxide-activated red mud for the elimination of Cd^{2+} was investigated by Khan *et al*. [88] under optimized conditions, including a pH of 6, an interaction time of 1.5 hours at 298 K, and an optimum uptake of 117.64 μg/g. The adsorption process was spontaneous and exhibited pseudo-first-order kinetics with intra- and film diffusion mechanisms. Additionally, the regenerated adsorbent was effective in removing Cd^{2+} for up to five cycles, achieving a recovery of nearly 91% of the Cd^{2+}. Abbasi *et al*. [89] synthesized a red mud/carbon nanotube composite as a sorbent for the removal of Pb^{2+}ions using a chemical vapour disposition method. The resulting composite, with a surface area of 78 m^2/g, demonstrated a higher adsorption capacity than pure red mud (11 m^2/g). The adsorption

capacity was highest for 0.05 g of the composite at pH 5, with equilibrium achieved within 50 minutes. García *et al*. [90] synthesized a ternary hybrid composite of red mud with iron oxide and alginate/chitosan for the removal of As(V). The results showed that the chitosan-immobilized materials exhibited the highest removal of As(V) at 100 mg/g with an adsorbent dose of 2.5 g/L at pH 7. The data was best fit with the Freundlich isotherm and pseudo-second-order kinetics.

In a study conducted by Pietrelli *et al*. [91], the utilization of pyrolusite and red mud was examined for the purpose of removing manganese and arsenic from drinking water. The researchers explored the effects of various factors, such as initial metal ion concentration, pH, temperature, and adsorbent performance, and employed an isotherm model to determine the optimal working conditions. The synergistic impact of red mud and pyrolusite improved the adsorption efficiency and stability, effectively and safely removing the targeted contaminants from water.

In another study by Pepper *et al*. [92], red mud was employed to prepare aganeite sorbent for the treatment of arsenic-contaminated water. The adsorption effect was evaluated using a kinetic model, which revealed that red mud exhibited stronger adsorption capacity and was less affected by pH compared to commercial adsorbents. However, the presence of carbonate and phosphate significantly reduced the adsorption efficiencies of both adsorbents.

Kalkan *et al*. [93] investigated the removal of cadmium from aqueous solutions using bacteria modified. The optimum results were reported at pH 4.0, contact time of 60 min, temperature of 30ºC, and an adsorbent dose of 1 mg/mL. The adsorption data was best fitted with Langmuir and Freundlich adsorption models. The maximum adsorption capacity obtained from Langmuir adsorption model was 83.034 mg/g. The kinetic processes of cadmium adsorption on bacteria-modified red mud were described by applying pseudo-first order and pseudo-second-order rate equations. The kinetic data for the adsorption process obeyed pseudo-second-order rate equations. Various thermodynamic parameters, such as $\Delta G°$, $\Delta H°$, and $\Delta S°$ were calculated and the negative value of $\Delta G°$ obtained indicate that the process was spontaneous, and the positive value of $\Delta H°$ confirms the reaction to be endothermic, and the positive value of $\Delta S°$ shows that the decrease in the degree of freedom of the adsorbed specie.

Luu *et al*. [94] investigated red mud modified by chitosan (RM/CS) as an adsorbent to effectively remove $Pb^{2+}$from aqueous solution. The surface area of RM/CS was found to

significantly increase by more than 50% compared to that of original red mud. They reported Pb^{2+} removal followed the intra-diffusion model. Additionally, the non-zero C value obtained from this model indicated that the removal was controlled by many different mechanisms. They also found that the interaction of Pb^{2+} and carbonate group on the material's surface played a primary role once the adsorption equilibrium was reached. The maximum adsorptive capacity was found to be about 209 mg/g.

Mi *et al.* [95] investigated removal of heavy metal ions by activating RM using Ca^{2+} and Mg^{2+} mixed solution neutralization and high-temperature treatment. Pb^{2+} and Zn^{2+} were selected as target contaminants. They used Fractional Factorial Design and Box-Behnken design to screen the significant preparation parameters and obtain the optimum preparation conditions. They determined as significant factors affecting the adsorption capacity of Pb^{2+} and Zn^{2+}, and the equilibrium optimum preparation parameters were the solution concentration of 1.5 mol/L, the liquid-solid ratio of 40 ml/g, the neutralization time of 114 min, calcination temperature of 518 °C, and the calcination time of 148 min. The physiochemical results revealed that the main mineral phase of NCRM was hematite, calcite, and cancrinite, and NCRM had a loose structure and abundant pores, which contributes to the sorption of heavy metal ions. The adsorption kinetics study was found to be via pseudo-first-order model and pseudo-second-order model, while pseudo- second-order model was the best model to describe adsorption of Zn^{2+} onto NCRM. Based on the batch experiment, the maximum adsorption capacities of Pb^{2+} and Zn^{2+} were 218.82 and 75.58 mg/g, respectively.

Sahu *et al*. [96] activated red mud by acid dilution followed by ammonia precipitation for adsorption of Cd^{2+}. The maximum adsorption capacities of Cd^{2+} on activated red mud (ARM) were found to be 12.046 and 12.548 mg/g at temperature 20 and 28 ˚C, respectively. Adsorption data of Cd^{2+} are best fitted to linearly transformed Langmuir isotherm with $R^2 > 0.99$. The pseudo-second-order model describes the kinetics of Cd^{2+} adsorption successfully to predict the rate constant of adsorption. Thermodynamic parameters revealed the endothermic, spontaneous and feasible nature of adsorption of Cd^{2+} onto ARM. The desorption efficiency of Cd^{2+} ions from ARM was 91.29% using 0.2 mol/L HCl.

Deihimi *et al*. [97] also utilized red mud to remove iron cyanide from water, and their experiment demonstrated that various pretreatment methods significantly improved the adsorption capacity of red mud. The researchers found that cetyltrimethylammonium bromide enhanced the ability of red mud to adsorb ferricyanide by altering the charge properties of the

red mud surface. Deihimi *et al.* [98] investigated the removal of ferricyanide anions from aqueous solutions using activated red mud as a ferricyanide adsorbent. They investigated the influence of various factors, including ferricyanide concentration, pH, adsorbent dosage, contact time, and adsorption process, on the removal of ferricyanide from aqueous solutions. The results of their study showed that the optimal conditions for adsorption were a ferricyanide concentration of 60 mg/L, a solution pH of 5.6, an adsorbent dosage of 2.59 g, and a contact time of 60 minutes, which resulted in a removal rate of 79.6% and 1.8 mg of ferricyanide adsorbed per gram of adsorbent. The activation process was found to enhance the capacity and efficiency of red mud adsorption of ferricyanide. The study demonstrated the potential of using red mud for water treatment, which embodies the principle of "using waste to treat waste." However, it is also crucial to consider the disposal of red mud if it is not utilized effectively as an adsorbent.

Petroleum coke

Petroleum coke (PC), a by-product from petrochemical industry, is a potential substance to replace activated carbon. PC is a by-product of the heavy oil or oil sand refining process. The composition of raw PC from different sources is slightly different, and the carbon content is the main content, accounting for more than 80% of the total elements. According to the difference of sulphur content in PC, it can be classified into high-sulphur (greater than 4%), medium-sulphur (2 - 4%) and low-sulphur (<2%) PC. Medium-sulphur and low-sulphur PC can be used in the aluminium and steel industries, where the sulphur content is required <3% and 0.5%, respectively. Since sulphur content of high-sulphur PC is greater than 4%, it cannot meet the requirement of some relevant industries.

Yuan *et al.* [99] synthesized a PCK3-450 adsorbent from PC for the removal of Cu^{2+} ion from aqueous solutions. A maximum Cu^{2+} ion adsorption capacity of 89.85 mg/g was attained at 30 °C using PCK3-450. Adsorption isotherms were analysed using the Langmuir, Freundlich, and Temkin models, and the experimental data fit well with the Freundlich model. Pseudo first-order, pseudo second-order, Elovich, and intra-particle diffusion models were used to describe the adsorption kinetics, and the rate of adsorption conformed to the pseudo second-order kinetic model.

The efficacy of metal-impregnated petroleum coke activated carbon for the adsorption of arsenite and arsenate in acidic waters was investigated by Fisher and Vreugdenhil [100].

Petroleum coke was modified with $FeCl_3$−$KMnO^{4-}$ to enhance the adsorption capacity for arsenate. Adsorption was significantly improved by the addition of an iron−manganese-loaded activated carbon, increasing adsorption from 8.12 to 50.93%. Ramírez Zamora [101] assessed the use of petroleum coke produced activated carbon for the adsorption of metal and phenol in water. The result present showed a clear increase in the adsorption capacity for Hg and methylene blue of the activated coke, especially when phosphoric acid is used. The also highlighted that for chemical process of activation still must be optimised to commercialise the product for its application in water.

Table 2.6: Absorbents reported for the removal of heavy metals from different water matrices.

Industrial waste material	Adsorbents	Heavy metals	Aquatic environment	Optimum condition				Adsorption capacity (mg/g)	Percentage removal (%)	Adsorption isotherm	Adsorption mechanism	Regeneration	Detection technique	Ref
				pH	Temperature (˚C)	Contact time (min)	Initial concentration (mg/L)							
Coal fly ash	MCFA	Mn^{2+}	Not reported	Not reported	Not reported	Not reported	Not reported	558.92	94.26	Physisorption	Freundlich	Not reported	Abs meter	[55]
		Cu^{2+}						0.434	95.88					
		Ni^{2+}						210.97	71.04					
		Pb^{2+}						12.16	99.91					
	CFA-ZA	Hg^{2+}	Not report	2.5	25	120	10	Not reported	94	Physisorption	Freundlich	Not reported	ICP -AES	[56]
	Na – X	Zn^{2+}	Not reported	5	Not reported	10	Not reported	656	Not reported	physisorption	Langmuir	Not reported	ICP – OES	[102]
		Pb^{2+}		5		120	Not reported							
	Na – X(C)	Zn^{2+}	Not reported	5	Not reported	10	Not reported	600	Not reported	physisorption	Langmuir	Not reported	ICP – OES	[102]
		Pb^{2+}		5		120								
	CFAPG	Zn^{2+}	Not reported	6	21±1	48	Not reported	13.42	Not reported		Bi -Langmuir	Not reported	AAS	[57]
	Fly ash	Pb^{2+}	Not reported	5	25±2	45	20–100	- 250	92–94	Not reported	Freundlich	Not reported	AAS	[58]
		Ni^{2+}		5		40	40 to 200	21.75	54–78.8		Temkin			
		Cr^{3+}		3 – 4		45	50 – 250	-83.3	35		Temkin			
	Coal fly ash	Pb^{2+}	Not report	5.04	Not reported	270	Not reported	99.082	99	Chemisorption	Langmuir	Not reported	ICP – MS	[59]
	NMFA	Cd^{2+}	Not reported	4 – 7	25	120	100	204.92	Not reported	Chemisorption	Langmuir	Not	AAS	[60]
	FA48	Pb^{2+}	Not reported	3	25	24 hours	50	55.53	Not reported	Chemisorption	Langmuir	Not reported	ICAP	[61]
	Z8	Cu^{2+}	wastewater	5	Not reported	120	Not reported	23.8	97	Physisorption	Not reported	Not reported	AAS	[62]
		Ni^{2+}		6	Not reported	40	Not reported	303	98					
		Pb^{2+}		9	Not reported	20	Not reported	1111	80-98					
	ZFA	Cd^{2+}	Not reported	5	25	7 hours	50	26.246	96	Chemisorption	Langmuir	Not reported	Not reported	[63]
	CFA – SH	Hg^{2+}	Not reported	8	25	50	Not reported	361.01	Not reported	Chemisorption	Langmuir	4	AAS	[103]
		Cd^{2+}		8		60		106.38						
	13 - X	Cd^{2+}	Not reported	7	30	120	250	321.54	99.65	Lagergren – chemisorption	Langmuir	Not reported	ICP – OES	[104]
	ANA-AC	Pb^{2+}	Not reported	5.4 - 6	25	360	100	125.57	100	Chemisorption	Langmuir	Not reported		[105]
Lignin	$MCCRM_2$	Cu^{2+}	Not reported	6	25	24 hours	Not reported	0.144mmol/g		Chemisorption	Langmuir	Not reported	AAS	[106]
		Pb^{2+}		5.3				0.161 mmol/g	Not reported					
	PAN/SL ACNFs	Pb^{2+}	Not reported	5		240	125	524	67	Chemisorption	Langmuir	Not reported	ICP – OES	[107]
	ECLNNPs	Pb^{2+}	Not reported	6	30	180	100	126	Not reported	Chemisorption	Langmuir	3	Not reported	[108]
		Cu^{2+}		5.5				54.4						
	SSAL	Pb^{2+}		5.35	45	12 hours	200	39.3	Not reported	Chemisorption	Langmuir	Not reported	Not reported	[109]
Petroleum coke	PCK3-450	Cu^{2+}	Not reported	5.24	30	120	100	89.85	Not reported	Chemisorption	Freundlich	Not reported		[99]

Industrial waste material	Adsorbents	Heavy metals	Aquatic environment	Optimum condition				Adsorption capacity (mg/g)	Percentage removal (%)	Adsorption isotherm	Adsorption mechanism	Regeneration	Detection technique	Ref
				pH	Temperature (˚C)	Contact time (min)	Initial concentration (mg/L)							
	BFS	Co^{2+}	Not reported	6	65	60		43.8	Not reported	Intra-particle diffusion		3	AAS	[70]
		Pb^{2+}		6	65	60	3.3e+6	30.8	Not reported	Avrami	Freundlich	3		
	WBFS	Cu^{2+}	Not reported	7	25 – 65 .	Not reported		21.32	Not reported	Chemisorption	Langmuir	Not reported	AAS	[74]
		Cd^{2+}		7	25 – 65			13.36						
		$Zn2^{+}$		7	25 – 65			14.86						
	S – nZVi@BFS	Cr^{6+}	Not reported	3.5	25	Not reported	10	184	Not reported	Chemisorption	Not reported	Not reported	ICP – OES	[71]
Blast furnace slag	BFS	Cr^{3+}	Not reported	4.8	20	60	Not reported	43.16	Not reported	Chemisorption	Langmuir	Not reported	AAS	[75]
		Pb^{2+}				50		50.12						
		Cr – Pb				80		39.91						
	Modified slag	Pb^{2+}	Not reported	7	60	120	40	96.46	64.32	Chemisorption	Langmuir	Not reported	AAS	[73]
	BFS-derived Ca – Ox/C – S – H	Pb^{2+}	Not reported			10		2117		Chemisorption	Sips	Not reported	AAS & ICP – OES	[76]
		Cd^{2+}						1083						
	WCBFS	Ni^{2+}	Not reported	2	24.5	30	100	12.66 &24.39	Not reported	chemisorption	Langmuir	Not reported	Uv – Vis	[77]
	SlagCS	Cu^{2+}	Not reported											
	BFS	Pb^{2+}	Not reported	5.4	20	50	60	34.26	87.93	Chemisorption	Langmuir	Not reported	AAS	[78]
	Fe^{0}/FeS_{x}@BFS	Cr^{6+}	Not reported	3.5.	60	20	Not reported	38	Not reported	Not reported	Not reported			
	Mn-RM	Pb^{2+}	Not reported	5.21	25	240	301.04	721.35	87.45	Chemisorption	Langmuir	Not reported	AAS	[110]
	Magnetic – 4A Zeolite	Zn^{2+}	Not reported	4	25±0.5	24 hours	100	331.4	Not reported	Chemisorption	Langmuir	Not reported	ICP – MS	[111]
		Cu^{2+}						136.3						
		Cd^{2+}						131.96						
		Ni^{2+}						119.70						
		Pb^{2+}						116.81						
	Red mud	Mn^{2+}	Drinking water	7	25	10 hours	2	Not reported	50	Not reported	Langmuir	Not reported	ICP – MS	[112]
Red mud		As^{3+}				5	1000		97					
	Bacteria-Modified Red Mud	Cd^{2+}	Not reported	4	30	60	Not reported	83.034	Not reported	Chemisorption	Langmuir	Not reported	Spectrophotometer	[93]
	RM/CM	Pb^{2+}	Not reported	5.5	25	180	500	208.02	Not reported	Intra-particle diffusion	Not reported	Not reported	AAS	[94]
	NCRM	Pb^{2+}	Not reported	4	25	240	200	218.82	Not reported	Chemisorption	Not reported	Not reported	ICP – OES	[95]
		Zn^{2+}					100	75.58						
	ARD	Cd^{2+}	Not reported	6	19 & 30	120	10	12.04 & 12.548	Not reported	Chemisorption	Langmuir	Not reported	AAS	[96]
	Red mud	Mn^{2+}	Not reported	6	28		5 – 95	56.81	Not reported	Chemisorption	Freundlich	Not reported	AAS	[113]

2.4. Factors affecting adsorption removal of heavy metals and antiretrovirals

The adsorption of heavy metals and antiretrovirals is influenced by different factors such as adsorbent particle size, solution pH, ionic strength, initial solution concentration, and contact time.

2.4.1. Adsorbent particle size

Studies on intra-particle diffusion reveal that the adsorption rate is significantly influenced by the waste materials' particle size [114]. Reduced particle size would result in increased surface area, which would raise the possibility of adsorption of the waste materials outside the surface. In addition to adsorption occurring at the waste material's exterior, intra-particle diffusion from the surface into the material's pores is also a possibility. For big particles, the diffusional barrier to mass transfer is larger. Most of the particle's interior surface may not be used for adsorption due to a variety of circumstances, including contact duration, blockage of some diffusional channel, mass transfer resistance or diffusional path length. As a result, the adsorption efficiency might drop [115,116].

2.4.2. Solution pH

For different types of industrial wastes adsorbent materials, the adsorption of metal ions and ARVs is significantly impacted by the pH of the solution [117]. Most metal ion and ARV compounds adsorption in a given pH range increases with pH up to a particular maximum threshold value and then decreases with an additional pH increase. Consequently, every metal ion and ARV has a preferred pH range within which to adsorb on a particular industrial waste material. The adsorbent's pHzpc, or the pH at which it is neutral, can also be used to explain the pH effect. When the medium pH is below the pHzpc value, the adsorbent's surface charge is positive; when the pH is higher than the pHzpc, it is negative.

Luu *et al*. [118] demonstrated that the Pb^{2+} removal increased with rising pH from 2 to 5.5, with the highest absorption occurring at 5.5. This is because when pH is low (below 5.5), the charge of the material surface is changed from positive to negative. Thus, the adsorption of cation Pb^{2+} is favoured. Additionally, at the low pH, more H^+ ions can exist, and more active adsorption sites are taken up, leading to the decrease in the uptake of Pb^{2+} as shown in Figure 2.9.

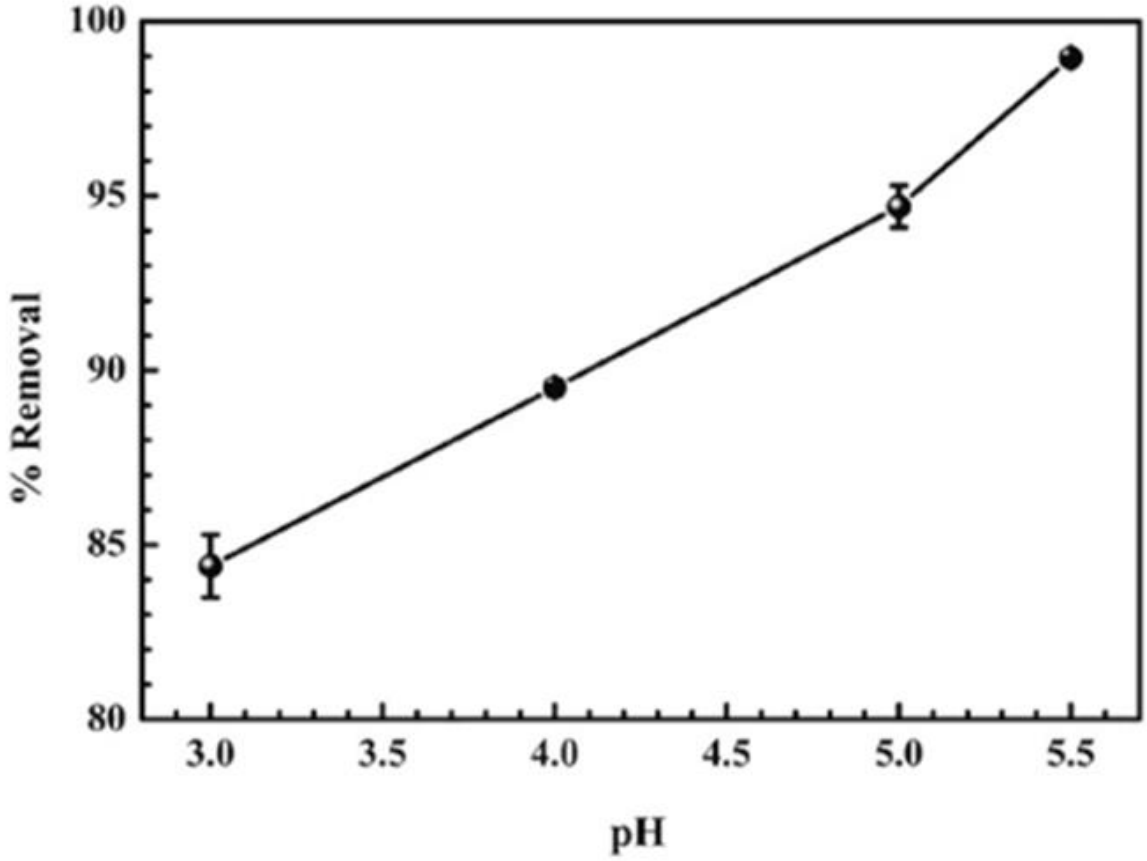

Figure 2.8: Effect of pH on the percentage removal of Pb^{2+} from aqueous using red mud modified by chitosan [118].

2.4.3. Ionic strength

Ionic strength is a general property of the solution affecting the affinity between the solute and the aqueous phase. This is among the significant variables affecting the equilibrium of the aqueous phase. Adsorption typically decreases as the aqueous solution's ionic strength rises. Surface chemistry hypothesis states that because of electrostatic interaction, two phases such as waste particles and metal species in an aqueous solution that come into contact will always be encircled by an electrical double layer [31]. Adsorption reduces with increasing ionic strength if electrostatic attraction plays a major role in the adsorption process. Certain inorganic anions, like chloride, can form complexes with certain metal ions, which might impact the adsorption process.

2.4.4. Contact time

Effect of contact time is investigated to find out how long it takes for the adsorption process to reach equilibrium. Wang *et al*. [119] performed kinetic studies to investigate the effect of contact time on Cu^{2+}, Cd^{2+}, and Zn^{2+}. **Figure 2.10** shows that the adsorption amount of Cu^{2+}, Cd^{2+}, and Zn^{2+} on WBFS reached a relatively high level within 20 min, and then slowly increased until it reached an equilibrium concentration. The adsorption process progression is certainly generated by the presence of vacant adsorption sites and by the presence of negative charges on the surface of the adsorbent. The total stop of the adsorption process reveals that the free adsorption sites are saturated.

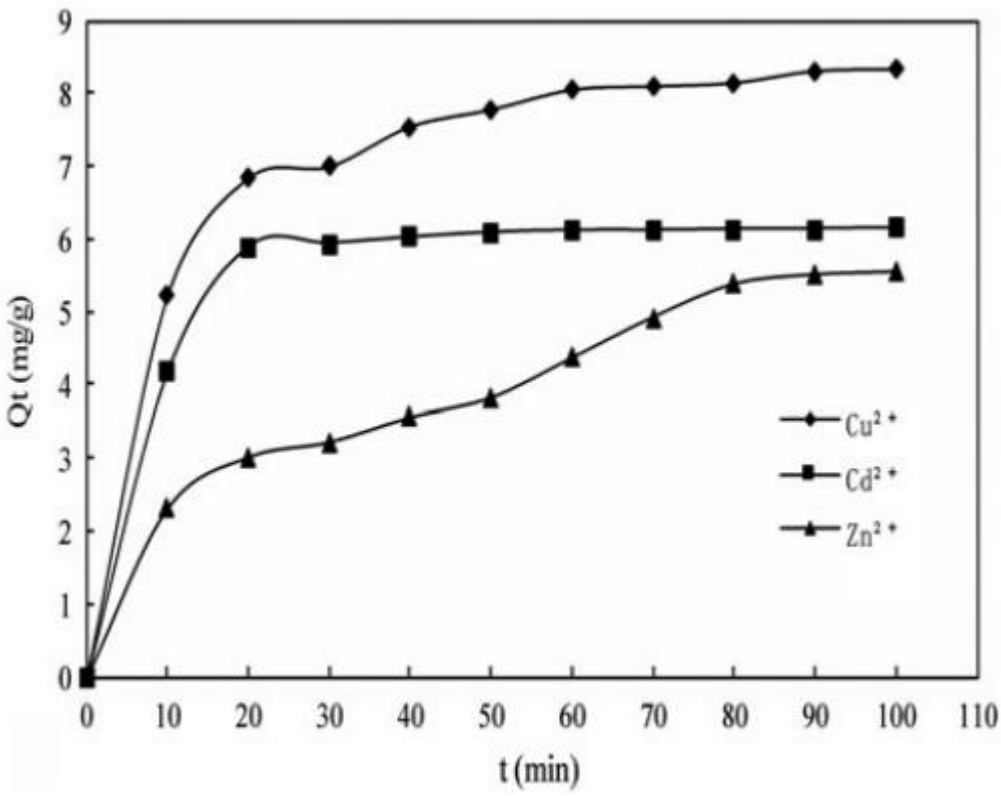

Figure 2.9: Adsorption kinetic curves of Cu^{2+}, Cd^{2+}, and Zn^{2+} onto WBFS [119].

2.4.5. Initial concentration

The adsorption capacity of different industrial waste materials is strongly influenced by the initial concentrations of metal ions and ARV compounds. Adsorption capacity generally increased as the heavy metals' and ARV's initial concentrations increased. When the initial

metal ion concentration becomes high, the removal efficiency decreases because the available active sites for adsorption becomes less demonstrated by Verma *et al* [120].

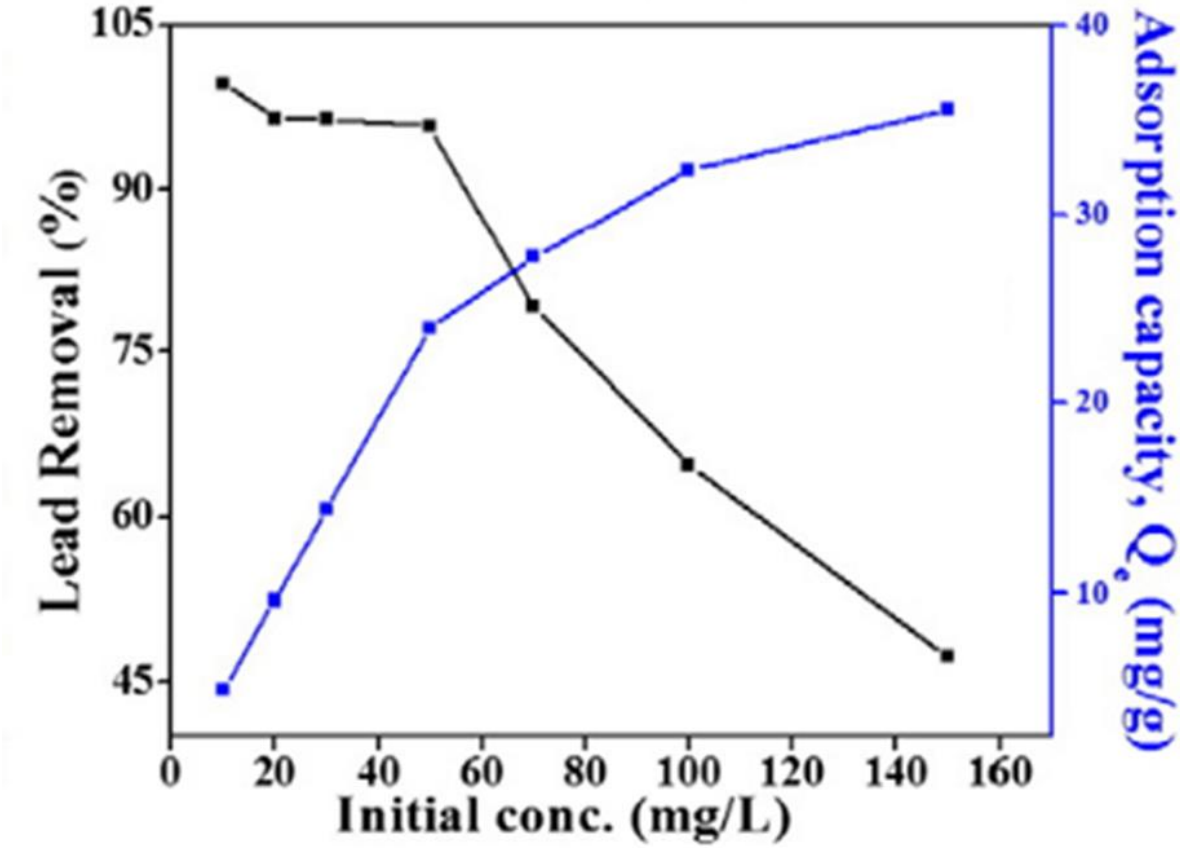

Figure 2.10: Effect of initial metal ion concentration on Pb^{2+} ions removal [120]

2.5. Summary of studies reported from 2013 to 2023 on adsorptive removal of heavy metals from aqueous solution.

The studies conducted depicted in **Figure 2.11**, demonstrated a considerable focus on the use of industrial waste materials, including coal fly ash, lignin, blast furnace slag, red mud, and petroleum coke, for the elimination of heavy metals in water. **Figure 2.11** revealed that lead (Pb^{2+}) has been the most extensively studied heavy metal for all these materials. Additionally, coal fly ash emerges as the most extensively studied material for all heavy metals, excluding arsenic (As^{3+}). This observation highlights the need for further research to explore the potential applications of other industrial waste materials, such as petroleum coke, for the removal of other heavy metals.

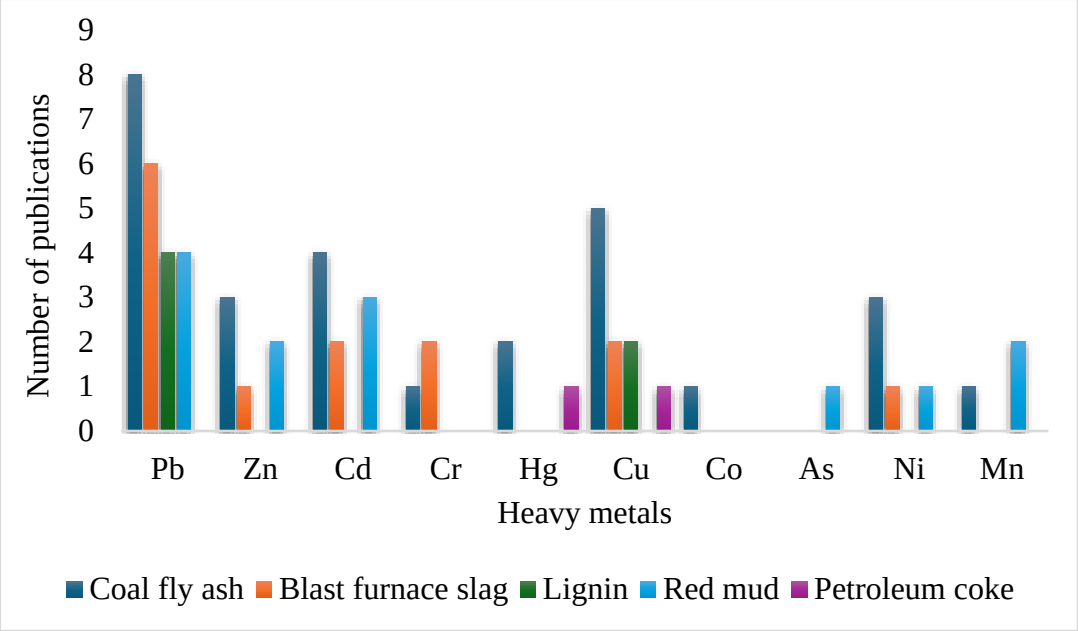

Figure 2.11: Number of publications reviewed for different heavy metals assessed from 2013 – 2023 using industrial waste-based adsorbents.

The **Figure 2.12** demonstrates the number of publications that have explored the potential of industrial waste in the removal of heavy metals between the years 2013 and 2023. The findings suggest that additional efforts are required, as the number of publications within this time frame is rather limited. Specifically, only 23 accessible publications were identified during this period, with research focusing on coal fly ash contributing to a high of >2 in certain years compared to other materials. In 2019, 2021 and 2023 more work were reported related to blast furnace slag, lignin and coal fly ash.

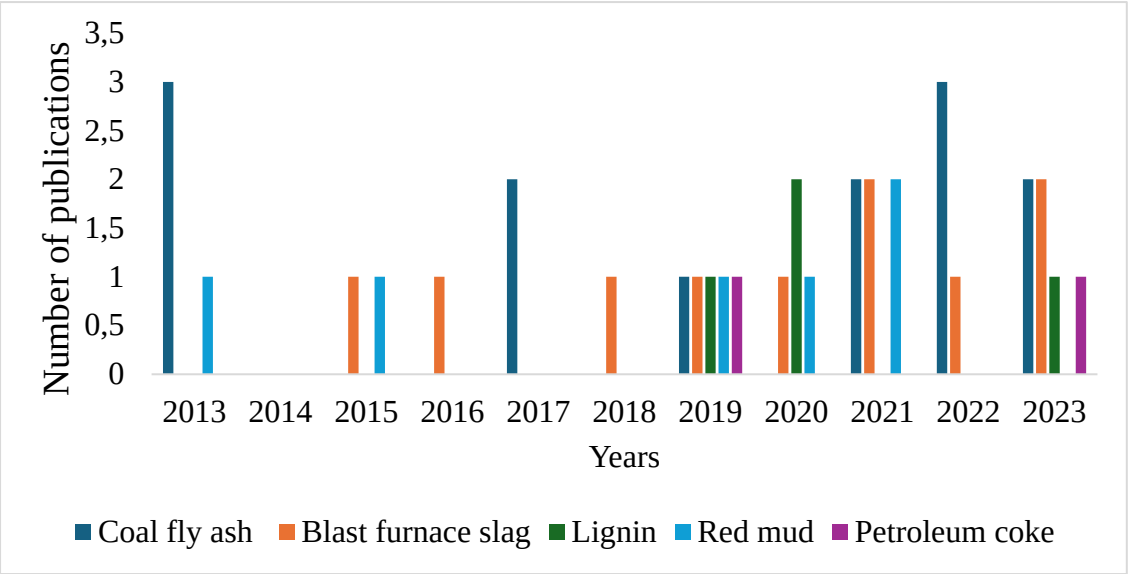

Figure 2.12: Number of publications between 2013 and 2023 on different waste material used for the removal of heavy metals from water.

Figure 2.13 depicts the various adsorption isotherms mechanisms that have been reported in the literature for the removal of heavy metals from water using industrial waste materials. Among these, the Langmuir isotherm was found to be the most reported, suggesting that the industrial waste material adsorbs onto the surface in a monolayer. The Freundlich isotherm was also observed, indicating the possibility of adsorption in multiple layers of the adsorbent.

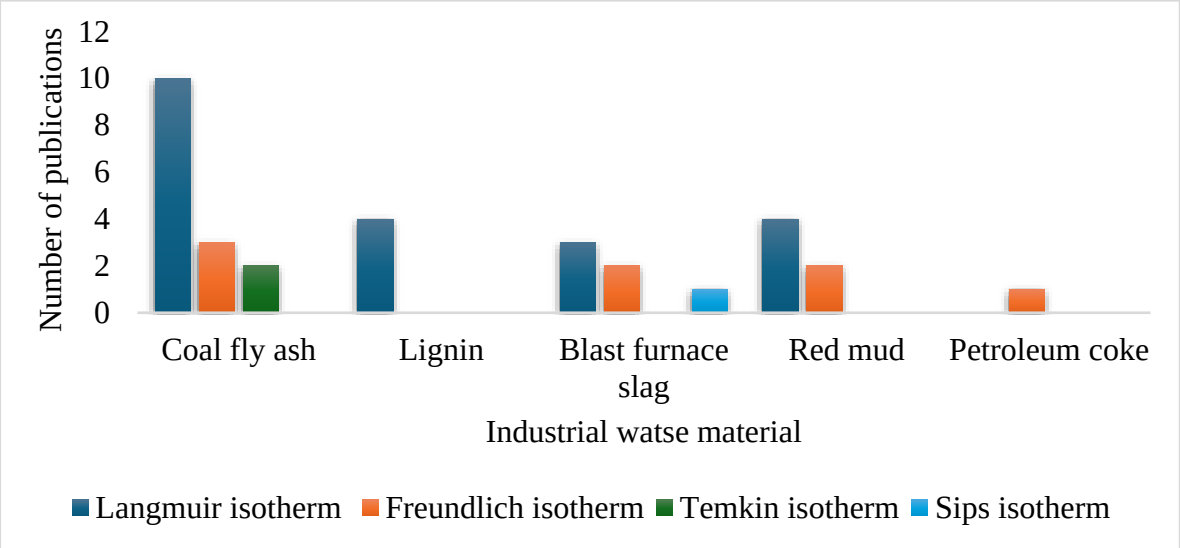

Figure 2.13: Reported adsorption isotherms related to different industrial waste material on removal of heavy metals from aqueous solution.

Figure 2.14 demonstrates the number of publications that have reported the various types of adsorption mechanisms involved in the adsorptive removal of heavy metals from industrial waste materials. It is evident from the figure that chemisorption is the most frequently reported mechanism for all industrial waste materials. Heavy metals bind to the active sites on the adsorbent surface, such as Al_2O_3, SiO_2, Fe_2O_4, etc., which possess a negative charge. This allows for chemisorption to occur, which is a monolayered phenomenon.

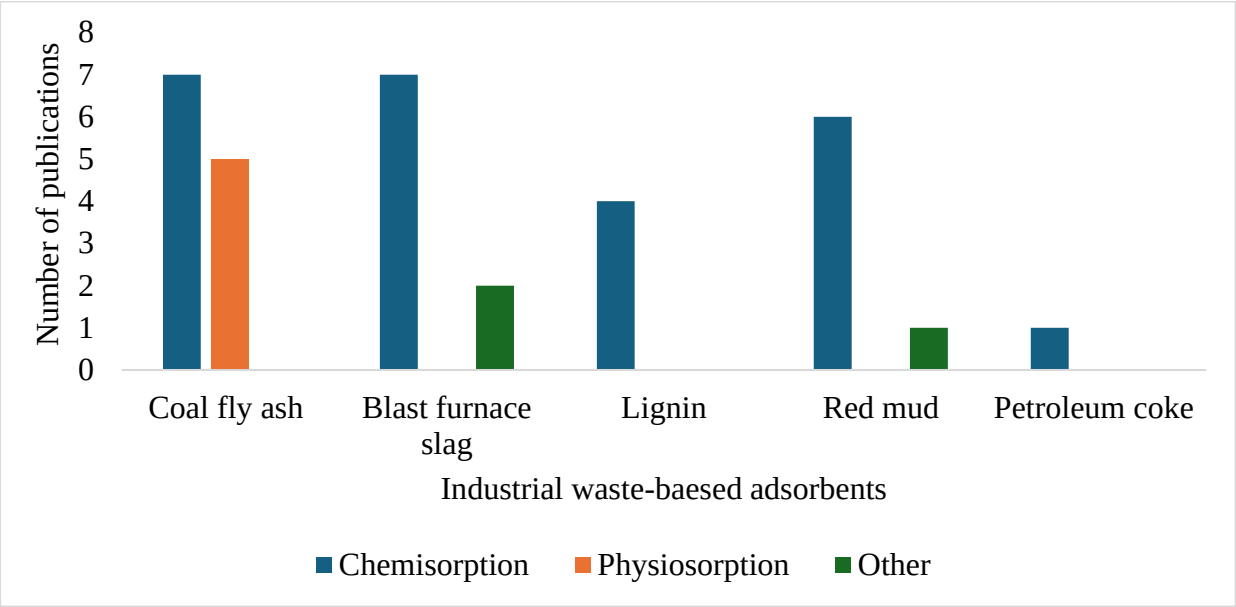

Figure 2.14: Number of publications that reported the mechanisms involved in the adsorptive removal of heavy metals using industrial waste materials.

The studies complied from 2013 until present. The data shows analytical techniques that have been adopted for the analysis of these heavy metal in aqueous solution over the years. the extensive studies have been shown in **Table 2.8**. **Figure 2.15** below have shown that the AAS method have been more preferred over the others analytical techniques, because most of the studies were analysing or investigating single elemental metrices. The ICP-OES technique has been the second most preferred method. ICP-OES allows simultaneous analysis of multiple elements, thus providing a more efficient workflow and saving valuable time and resources. ICP-MS was also preferred after ICP-OES because ICP-MS is useful for analysing samples with low regulatory limits.

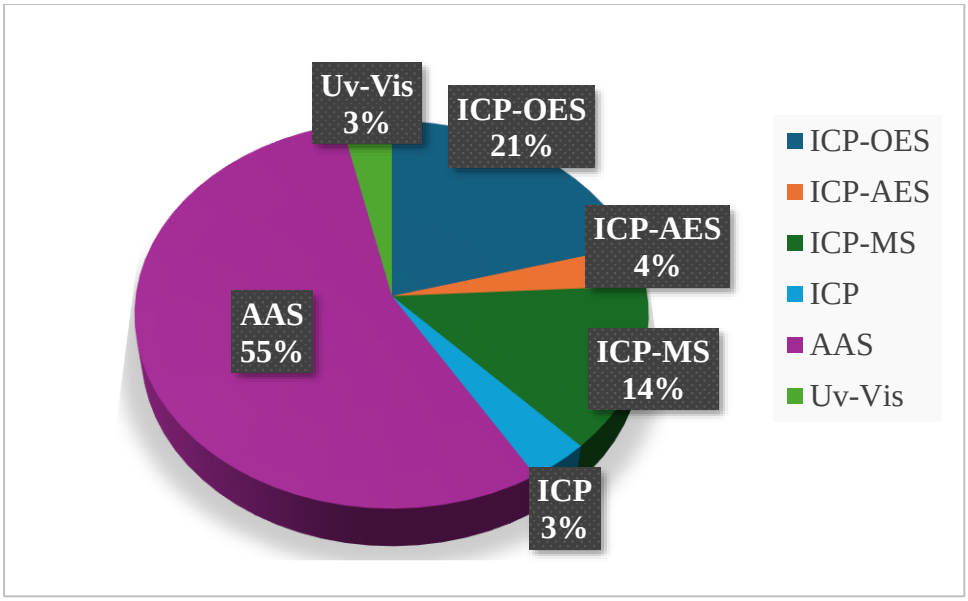

Figure 2.15: Reported analytical techniques for analysis of heavy metals.

2.6. Conclusion

Aquatic environments contain both antiretrovirals and heavy metals, which are not fully metabolizable by either human or animal digestive systems. The unmetabolized remnants of these substances, originating from sources such as hospital effluents, wastewater treatment plants, industrial activities, agricultural activities, and domestic/residential wastewater, pose significant threats to both human and environmental health. In this review, the industrial materials and methods for treating antiretroviral and heavy metal contaminants in aqueous solutions has been discussed. We also examine the industrial waste-based adsorbents, such as coal fly ash, blast furnace slag, lignin, red mud, petroleum coke, and other materials, which have been investigated for their high adsorption capacity and potential for removing antiretrovirals and heavy metals from aqueous solutions.

REFERENCE

[1] T.P. Wood, A.E. Basson, C. Duvenage, E.R. Rohwer, The chlorination behaviour and environmental fate of the antiretroviral drug nevirapine in South African surface water, (2016) 349–360. https://doi.org/10.1016/J.WATRES.2016.08.038.

[2] F.C. Moreira, J. Soler, M.F. Alpendurada, R.A.R. Boaventura, E. Brillas, V.J.P. Vilar, Tertiary treatment of a municipal wastewater toward pharmaceuticals removal by chemical and electrochemical advanced oxidation processes, (2016) 251–263. https://doi.org/10.1016/J.WATRES.2016.08.036.

[3] A.B. Zitha, S. Ncube, N. Mketo, H. Nyoni, L.M. Madikizela, Antiretroviral Drugs in Water: An African Challenge with Kenya and South Africa as Hotspots and Plausible Remediation Strategies, (2022) 1237–1253. https://doi.org/10.1007/s42250-022-00417-1.

[4] O.A. Abafe, J. Späth, J. Fick, S. Jansson, C. Buckley, A. Stark, B. Pietruschka, B.S. Martincigh, LC-MS/MS determination of antiretroviral drugs in influents and effluents from wastewater treatment plants in KwaZulu-Natal, South Africa, (2018) 660–670. https://doi.org/10.1016/j.chemosphere.2018.02.105.

[5] R.F. Waris, I.H. Farooqi, Different advanced oxidation processes for the abatement of pharmaceutical compounds, International Journal of Environmental Science and (2023) 2325–2338. https://doi.org/10.1007/s13762-023-05127-w.

[6] A.B. Zitha, S. Ncube, N. Mketo, H. Nyoni, L.M. Madikizela, Antiretroviral Drugs in Water: An African Challenge with Kenya and South Africa as Hotspots and Plausible Remediation Strategies, (2022) 1237–1253. https://doi.org/10.1007/s42250-022-00417-1.

[7] L.M. Madikizela, S. Ncube, L. Chimuka, Analysis, occurrence and removal of pharmaceuticals in African water resources: A current status, (2020) 109741. https://doi.org/10.1016/j.jenvman.2019.109741.

[8] O.A. Abafe, J. Späth, J. Fick, S. Jansson, C. Buckley, A. Stark, B. Pietruschka, B.S. Martincigh, LC-MS/MS determination of antiretroviral drugs in influents and effluents from wastewater treatment plants in KwaZulu-Natal, South Africa, (2018) 660–670. https://doi.org/10.1016/j.chemosphere.2018.02.105.

[9] T.T. Mosekiemang, M.A. Stander, A. de Villiers, Simultaneous quantification of commonly prescribed antiretroviral drugs and their selected metabolites in aqueous environmental samples by direct injection and solid phase extraction liquid chromatography - tandem mass spectrometry, (2019) 983–992. https://doi.org/10.1016/j.chemosphere.2018.12.205.

[10] S.P. Mahlambi, P.N. Mahlambi, L.M. Madikizela, Synthesis and application of a molecularly imprinted polymer in selective solid-phase extraction of efavirenz from water, (2019) 356–365. https://doi.org/10.2166/wst.2019.054.

[11] C. Rimayi, D. Odusanya, J.M. Weiss, J. de Boer, L. Chimuka, Contaminants of emerging concern in the Hartbeespoort Dam catchment and the uMngeni River estuary 2016 pollution incident, South Africa, (2018) 1008–1017. https://doi.org/10.1016/j.scitotenv.2018.01.263.

[12] C. Schoeman, M. Dlamini, O.J. Okonkwo, The impact of a Wastewater Treatment Works in Southern Gauteng, South Africa on efavirenz and nevirapine discharges into the aquatic environment, (2017) 95–106. https://doi.org/10.1016/j.emcon.2017.09.001.

[13] T.S. Anirudhan, C.D. Bringle, P.G. Radhakrishnan, Heavy metal interactions with phosphatic clay: Kinetic and equilibrium studies, (2012) 149–157. https://doi.org/10.1016/J.CEJ.2012.06.024.

[14] M.K. Abd Elnabi, N.E. Elkaliny, M.M. Elyazied, S.H. Azab, S.A. Elkhalifa, S. Elmasry, M.S. Mouhamed, E.M. Shalamesh, N.A. Alhorieny, A.E. Abd Elaty, I.M. Elgendy, A.E. Etman, K.E. Saad, K. Tsigkou, S.S. Ali, M. Kornaros, Y.A.G. Mahmoud, Toxicity of Heavy Metals and Recent Advances in Their Removal: A Review, (2023). https://doi.org/10.3390/toxics11070580.

[15] M. Ahmaruzzaman, Industrial wastes as low-cost potential adsorbents for the treatment of wastewater laden with heavy metals, (2011) 36–59. https://doi.org/10.1016/j.cis.2011.04.005.

[16] L.M. Madikizela, S. Ncube, L. Chimuka, Analysis, occurrence and removal of pharmaceuticals in African water resources: A current status, (2020) 109741. https://doi.org/10.1016/j.jenvman.2019.109741.

[17] A. Awwad, N. Salem, M. Amer, M. Shammout, Adsorptive removal of Pb (II) and Cd (II) ions from aqueous solution onto modified Hiswa iron-kaolin clay: Equilibrium and thermodynamic aspects, (2021) 139–144.

[18] P. Rajasulochana, V. Preethy, Comparison on efficiency of various techniques in treatment of waste and sewage water – A comprehensive review, (2016) 175–184. https://doi.org/10.1016/j.reffit.2016.09.004.

[19] A.O. Adeola, J. de Lange, P.B.C. Forbes, Adsorption of antiretroviral drugs, efavirenz and nevirapine from aqueous solution by graphene wool: Kinetic, equilibrium, thermodynamic and computational studies, (2021) 100157. https://doi.org/10.1016/j.apsadv.2021.100157.

[20] M. Ahmaruzzaman, Industrial wastes as low-cost potential adsorbents for the treatment of wastewater laden with heavy metals, (2011) 36–59. https://doi.org/10.1016/j.cis.2011.04.005.

[21] A.H. Mhemeed, A General Overview on the Adsorption *Address for Correspondence, Indian Journal of Natural Sciences Www.Tnsroindia.Org.in ©IJONS 9 (2018) 16127–16131. www.tnsroindia.org.in.

[22] A. Kaushal, Adsorption Phenomenon and its Application in Removal of Lead from Waste Water: A Review, (2017) 1–11. https://doi.org/10.15406/ijh.2017.01.00008.

[23] S. Michael Abegunde, K. Solomon Idowu, O. Morayo Adejuwon, T. Adeyemi-Adejolu, A review on the influence of chemical modification on the performance of adsorbents, Resources, Environment and (2020) 100001. https://doi.org/10.1016/j.resenv.2020.100001.

[24] 5 Difference Between Chemisorption And Physisorption, Types, Important Topics | PW, (n.d.). https://www.pw.live/exams/jee/difference-between-chemisorption-and-physisorption/ (accessed February 15, 2024).

[25] S. Afroze, T.K. Sen, A Review on Heavy Metal Ions and Dye Adsorption from Water by Agricultural Solid Waste Adsorbents, (2018) 1–50. https://doi.org/10.1007/S11270-018-3869-Z.

[26] X. Wang, A. Hussain, H. Zhu, Y. Li, X. Wang, D. Li, Simultaneous Adsorption of Multi-Heavy Metal Ions from Wastewater via Grafted Phosphate Functionality on Polyvinyl Alcohol, (2023) 1–17. https://doi.org/10.1007/S11270-023-06666-1/METRICS.

[27] X.L. Sun, Y. Wang, H.Q. Xiong, F. Wu, T.X. Lv, Y.C. Fang, H. Xiang, The Role of Surface Functional Groups of Iron Oxide, Organic Matter, and Clay Mineral Complexes in Sediments on the Adsorption of Copper Ions, (2023) 6711. https://doi.org/10.3390/SU15086711.

[28] H. Zeng, Y. Su, X. Gong, L. Zheng, L. Zhang, P. Meng, Q. Zhou, J. Ren, Competitive adsorption behavior of typical heavy metal ions from acid mine drainage by multigroup-functionalization cellulose: qualitative and quantitative mechanism, (2023) 68191–68205. https://doi.org/10.1007/S11356-023-27188-7/METRICS.

[29] D.G. Chandran, L. Muruganandam, R. Biswas, A review on adsorption of heavy metals from wastewater using carbon nanotube and graphene-based nanomaterials, (2023) 110010–110046. https://doi.org/10.1007/S11356-023-30192-6/METRICS.

[30] A. Prajapati, A. Narayan Vaidya, A.R. Kumar, Microplastic properties and their interaction with hydrophobic organic contaminants: a review, (2022) 49490–49512. https://doi.org/10.1007/S11356-022-20723-Y.

[31] M. Zhai, B. Fu, Y. Zhai, W. Wang, A. Maroney, A.A. Keller, H. Wang, J.M. Chovelon, Simultaneous removal of pharmaceuticals and heavy metals from aqueous phase via adsorptive strategy: A critical review, (2023) 119924. https://doi.org/10.1016/j.watres.2023.119924.

[32] M.K. Sahu, S. Mandal, L.S. Yadav, S.S. Dash, R.K. Patel, Equilibrium and kinetic studies of Cd(II) ion adsorption from aqueous solution by activated red mud, (2016) 14251–14265. https://doi.org/10.1080/19443994.2015.1062428.

[33] H. Xiyili, S. Çetintaş, D. Bingöl, Removal of some heavy metals onto mechanically activated fly ash: Modeling approach for optimization, isotherms, kinetics and thermodynamics, (2017) 288–300. https://doi.org/10.1016/j.psep.2017.04.012.

[34] K.O. K'oreje, K. Demeestere, P. De Wispelaere, L. Vergeynst, J. Dewulf, H. Van Langenhove, From multi-residue screening to target analysis of pharmaceuticals in water: Development of a new approach based on magnetic sector mass spectrometry and

application in the Nairobi River basin, Kenya, (2012) 153–164. https://doi.org/10.1016/j.scitotenv.2012.07.052.

[35] T.P. Wood, C.S.J. Duvenage, E. Rohwer, The occurrence of anti-retroviral compounds used for HIV treatment in South African surface water, (2015) 235–243. https://doi.org/10.1016/j.envpol.2015.01.030.

[36] S.C. Mashiane M, Quantification of Selected Antiretroviral Drugs in a Wastewater Treatment Works in South Africa Using GC-TOFMS, (2015). https://doi.org/10.4172/2157-7064.100027 2.

[37] N.Y. Mlunguza, S. Ncube, P.N. Mahlambi, L. Chimuka, L.M. Madikizela, Determination of selected antiretroviral drugs in wastewater, surface water and aquatic plants using hollow fibre liquid phase microextraction and liquid chromatography - tandem mass spectrometry, (2020) 121067. https://doi.org/10.1016/j.jhazmat.2019.121067.

[38] T.G. Kebede, M.B. Seroto, R.C. Chokwe, S. Dube, M.M. Nindi, Adsorption of antiretroviral (ARVs) and related drugs from environmental wastewaters using nanofibers, (2020) 104049. https://doi.org/10.1016/j.jece.2020.104049.

[39] P.S.M. and L.M.M. Sharlott N. Qwane, Synthesis, Characterization and Application of a Molecularly Imprinted Polymer in Selective Adsorption of Abacavir from Polluted Water, (2020) 84–91. https://doi.org/https://doi.org/10.17159/0379-4350/2020/v73a13 .

[40] A.O. Adeola, J. de Lange, P.B.C. Forbes, Adsorption of antiretroviral drugs, efavirenz and nevirapine from aqueous solution by graphene wool: Kinetic, equilibrium, thermodynamic and computational studies, (2021) 100157. https://doi.org/10.1016/j.apsadv.2021.100157.

[41] T.G. Kebede, M.B. Seroto, R.C. Chokwe, S. Dube, M.M. Nindi, Adsorption of antiretroviral (ARVs) and related drugs from environmental wastewaters using nanofibers, (2020) 104049. https://doi.org/10.1016/j.jece.2020.104049.

[42] I. Chianella, K. Karim, E. V. Piletska, C. Preston, S.A. Piletsky, Computational design and synthesis of molecularly imprinted polymers with high binding capacity for pharmaceutical applications-model case: Adsorbent for abacavir, (2006) 73–78. https://doi.org/10.1016/j.aca.2005.11.068.

[43] Z. Terzopoulou, M. Papageorgiou, G.Z. Kyzas, D.N. Bikiaris, D.A. Lambropoulou, Preparation of molecularly imprinted solid-phase microextraction fiber for the selective removal and extraction of the antiviral drug abacavir in environmental and biological matrices, (2016) 63–75. https://doi.org/10.1016/j.aca.2016.01.059.

[44] J. Späth, P. Arumugam, R.H. Lindberg, O.A. Abafe, S. Jansson, J. Fick, C.A. Buckley, Biochar for the removal of detected micropollutants in south african domestic wastewater: A case study from a demonstration-scale decentralised wastewater treatment system in ethekwini, (2021) 396–416. https://doi.org/10.17159/WSA/2021.V47.I4.3861.

[45] M. Ndilimeke Akawa, K. Mogolodi Dimpe, P. Nosizo Nomngongo, An adsorbent composed of alginate, polyvinylpyrrolidone and activated carbon (AC@PVP@alginate) for ultrasound-assisted dispersive micro-solid phase extraction of nevirapine and zidovudine in environmental water samples, (2021) 100559. https://doi.org/10.1016/j.enmm.2021.100559.

[46] N.S.G.F.R.A.-H. G Abd Ali, Adsorption technique for the removal of heavy metals from wastewater using low-cost natural adsorbent, IOP Conf Ser: Earth Environ Sci 2023 (2023) 012012.

[47] D.G. Chandran, L. Muruganandam, R. Biswas, A review on adsorption of heavy metals from wastewater using carbon nanotube and graphene-based nanomaterials, (2023) 110010–110046. https://doi.org/10.1007/S11356-023-30192-6/METRICS.

[48] M. Ghaedi, N. Mosallanejad, Removal of Heavy Metal Ions from Polluted Waters by Using of Low Cost Adsorbents: Review, (2013) 7–22.

[49] L. Panda, S. Dash, Characterization and utilization of coal fly ash: A review, Emerging Materials Research 9 (2020) 921–934. https://doi.org/10.1680/jemmr.18.00097.

[50] J.K. Ahmed, M. Ahmaruzzaman, Journal of Water Process Engineering A review on potential usage of industrial waste materials for binding heavy metal ions from aqueous solutions, (2016) 39–41.

[51] A.R.K. Gollakota, V. Volli, C.M. Shu, Progressive utilisation prospects of coal fly ash: A review, (2019) 951–989. https://doi.org/10.1016/j.scitotenv.2019.03.337.

[52] M. Harja, G. Buema, D. Bucur, Recent advances in removal of Congo Red dye by adsorption using an industrial waste, (2022) 1–18. https://doi.org/10.1038/s41598-022-10093-3.

[53] M. Harja, G. Buema, N. Lupu, H. Chiriac, D.D. Herea, G. Ciobanu, Fly ash coated with magnetic materials: Improved adsorbent for cu (ii) removal from wastewater, (2021) 1–18. https://doi.org/10.3390/ma14010063.

[54] L. Forminte, G. Ciobanu, G. Buema, N. Lupu, H. Chiriac, C.G. de Castro, M. Harja, New materials synthesized by sulfuric acid attack over power plant fly ash, (2020) 48–58. https://doi.org/10.37358/RC.20.7.8224.

[55] Z. Hussain, H. Zhang, N. Chang, H. Wang, Synthesis of porous materials by the modification of coal fly ash and its environmentally friendly use for the removal of heavy metals from wastewater, (2022) 1–13. https://doi.org/10.3389/fenvs.2022.1085326.

[56] M. Attari, S.S. Bukhari, H. Kazemian, S. Rohani, A low-cost adsorbent from coal fly ash for mercury removal from industrial wastewater, (2017) 391–399. https://doi.org/10.1016/j.jece.2016.12.014.

[57] J. Tang, P. Liu, S. Xue, Y. Li, Y. Zhao, K. Huang, Z. Liu, Optimization of coal fly ash-based porous geopolymer synthesis and application for zinc removal from water, (2023) 5828–5833. https://doi.org/10.1016/j.ceramint.2022.10.028.

[58] R. Shyam, J.K. Puri, H. Kaur, R. Amutha, A. Kapila, Single and binary adsorption of heavy metals on fly ash samples from aqueous solution, (2013) 31–36. https://doi.org/10.1016/j.molliq.2012.10.031.

[59] W. Wang, Z. Zheng, C. Feng, X. Gao, Y. Qiao, M. Xu, Application of zeolite synthesized from coal fly ash via wet milling as a sustainable resource on lead(II) removal, (2023) 1246–1254. https://doi.org/10.1177/0734242X231160077.

[60] X. Zhao, H. Zhao, X. Huang, L. Wang, F. Liu, X. Hu, J. Li, G. Zhang, P. Ji, Effect and mechanisms of synthesis conditions on the cadmium adsorption capacity of modified fly ash, (2021) 112550. https://doi.org/10.1016/j.ecoenv.2021.112550.

[61] Siahaan, Removal of Pb2+ from Aqueous Solutions Using K-Type Zeolite Synthesized from Coal Fly Ash, (2019).

[62] M. Harja, G. Buema, D.M. Sutiman, I. Cretescu, Removal of heavy metal ions from aqueous solutions using low-cost sorbents obtained from ash, (2013) 497–508. https://doi.org/10.2478/s11696-012-0303-7.

[63] H. Javadian, F. Ghorbani, H. allah Tayebi, S.M.H. Asl, Study of the adsorption of Cd (II) from aqueous solution using zeolite-based geopolymer, synthesized from coal fly ash; kinetic, isotherm and thermodynamic studies, (2015) 837–849. https://doi.org/10.1016/j.arabjc.2013.02.018 .

[64] S.M. Abdelbasir, M.A.A. Khalek, From waste to waste: iron blast furnace slag for heavy metal ions removal from aqueous system, (2022) 57964–57979. https://doi.org/10.1007/S11356-022-19834-3/TABLES/3.

[65] M. Yusuf, L. Chuah, M.A. Khan, T.S.Y. Choong, Adsorption of Nickel on Electric Arc Furnace Slag: Batch and Column Studies, (2014) 388–397. https://doi.org/10.1080/01496395.2013.843099.

[66] T.J. Medina, S.P. Arredondo, R. Corral, A. Jacobo, R.A. Zárraga, C.A. Rosas, F.G. Cabrera, J.M. Bernal, Microstructure and pb2+ adsorption properties of blast furnace slag and fly ash based geopolymers, (2020) 1–17. https://doi.org/10.3390/min10090808.

[67] X. Zhan, L. Xiao, B. Liang, Removal of Pb(II) from acid mine drainage with bentonite-steel slag composite particles, (2019). https://doi.org/10.3390/su11164476.

[68] P. Bhunia, S. Chatterjee, P. Rudra, S. De, Chelating polyacrylonitrile beads for removal of lead and cadmium from wastewater, (2018) 202–213. https://doi.org/10.1016/j.seppur.2017.11.001.

[69] Y. Xue, S. Wu, M. Zhou, Adsorption characterization of Cu(II) from aqueous solution onto basic oxygen furnace slag, (2013) 355–364. https://doi.org/10.1016/j.cej.2013.07.045.

[70] S.M. Abdelbasir, M.A.A. Khalek, From waste to waste: iron blast furnace slag for heavy metal ions removal from aqueous system, (2022) 57964–57979. https://doi.org/10.1007/s11356-022-19834-3.

[71] M. Deng, X. Wang, Y. Li, F. Wang, Z. Jiang, Y. Liu, Z. Gu, S. Xia, J. Zhao, Reduction and immobilization of Cr(VI) in aqueous solutions by blast furnace slag supported

sulfidized nanoscale zerovalent iron, (2020) 140722. https://doi.org/10.1016/j.scitotenv.2020.140722.

[72] S. V. Dimitrova, D.R. Mehandgiev, Lead removal from aqueous solutions by granulated blast-furnace slag, (1998) 3289–3292. https://doi.org/10.1016/S0043-1354(98)00119-5.

[73] Y. Wang, H. Li, S. Cui, Q. Wei, Adsorption behavior of lead ions from wastewater on pristine and aminopropyl-modified blast furnace slag, (2021). https://doi.org/10.3390/w13192735.

[74] Z. Wang, G. Huang, C. An, L. Chen, J. Liu, Removal of copper, zinc and cadmium ions through adsorption on water-quenched blast furnace slag, (2016) 22493–22506. https://doi.org/10.1080/19443994.2015.1135084.

[75] T. Chouchane, O. Khireddine, S. Chibani, A. Boukari, Removal of Cr(III), Pb(II) and Cr-Pb Mixture by Blast Furnace Slag (BFS) in Solution, (2023) 251–268. https://doi.org/10.22036/ABCR.2022.365182.1843.

[76] Q.T.N. Le, E.L. Vivas, K. Cho, Calcium oxalate/calcium silicate hydrate (Ca-Ox/C-S-H) from blast furnace slag for the highly efficient removal of Pb2+ and Cd2+ from water, (2021) 106287. https://doi.org/10.1016/j.jece.2021.106287.

[77] F.M.S.E. El-Dars, M.A.G. Elngar, S.T. Abdel-Rahim, N.A. El-Hussiny, M.E.H. Shalabi, Kinetic of nickel (II) removal from aqueous solution using different particle size of water-cooled blast furnace slag, (2015) 769–778. https://doi.org/10.1080/19443994.2014.883578.

[78] T. Chouchane, S. Chibani, O. Khiriddine, A. Boukari, Adsorption Study of Pb(II) Ions on the Blast Furnace Slag (BFS) from Aqueous Solution, (2023) 1–13. https://doi.org/10.22068/ijmse.3011.

[79] R. Garcia-Valls, T.A. Hatton, Metal ion complexation with lignin derivatives, (2003) 99–105. https://doi.org/10.1016/S1385-8947(03)00007-X.

[80] V. Nair, A. Panigrahy, R. Vinu, Development of novel chitosan-lignin composites for adsorption of dyes and metal ions from wastewater, (2014) 491–502. https://doi.org/10.1016/j.cej.2014.05.045.

[81] Z. Mahmood, M. Yameen, M. Jahangeer, M. Riaz, A. Ghaffar, I. Javid, Lignin as Natural Antioxidant Capacity, (2018). https://doi.org/10.5772/intechopen.73284.

[82] F. Zhou, X. Feng, J. Yu, X. Jiang, High performance of 3D porous graphene/lignin/sodium alginate composite for adsorption of Cd(II) and Pb(II), Environmental Science and Pollution Research 25 (2018) 15651–15661. https://doi.org/10.1007/s11356-018-1733-8.

[83] X. Vecino, R. Devesa-Rey, A.B. Moldes, J.M. Cruz, Formulation of an alginate-vineyard pruning waste composite as a new eco-friendly adsorbent to remove micronutrients from agroindustrial effluents, (2014) 24–31. https://doi.org/10.1016/j.chemosphere.2014.03.004.

[84] G. Bustos, S. Calvar, X. Vecino, J.M. Cruz, A.B. Moldes, Industrial Symbiosis Between the Winery and Environmental Industry Through the Utilization of Grape Marc for Water Desalination Containing Copper(II), (2018). https://doi.org/10.1007/s11270-018-3697-1.

[85] F. Lyu, S. Niu, L. Wang, R. Liu, W. Sun, D. He, Efficient removal of Pb(II) ions from aqueous solution by modified red mud, (2021) 124678. https://doi.org/10.1016/j.jhazmat.2020.124678.

[86] F.T. da Conceição, B.C. Pichinelli, M.S.G. Silva, R.B. Moruzzi, A.A. Menegário, M.L.P. Antunes, Cu(II) adsorption from aqueous solution using red mud activated by chemical and thermal treatment, (2016) 1–7. https://doi.org/10.1007/s12665-015-4929-y.

[87] C.G. Joseph, Y.H. Taufiq-Yap, V. Krishnan, G. Li Puma, Application of modified red mud in environmentally-benign applications: A review paper, (2020) 795–806. https://doi.org/10.4491/eer.2019.374.

[88] T.A. Khan, S.A. Chaudhry, I. Ali, Equilibrium uptake, isotherm and kinetic studies of Cd(II) adsorption onto iron oxide activated red mud from aqueous solution, (2015) 165–175. https://doi.org/10.1016/j.molliq.2014.12.021.

[89] S. Mesgari Abbasi, A. Rashidi, A. Ghorbani, G. Khalaj, Synthesis, processing, characterization, and applications of red mud/carbon nanotube composites, (2016) 16738–16743. https://doi.org/10.1016/j.ceramint.2016.07.146.

[90] M. López-García, M. Martínez-Cabanas, T. Vilariño, P. Lodeiro, P. Rodríguez-Barro, R. Herrero, J.L. Barriada, New polymeric/inorganic hybrid sorbents based on red mud and

nanosized magnetite for large scale applications in As(V) removal, (2017) 117–125. https://doi.org/10.1016/j.cej.2016.11.081.

[91] L. Pietrelli, N.M. Ippolito, S. Ferro, V.G. Dovì, M. Vocciante, Removal of Mn and As from drinking water by red mud and pyrolusite, (2019) 526–533. https://doi.org/10.1016/j.jenvman.2019.02.093.

[92] R.A. Pepper, S.J. Couperthwaite, G.J. Millar, A novel akaganeite sorbent synthesised from waste red mud: Application for treatment of arsenate in aqueous solutions, (2018) 6308–6316. https://doi.org/10.1016/j.jece.2018.09.036.

[93] E. Kalkan, H. Nadaroglu, N. Dikbaş, E. Taşgin, N. Çelebi, Bacteria-modified red mud for adsorption of cadmium ions from aqueous solutions, (2013) 417–429.

[94] T.T. Luu, V.P. Dinh, Q.H. Nguyen, N.Q. Tran, D.K. Nguyen, T.H. Ho, V.D. Nguyen, D.X. Tran, H.A.T. Kiet, Pb(II) adsorption mechanism and capability from aqueous solution using red mud modified by chitosan, (2022) 132279. https://doi.org/10.1016/j.chemosphere.2021.132279.

[95] H. Mi, L. Yi, Q. Wu, J. Xia, B. Zhang, Preparation and optimization of a low-cost adsorbent for heavy metal ions from red mud using fraction factorial design and Box-Behnken response methodology, (2021) 127198. https://doi.org/10.1016/j.colsurfa.2021.127198.

[96] M.K. Sahu, S. Mandal, L.S. Yadav, S.S. Dash, R.K. Patel, Equilibrium and kinetic studies of Cd(II) ion adsorption from aqueous solution by activated red mud, (2016) 14251–14265. https://doi.org/10.1080/19443994.2015.1062428.

[97] N. Deihimi, M. Irannajad, B. Rezai, Characterization studies of red mud modification processes as adsorbent for enhancing ferricyanide removal, (2018) 266–275. https://doi.org/10.1016/j.jenvman.2017.10.037.

[98] N. Deihimi, M. Irannajad, B. Rezai, Equilibrium and kinetic studies of ferricyanide adsorption from aqueous solution by activated red mud, (2018) 277–285. https://doi.org/10.1016/j.jenvman.2018.08.089.

[99] X. Yuan, S.I. Im, S.W. Choi, K.B. Lee, Removal of Cu(II) ions from aqueous solutions using petroleum coke-derived microporous carbon: investigation of adsorption

equilibrium and kinetics, (2019) 1205–1218. https://doi.org/10.1007/s10450-019-00059-9.

[100] K.S. Fisher, A.J. Vreugdenhil, Metal-Impregnated Petroleum Coke-Derived Activated Carbon for the Adsorption of Arsenic in Acidic Waters, (2023) 29083–29100. https://doi.org/10.1021/acsomega.3c02078.

[101] R.M. Ramírez Zamora, R. Schouwenaars, A. Durán Moreno, G. Buitrón, Production of activated carbon from petroleum coke and its application in water treatment for the removal of metals and phenol, (2000) 119–126. https://doi.org/10.2166/wst.2000.0505.

[102] R. Panek, M. Medykowska, M. Wi´sniewska, K. Szewczuk-Karpisz, K. J¸edruchniewicz, M. Franus, Simultaneous Removal of Pb2+ and Zn 2+ Heavy Metals Using, (2021) 1–17.

[103] S. Dash, H. Chaudhuri, R. Gupta, U.G. Nair, A. Sarkar, Fabrication and Application of Low-Cost Thiol Functionalized Coal Fly Ash for Selective Adsorption of Heavy Toxic Metal Ions from Water, (2017) 1461–1470. https://doi.org/10.1021/acs.iecr.6b03869.

[104] L. Kang, S.F. Liu, D.W. Yi, K. Wang, H.L. Du, H.Q. Huang, P. Chen, Renewable conversion of coal gangue to 13-X molecular sieve for Cd2+-containing wastewater adsorption performance, (2023) 702–710. https://doi.org/10.1007/s12598-023-02461-3.

[105] Q. Li, L. Lv, X. Zhao, Y. Wang, Y. Wang, Cost-effective microwave-assisted hydrothermal rapid synthesis of analcime-activated carbon composite from coal gangue used for Pb2+ adsorption, (2022) 77788–77799. https://doi.org/10.1007/s11356-022-20942-3.

[106] X. Shen, Y. Xie, Q. Wang, X. Yi, J.L. Shamshina, R.D. Rogers, Enhanced heavy metal adsorption ability of lignocellulosic hydrogel adsorbents by the structural support effect of lignin, 2019) 4005–4019. https://doi.org/10.1007/s10570-019-02328-w.

[107] N.A. Nordin, N.A. Rahman, A.H. Abdullah, Effective Removal of Pb(II) Ions by Electrospun PAN/Sago Lignin-Based Activated Carbon Nanofibers, (2020). https://doi.org/10.3390/molecules25133081.

[108] B. Xie, Y. Hou, Y. Li, Modified Lignin Nanosphere Adsorbent for Lead and Copper Ions, (2020) 249–262. https://doi.org/10.15376/BIORES.16.1.249-262.

[109] Y. Jin, C. Zeng, Q.F. Lü, Y. Yu, Efficient adsorption of methylene blue and lead ions in aqueous solutions by 5-sulfosalicylic acid modified lignin, (2019) 50–58. https://doi.org/10.1016/j.ijbiomac.2018.10.213.

[110] Y. Bai, Y. Pang, Z. Wu, X. Li, J. Jing, H. Wang, Z. Zhou, Adsorption of Lead from Water Using MnO2-Modified Red Mud: Performance, Mechanism, and Environmental Risk, (2023). https://doi.org/10.3390/w15244314.

[111] W.M. Xie, F.P. Zhou, X.L. Bi, D.D. Chen, J. Li, S.Y. Sun, J.Y. Liu, X.Q. Chen, Accelerated crystallization of magnetic 4A-zeolite synthesized from red mud for application in removal of mixed heavy metal ions, (2018) 441–449. https://doi.org/10.1016/j.jhazmat.2018.07.007.

[112] L. Pietrelli, N.M. Ippolito, S. Ferro, V.G. Dovì, M. Vocciante, Removal of Mn and As from drinking water by red mud and pyrolusite, (2019) 526–533. https://doi.org/10.1016/j.jenvman.2019.02.093.

[113] Y. Li, H. Huang, Z. Xu, H. Ma, Y. Guo, Mechanism study on manganese(II) removal from acid mine wastewater using red mud and its application to a lab-scale column, (2020) 119955. https://doi.org/10.1016/j.jclepro.2020.119955.

[114] A. Phounglamcheik, M. Bäckebo, R. Robinson, K. Umeki, The significance of intraparticle and interparticle diffusion during CO2 gasification of biomass char in a packed bed, (2022). https://doi.org/10.1016/j.fuel.2021.122302.

[115] X. Guo, S. Zhang, X. quan Shan, Adsorption of metal ions on lignin, (2008) 134–142. https://doi.org/10.1016/j.jhazmat.2007.05.065.

[116] V. Nair, A. Panigrahy, R. Vinu, Development of novel chitosan-lignin composites for adsorption of dyes and metal ions from wastewater, (2014) 491–502. https://doi.org/10.1016/j.cej.2014.05.045.

[117] T.G. Kebede, M.B. Seroto, R.C. Chokwe, S. Dube, M.M. Nindi, Adsorption of antiretroviral (ARVs) and related drugs from environmental wastewaters using nanofibers, (2020) 104049. https://doi.org/10.1016/j.jece.2020.104049.

[118] T.T. Luu, V.P. Dinh, Q.H. Nguyen, N.Q. Tran, D.K. Nguyen, T.H. Ho, V.D. Nguyen, D.X. Tran, H.A.T. Kiet, Pb(II) adsorption mechanism and capability from aqueous

solution using red mud modified by chitosan, (2022) 132279. https://doi.org/10.1016/j.chemosphere.2021.132279.

[119] Z. Wang, G. Huang, C. An, L. Chen, J. Liu, Removal of copper, zinc and cadmium ions through adsorption on water-quenched blast furnace slag, (2016) 22493–22506. https://doi.org/10.1080/19443994.2015.1135084.

[120] M. Verma, I. Tyagi, R. Chandra, V.K. Gupta, Adsorptive removal of Pb (II) ions from aqueous solution using CuO nanoparticles synthesized by sputtering method, (2017) 936–944. https://doi.org/10.1016/j.molliq.2016.04.045.

CHAPTER 3: METHODOLOGY

PREAMBLE

This chapter describes in detail the materials and methods used to prepare the magnetic mesoporous adsorbents. The chapter further outlines instrumentation used for characterization of the raw, active and Fe_3O_4 coated adsorbents and characterization results are also interpreted.

3.1. Experimental procedure

3.1.1. Chemicals and methods

The glassware used were washed using soap and water, then socked in 5% nitric acid and finally rinsed with deionized water prior to drying in an oven at 100 ℃ for overnight. 1000 mg/L efavirenz standard (Sigma-Aldrich, South Africa) solutions were prepared by weighing 10 mg into 10 mL volumetric flask followed by dilution to gain required concentrations. Lead standards were prepared from appropriate dilution of 1000 mg/L lead standard solution (Sigma-Aldrich, South Africa). lead standards 1000 mg/L, 70% ultra-pure nitric acid (HNO_3), sodium hydroxide (NaOH) and efavirenz were purchased from Sigma-Aldrich, South Africa. Nylon microfilters (0.45 µm) were purchased from Anatech instrument, South Africa.

3.1.2. Collection and pre-treatment of coal fly ash and petroleum coke

Calcined petroleum coke standard reference material was purchased from National Institute of Standards and Technology, United States Department of Commerce. Coal fly ash samples were collected from Majuba Power Station (ESKOM), South Africa with collection point (27.1001° S, 29.7694° E). The fly ash was taken from the bottom of the precipitators at the silos, before being mixed with 210 L of water. The bottom ash was collected from the Ash Emergency loading point at the station using a 210 L container. Upon arrival at the lab, excess water was removed from the drums to allow the samples to dry, making it easier for further sampling processing. The samples and their abbreviations are presented in **Table 3.1**.

Table 3.1: Sample labels used in the current study.

Industrial waste	Raw	Activation	Coating with Fe_3O_4
Petroleum coke	RPC	APC	Fe_3O_4 @APC
Coal fly ash	RCFA	ACFA	Fe_3O_4 @ACFA
Bottom ash	RBA	ABA	Fe_3O_4 @ABA
Fly ash	RFA	AFA	Fe_3O_4 @AFA

3.1.3. Sampling and sample pre-treatment of real water samples

Grab sampling method was used to collect samples around the Gauteng province (South Africa). Wastewater samples, such as influent and effluent were collected from the Daspoort wastewater treatment plant which discharges its effluent into Apies River. Influent, effluent and river samples were collected into 2.5 L amber bottles and kept in an ice box while being transported to the laboratory. Then, the samples were filtered using glass wool and stored at 4 °C in the cold room until the analysis.

3.1.4. Preparation of magnetic mesoporous adsorbents

Activation of raw materials

Raw coal fly ash (RCFA), bottom ash (RBA), fly ash (RFA) and petroleum coke (RPC) were crushed at 25 rpm for 90 min with Retch MM 200 ball miller and then sieved with Kingtest laboratory sieve of 75 µm aperture. Then, the material was soaked in 0.1 mol/L HNO_3 to remove impurities for 2 hours followed by washing with Milli-Q water obtained from a water purification system with water conductivity of 18.2 µS/cm and oven-dried overnight at 85 ˚C to remove moisture.

RFCA, RBA, RFA and RPC were mixed with the NaOH at 5:8 mass ratios. The resultant mixture was then calcinated in a Lenton TM-104 TOHO furnace at 350 ˚C for 4 hours. The product was washed with Milli-Q water until a pH of 7 was achieved and then dried at 105 ˚C for 6 hours. This resulted in the desired activated coal fly ash (ACFA), activated bottom ash (ABA), activated fly ash (AFA), and activated petroleum coke (APC) [1].

Coating of activated materials

Activated coal fly ash (ACFA), activated bottom ash (ABA), activated fly ash (AFA), and activated petroleum coke (APC) were obtained and mixed with Fe_3O_4 in a ratio of 1:9 [2] . The mixture was then ball-milled for 4 hours using a Retch MM 200 machine, followed by washing with Milli-Q water. The resulting product was then oven-dried at 105 ˚C overnight, resulting in the final magnetic mesoporous adsorbent products: Fe_3O_4@ACFA, Fe_3O_4@ABA, Fe_3O_4@AFA, and Fe_3O_4@APC [2].

3.2. Characterization of magnetic mesoporous adsorbents

3.2.1. Fourier-transformed infrared spectroscopy

Fourier-transformed infrared (FTIR) spectroscopy was used to identify the functional groups present in all samples. Fourier transformed infrared (FTIR) spectra of RCFA, RBA, RFA, RPC. ACFA, ABA, AFA, APC, Fe_3O_4@ACFA, Fe_3O_4@ABA, Fe_3O_4@AFA and Fe_3O_4@APC were measured by using a Bruker Tensor 27 (Bruker Optics, GmbH, Germany) FTIR spectrophotometer with the KBr wafer technique. The synthesized samples were mixed with KBr and compressed to pellet. During the analysis the data was recorded from 400 to 4000 cm^{-1} range.

3.2.2. Thermogravimetric analysis

The RCFA, RBA, RFA, RPC. ACFA, ABA, AFA, APC, Fe_3O_4@ACFA, Fe_3O_4@ABA, Fe_3O_4@AFA and Fe_3O_4@APC's thermal stability and thermal decomposition temperatures were examined using thermogravimetric (TGA) analyser device model Q500 from TA Instruments-Waters LLC. The samples were placed individually in silica pan as a sample holder under nitrogen atmosphere with nitrogen gas flow rate of 40 mL/min. All samples were heated from 10 to 600 ˚C with heating rate increasing of 30 ˚C/min [3,4].

3.2.3. Brunauer-Emmett-Teller analysis

The Brunauer-Emmett teller (BET) analysis was conducted using a Micromeritics ASAP 2460 to determine the surface area, particle size, pore size, pore volume and porosity of RCFA, RBA, RFA, RPC. ACFA, ABA, AFA, APC, Fe_3O_4@ACFA, Fe_3O_4@ABA, Fe_3O_4@AFA and Fe_3O_4@APC. During the analysis, the materials were degassed with nitrogen gas at 200 °C for

2 hours. The measurements were conducted at 200 °C. The pore sizes and volumes were calculated by using adsorption curves with BJ H model.

3.2.4. Scanning electron microscopy-energy dispersive X-ray spectroscopy

To analyse the morphology and elemental composition of the RCFA, RBA, RFA, RPC. ACFA, ABA, AFA, APC, Fe_3O_4@ACFA, Fe_3O_4@ABA, Fe_3O_4@AFA and Fe_3O_4@APC, the Scanning electron microscope- energy dispersive spectroscopy (SEM/EDS, Tescan, Brno, Czech Republic) was used. The Scanning electron microscope (SEM) measurements were carried out using a Tescan Vega 3 LMH, operated at 20 kV accelerating voltage, using secondary electron detector (SED) and energy dispersive spectroscopy (EDS). The samples were firstly carbon-coated with the Agar Turbo Carbon coater, thereby improving their conductivity prior to each measurement.

3.2.5. Ultra-violet visible spectroscopy

The UV spectra of RCFA, RBA, RFA, RPC, ACFA, ABA, AFA, APC, Fe_3O_4@ACFA, Fe_3O_4@ABA, Fe_3O_4@AFA, and Fe_3O_4@APC were confirmed using a Shimadzu plate number 1 spectrophotometer (RF-5301PC, Shimadzu). The spectrophotometer was connected to a light source of 150 W Xenon lamp, which was utilized to generate the UV spectra. The data obtained from these samples were analysed to determine the properties and characteristics of the compounds.

3.2.6. Transmission electron microscopy

To confirm the particle size, the RCFA, RBA, RFA, RPC. ACFA, ABA, AFA, APC, Fe_3O_4@ACFA, Fe_3O_4@ABA, Fe_3O_4@AFA and Fe_3O_4@APC samples were analysed by using Jeol JEM-2100F transmission electron microscope instrument (TEM, JOEL Ltd., Tokyo, Japan). The analysis was done instrument at 200 kV and was equipped with LaB6 source and charge coupled device (CCD) digital camera. Before TEM analysis, small amount of iron oxide material was dispersed onto the TEM grid (200 mesh size Cu-grid), coated with a thin film made of lacy carbon material.

3.3. Results and discussion

3.3.1. Fourier-transformed infrared spectroscopy

The surface functional groups of RCFA, RBA, RFA, RPC. ACFA, ABA, AFA, APC, Fe_3O_4@ACFA, Fe_3O_4@ABA, Fe_3O_4@AFA, Fe_3O_4@APC and Fe_3O_4 nanoparticles were characterized by FT-IR spectra as shown in **Figure 3.1**. **Figure 3.1a** shows the FT-IR spectra of RPC, APC, Fe_3O_4 and Fe_3O_4@APC. The vibration band at 1114.8 cm^{-1} is attributed to S=O symmetric stretching and asymmetric stretching. The peak at 1628 cm^{-1} is assigned to C=O stretching vibration. Also, the peak at 1340 c m^{-1} is due to the –OH stretching mode of –COOH, and phenolic –OH groups which represent the introduction of –OH by NaOH [3].

The FTIR spectra for RBA (**Figure 3.1b**), RCFA (**Figure 3.1c**), and RFA (**Figure 3.1d**) show similar functional groups. Broad peaks representative of aluminosilicates were observed. The spectra showed that the materials contained predominately silica and alumina functional groups. This was confirmed by the presence of an asymmetric stretching vibration between 900 cm^{-1} and 1050 cm^{-1} of Si– O–Si. This results from the overlapping of the FTIR spectra of glass, mullite and quartz. The peak at around 580 cm^{-1} was due to Al–O stretching vibrations (mullite), and the peak at around 450 cm^{-1} is associated with Si–O–Si and Al–O–Al symmetric bending vibrations. The peak at 670 cm^{-1} was attributed to Al–O–Al bending vibrations of quartz and mullite [4].

The spectra also showed two broad bands at ~1600 cm^{-1} and ~3500 cm^{-1}. These bands are attributed to the bending vibration of water molecules and the Fe–OH complex [5]. The bands in the region of 400 cm^{-1} to 750 cm^{-1} in all the samples signified the presence of Fe–O (magnetite) and Fe–O–Fe (maghemite) bonds [6]. The presence of an absorption band corresponding to the stretching vibration of Fe–O confirmed the successful coating with Fe_3O_4 onto APC, ABA, AFA and ACFA.

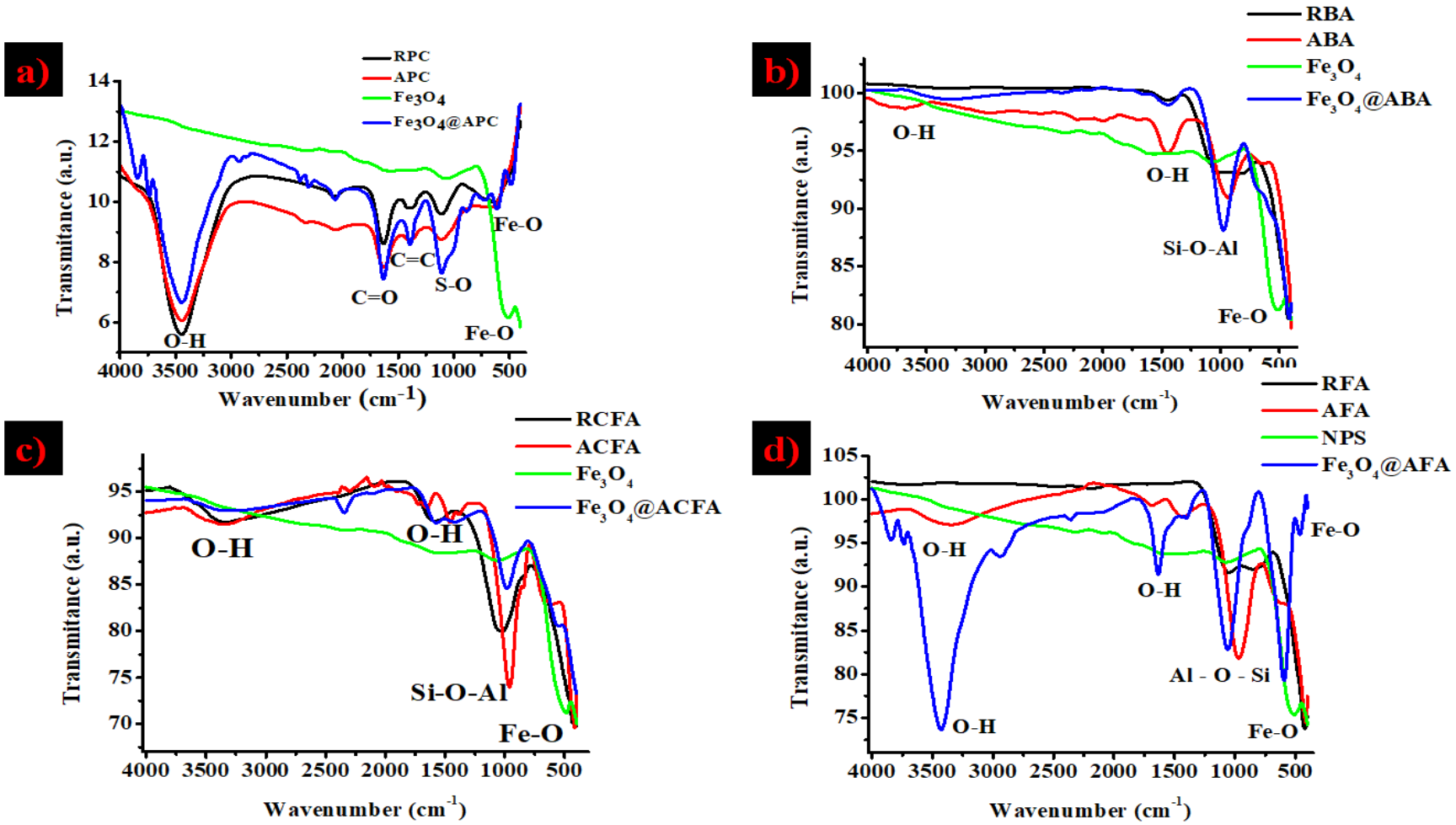

Figure 3.1: The FT-IR spectra of a) RPC, APC, Fe_3O_4@APC, b) RBA, ABA, Fe_3O_4@ABA c) RCFA, ACFA, Fe_3O_4@ACFA, d) RFA, AFA, and Fe_3O_4@AFA

3.3.2. Thermogravimetric analysis

Thermogravimetric (TGA) analysis was conducted to investigate the thermal stability of the synthesized materials. **Figure 3.2** demonstrates the thermograms of RPC, APC, Fe_3O_4@APC, RBA, ABA, Fe_3O_4@ABA, RFCA, ACFA, Fe_3O_4@ACFA, RFA, AFA, Fe_3O_4@AFA. It can be seen in **Figure 3.2a** that the weight loss happened at 400°C which was due to the carbon combustion derived from petroleum coke. This observation was consistent in RPC, APC and Fe_3O_4@APC. Weight loss at 100 ˚C presents evaporation of moisture on APC which was also observed on the Fe_3O_4@APC.

Figure 3.2b shows RBA, ABA and Fe_3O_4@ABA. RBA shows the three weight losses for the ash samples, with local minima at temperatures of 350 ˚C, 400 ˚C and 650 ˚C. The first loss was attributed to the evaporation of water. The second loss was due to the dehydration of $Ca(OH)_2$. At 650 ˚C, there was a mass loss resulting from the decomposition of $CaCO_3$. However, the RBA and Fe_3O_4@ABA had similar mass loss at 550 ˚C, resulting from the decomposition of $Ca(OH)_2$ as suggested in a previous study [4,7]. The mass losses at around 600 °C can be assigned to CO_2 escape, mainly from calcite [8].

Figure 3.2c and d show the thermograms of different samples under study. In **Figure 3.2c**, you can observe the thermogram of RFCA, ACFA, and Fe_3O_4@ACFA, which depicts the variation in temperature with respect to time. Similarly**, Figure 3.2d** presents the thermograms for RFA, AFA, and Fe_3O_4@AFA. It's important to note that the bottom ash, fly ash, and coal fly ash share a similar composition and hence exhibit a similar pattern of decomposition. The thermograms of these samples show the changes in temperature due to the decomposition of moisture, $CaCO_3$, $Ca(OH)_2$, and CO_2.

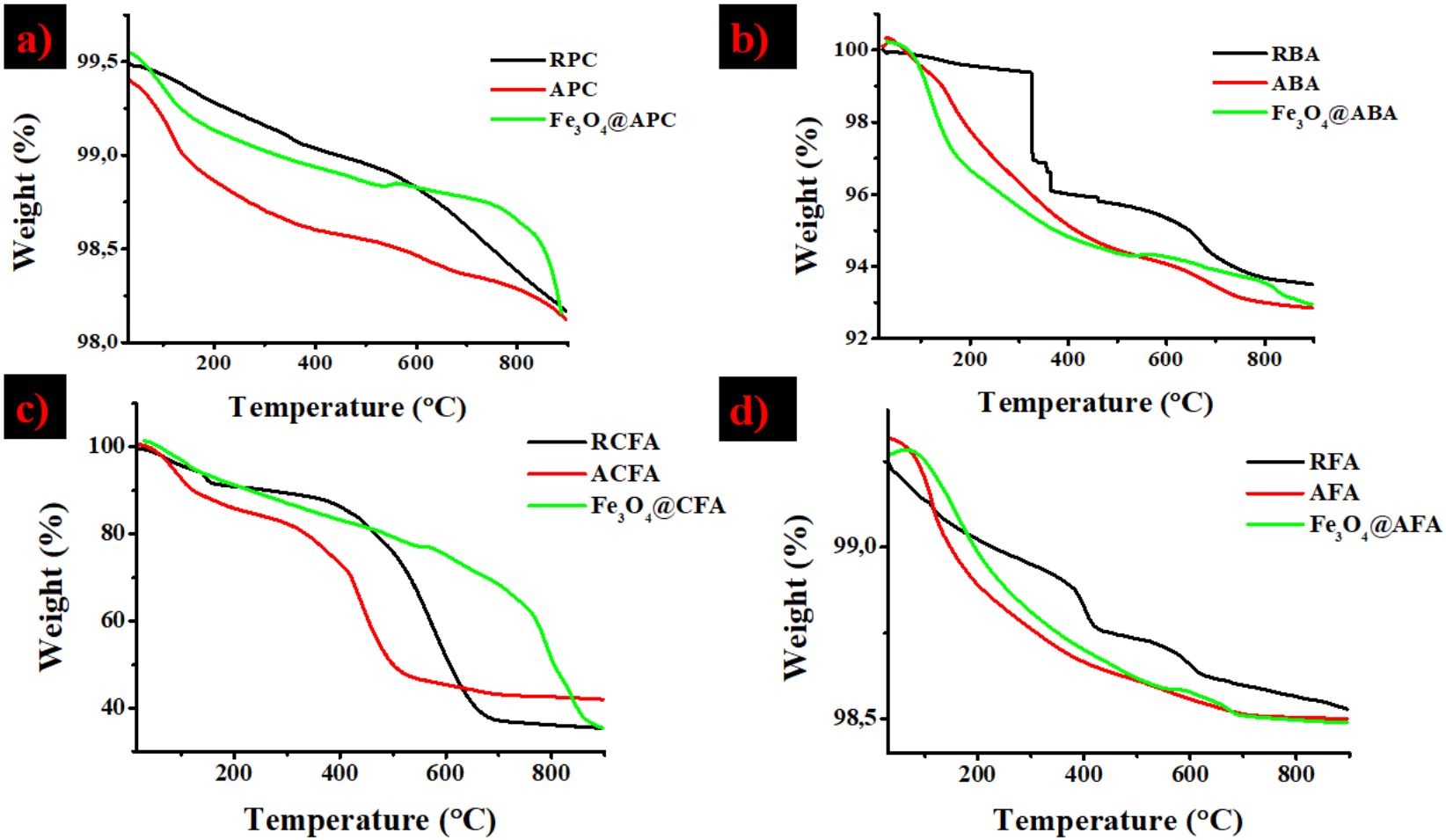

Figure 3.2: Thermogravimetric curves of a) RPC, APC, Fe_3O_4@APC, b) RBA, ABA, Fe_3O_4@ABA c) RCFA, ACFA, Fe_3O_4@ACFA, d) RFA, AFA, and Fe_3O_4@AFA.

3.3.3. Brunauer-Emmett-Teller analysis

The nitrogen adsorption-desorption isotherm for the (a) RPC, APC, Fe_3O_4@APC, (b) RBA, ABA, Fe_3O_4@ABA, (c) RCFA, ACFA, Fe_3O_4@ACFA, (d) RFA, AFA, and Fe_3O_4@AFA are shown in **Figure 3.3**. From the results, it was observed that the hysteresis loop for Fe_3O_4@APC, Fe_3O_4@ABA, Fe_3O_4@ACFA and Fe_3O_4@AFA closes near to a relative pressure of 0.99, which indicates mesoporous characteristics of the adsorbents. The adsorption–desorption isotherm shape shows a typical type – IV, which agrees with the nature of mesoporous adsorbents according to IUPAC [4]. From **Table 3.2,** it was observed that the activation by NaOH increased the pore diameter. However, coating ABA, ACFA and APC decreased the pore which is characterized as mesoporous thus confirmed the mesoporous nature of the Fe_3O_4@APC, Fe_3O_4@ABA, Fe_3O_4@ACFA and Fe_3O_4@AFA. The Barrett, Joyner and Halenda (BJH) cumulative volume of pores, BJH average pore diameter and surface area were determined shown in **Table 3.2**.

RCFA has a moderate surface area of 6.667 m^2/g and a relatively larger pore diameter, while ACFA has a higher surface area of 7.799 m^2/g and a smaller pore diameter compared to RCFA. Fe_3O_4@AFA has a similar surface area of 7.479 m^2/g to ACFA but a significantly larger pore volume. RBA has a lower surface area of 3.684 m^2/g and a much larger pore diameter, while ABA boasts the highest surface area of 12.578 m^2/g and the largest pore diameter. Fe_3O_4@ABA has a moderate surface area of 6.885 m^2/g and a smaller pore diameter. RFA exhibits the lowest surface area of 1.928 m^2/g and a small pore diameter. Fe_3O_4@AFA has a similar surface area of 12.337 m^2/g to AFA with a smaller pore diameter. RPC has a moderate surface area of 6.224 m^2/g and a small pore diameter, whereas APC has a higher surface area of 11.457 m^2/g and a similar pore diameter to RPC. Fe_3O_4@APC has a moderate surface area of 6.579 m^2/g and a slightly smaller pore diameter. Generally, a higher surface area correlates with better adsorption capacity, while a smaller pore diameter enhances selectivity for specific pollutants. Activated samples (ACFA, ABA, AFA) demonstrate improved properties for adsorption.

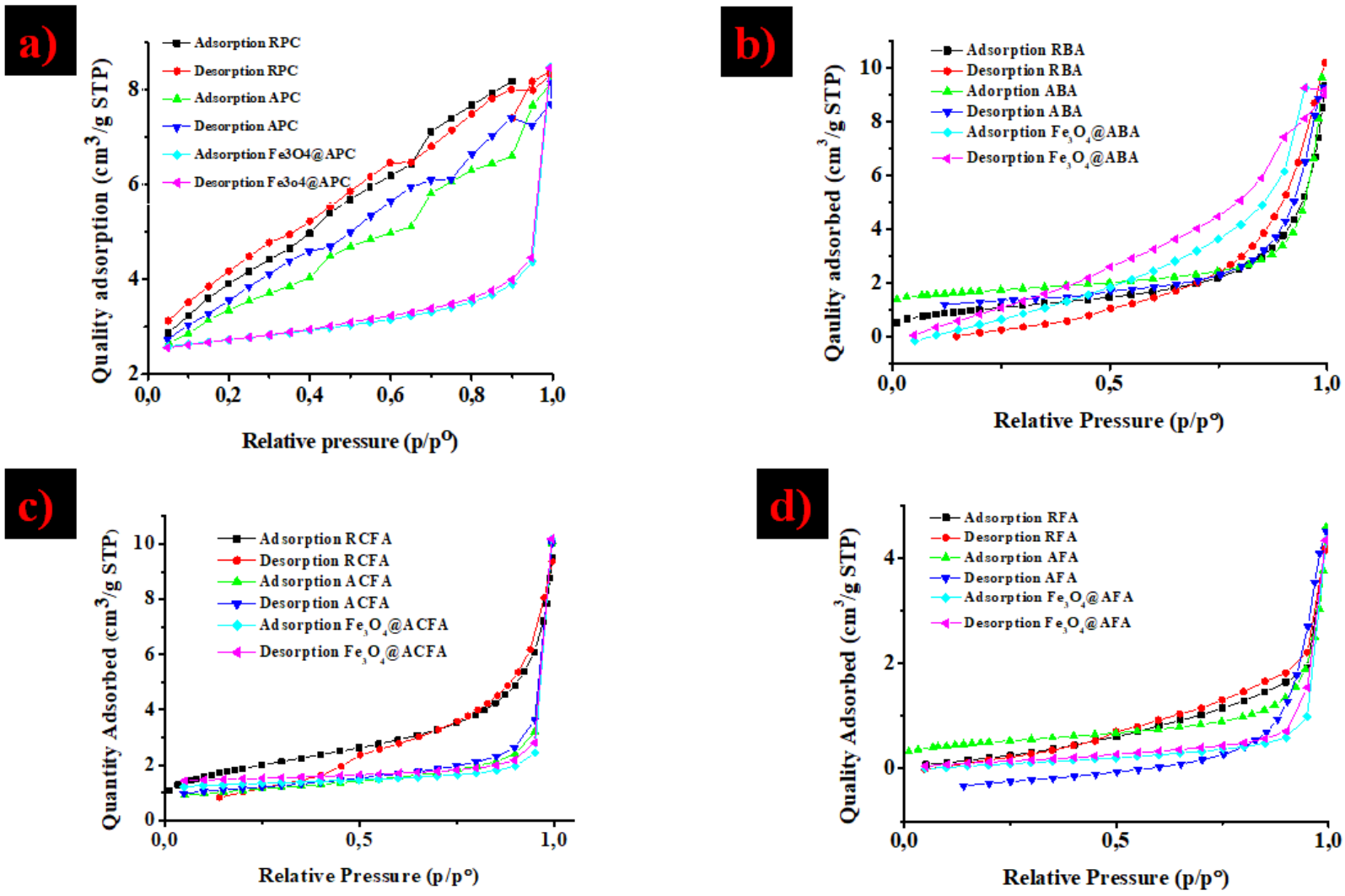

Figure 3.3: The nitrogen adsorption isotherm curve of a) RPC, APC, Fe_3O_4@APC, b) RBA, ABA, Fe_3O_4@ABA c) RCFA, ACFA, Fe_3O_4@ACFA, d) RFA, AFA, and Fe_3O_4@AFA.

Table 3.2: The total pore volume, mean pore diameter, and surface area properties.

Sample	Surface area (m^2/g)	Pore volume (cm^3/g)	Pore diameter (nm)
RCFA	6.667	0.013	8.122
ACFA	7.799	0.048	3.835
Fe_3O_4@AFA	7.479	0.140	3.417
RBA	3.684	0.0132	14.32
ABA	12.58	0.0668	21.24
Fe_3O_4@ABA	6.885	0.063	3.826
RFA	1.928	0.007	3.065
AFA	17.38	0.058	13.38
Fe_3O_4@AFA	12.33	0.0820	4.009
RPC	6.224	0.036	3.415
APC	11.46	0.012	3.421
Fe_3O_4@APC	6.579	0.010	3.414

3.3.4. Scanning electron microscopy-energy dispersive X-ray spectroscopy

Figure 3.4 shows the SEM-EDS of RPC, APC and Fe_3O_4@APC. The SEM images of RPC (**Figure 3.4a**) shows smooth flat surface. APC (**Figure 3.4b**) is composed primarily of agglomerated combination of spherical and rodlike structures which were destroyed during ball milling resulting in the smooth flaky particles as shown in **Figure 3.4c** representing Fe_3O_4@APC. The EDS shows that RPC, APC and Fe_3O_4@APC are primarily composed of carbon, oxygen and sulphur atoms. The presence of Fe on Fe_3O_4@APC confirms the successful coating with Fe_3O_4 onto APC. This is also confirmed by the FTIR results.

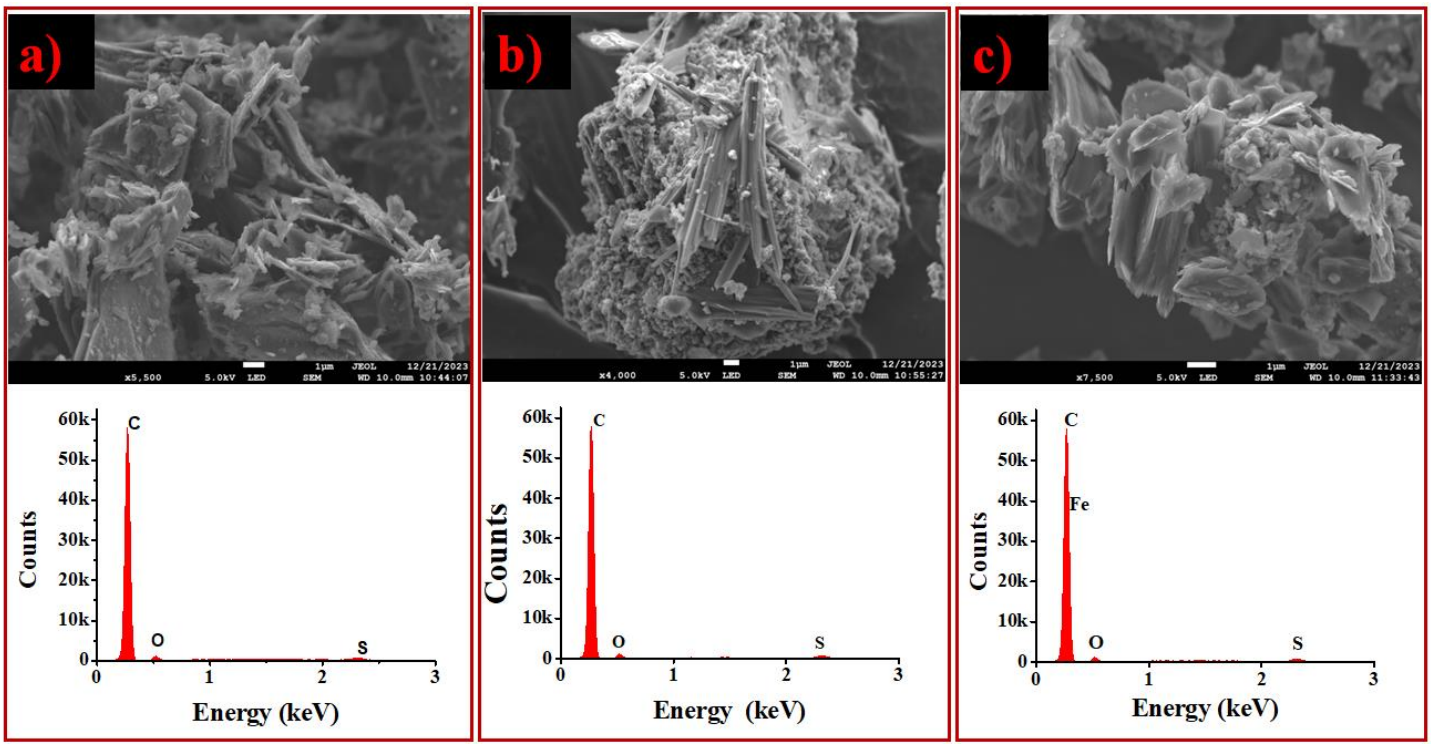

Figure 3.4: SEM-EDS of a) RPC, b) APC and c) Fe_3O_4@APC.

Figure 3.5 illustrates SEM images of RBA, ABA, Fe_3O_4@ABA, RCFA, ACFA, Fe_3O_4@ACFA, RFA, AFA, and Fe3O4@AFA. Specifically, **Figure 3.5a**, **Figure 3.5d**, and **Figure 3.5g** show the SEM images of RBA, RCFA, and RFA before activation, respectively. As shown by the images, RFA exhibited a smooth surface with large pores, while RCFA comprised of rough surfaces with sheet-like structures, and RFA consisted of spherical particles of varying sizes with a relatively smooth surface.

Following activation with NaOH, these materials undergo changes in their surface morphology presented by **Figure 3.5b** (ABA), **Figure 3.5e** (ACFA) and **Figure 3.5h** (AFA). ABA, ACFA, and AFA exhibit agglomerated particles of different shapes on their surfaces, compared to RBA, RCFA, and RFA. ABA primarily comprised spherical structures of various sizes, ACFA features a combination of spherical and rod-like structures, and AFA primarily consisted of rod – like structures. Additionally, when ABA, ACFA, and AFA were coated with Fe_3O_4 nanoparticles, noticeable changes were observed in the obtained products, Fe_3O_4@ABA (**Figure 3.5d**), Fe_3O_4@ACFA (**Figure 3.5f**), and Fe_3O_4@AFA (**Figure 3.5i**).

The use of milling destroyed the agglomerated particles of ABA, ACFA, and AFA, and uniformly distributed the Fe_3O_4 nanoparticles. The SEM images showed a uniform distribution of both small particles and Fe_3O_4 nanoparticles within the composite. The SEM of

Fe_3O_4@ABA demonstrated that the bottom ash was well crushed, and the shapes of the particles became more uniform. The sizes were significantly reduced, indicating the breakdown of the original spherical-shaped bottom ash. Similarly, Fe_3O_4@ACFA demonstrated the distribution of Fe_3O_4 nanoparticles on the surface, while Fe_3O_4@AFA exhibited a similar trend to that of Fe_3O_4@ACFA. The observations align with existing literature on the effects of milling and Fe_3O_4 nanoparticle coating.

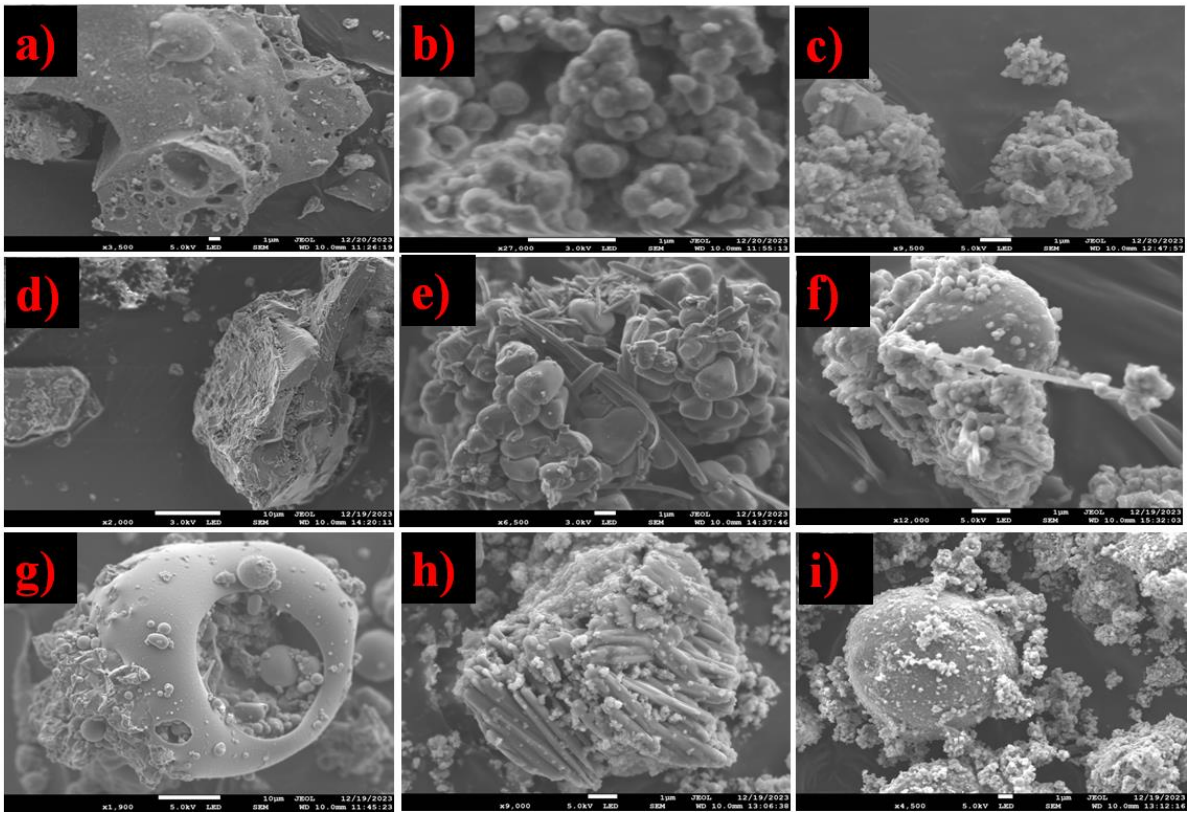

Figure 3.5: SEM images of a) RBA, b) ABA, c) Fe_3O_4@ABA, d) RCFA, e) ACFA, f) Fe_3O_4@ACFA, g) RFA, h) AFA, and i) Fe_3O_4@AFA.

As determined by EDS (**Figure 3.6**), the predominant elements in the RBA, ABA, Fe_3O_4@ABA, RCFA, ACFA, Fe_3O_4@ACFA, RFA, AFA, and Fe3O4@AFA, were oxygen, unburned carbon, silicon, aluminium, iron, and calcium. Minor amounts of magnesium, titanium, sodium, and potassium were found in analysed samples. By comparing the data obtained for Fe in the case of Fe_3O_4@ABA, Fe_3O_4@ACFA and Fe_3O_4@AFA, the SEM-EDS was inconclusive to determine the successful preparation of the magnetic mesoporous adsorbents.

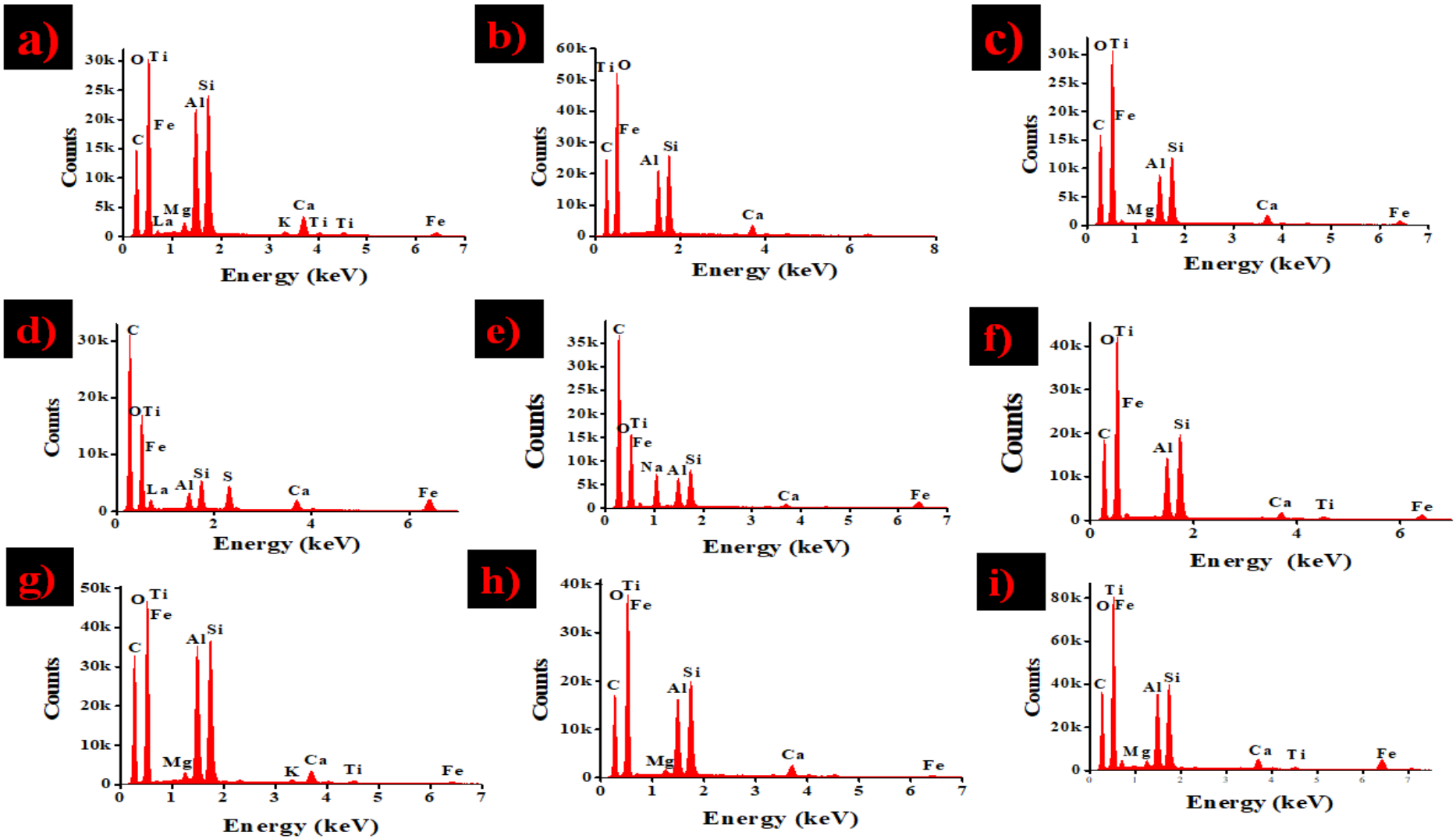

Figure 3.6: EDS of a) RBA, b) ABA, c) Fe_3O_4@ABA, d) RCFA, e) ACFA, f) Fe_3O_4@ACFA, g) RFA, h) AFA, and i) Fe_3O_4@

3.3.5. Ultra-Violet Visible spectroscopy

Ultraviolet visible spectroscopy was conducted to evaluate the absorbance of the samples and to confirm the successful incorporation of Fe_3O_4 nanoparticles. **Figure 3.7a** shows the Uv–Vis spectra of RPC, APC, Fe_3O_4 and Fe_3O_4@APC. It is illustrated that both the Uv and visible regions are light active for RPC. The optimum absorbance peak is the range of 400 – 600 cm^{-1}. This implies that within the visible region the material is active. There is a noticeable decrease in absorbance in the visible region, indicating weaker light adsorption of RPC in the visible region compared to the UV region. The absorbance of APC was reduced. Fe_3O_4@APC demonstrates increased absorbance upon the introduction of Fe_3O_4 nanoparticles, indicating successful incorporation. A similar trend was observed for ABA, ACFA, AFA, Fe_3O_4@ABA, Fe_3O_4@ACFA and Fe_3O_4@AFA. Spectra show a broad band between 200–300 nm region for all samples, which indicates the presence of a tetrahedral coordinated Fe^{2+} or Fe^{3+} [9,10]. Absorption band in the range 350–450 nm was due to the absorption and scattering of light by the nanoparticles. Fe^{2+} was found in the RBA, RCFA, and RFA of all three ash samples in the same spectral range as the Fe_3O_4 nanoparticle-coated samples. This observation was supported by the FTIR and SEM-EDS.

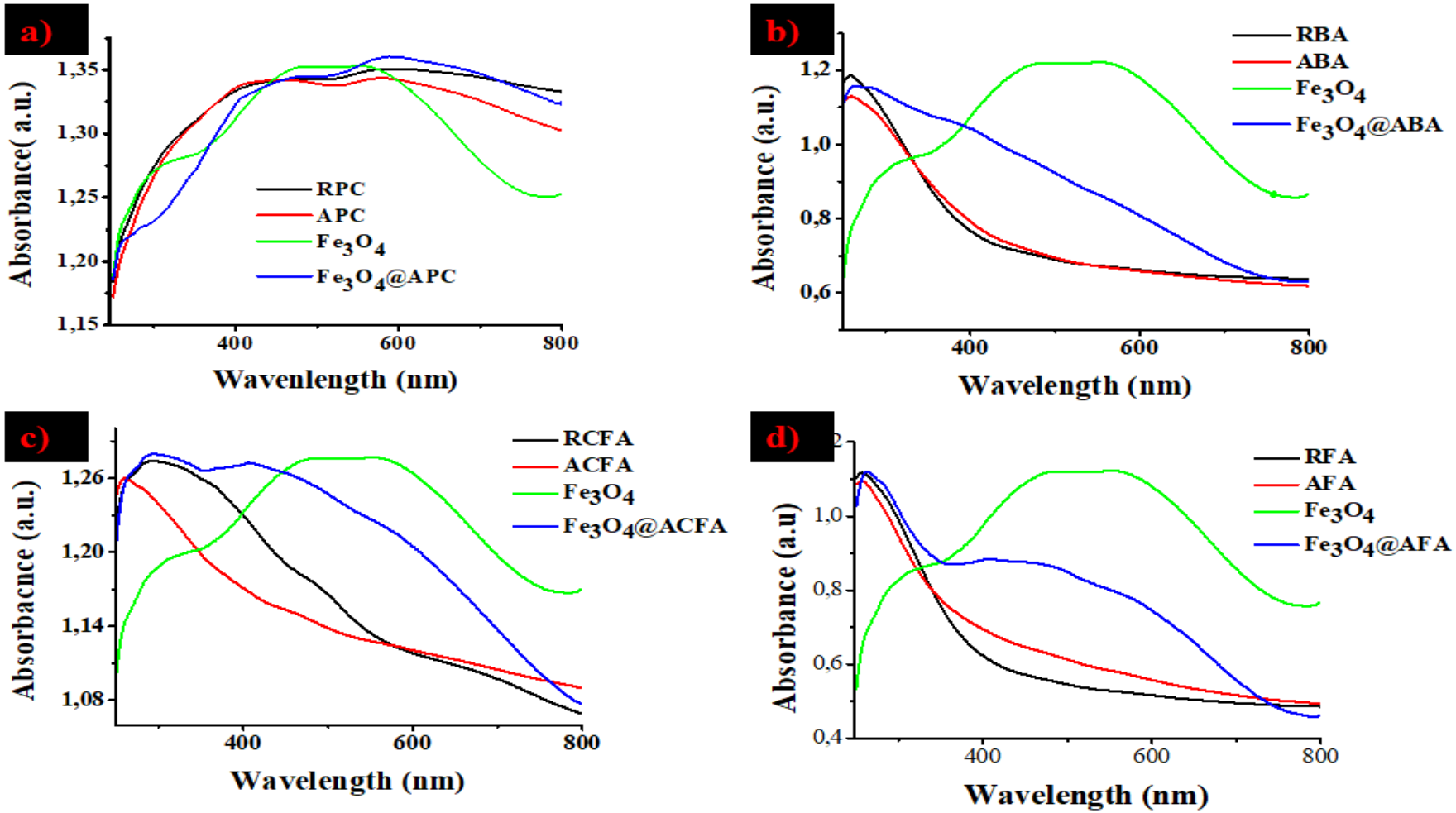

Figure 3.7: UV-vis spectra of a) RPC, APC, Fe_3O_4@APC, b) RBA, ABA, Fe_3O_4@ABA c) RCFA, ACFA, Fe_3O_4@ACFA, d) RFA, AFA, and Fe_3O_4@AFA.

3.3.6. Transmission electron microscopy

Figure 3.8 shows the TEM bright-field images of Fe_3O_4@APC, Fe_3O_4@ABA, Fe_3O_4@ACF and Fe_3O_4@AFA along with corresponding selected area electron diffraction (SAED) pattern. There is uniform coating of Fe_3O_4 nanoparticles onto APC, ABA, ACFA and AFA surface which is clearly showed with the aid of these images. The SAED pattern depicts the polycrystalline nature of the adsorbents. These particles can be crystalline or semicrystalline, which can be observed in the corresponding selected area electron diffraction patterns.

The SAED pattern with cloudy ring represents the presence of amorphous particles, and the presence of a dotted ring shape indicates the presence of semicrystalline or crystalline particles, which could be quartz and mullite [11,12]. **Figure 3.8** also shows the particle size distribution of the Fe_3O_4@APC, Fe_3O_4@ABA, Fe_3O_4@ACF and Fe_3O_4@AFA., which was calculated using image J software. An average particle size of 35 nm was obtained which is comparable with SEM results.

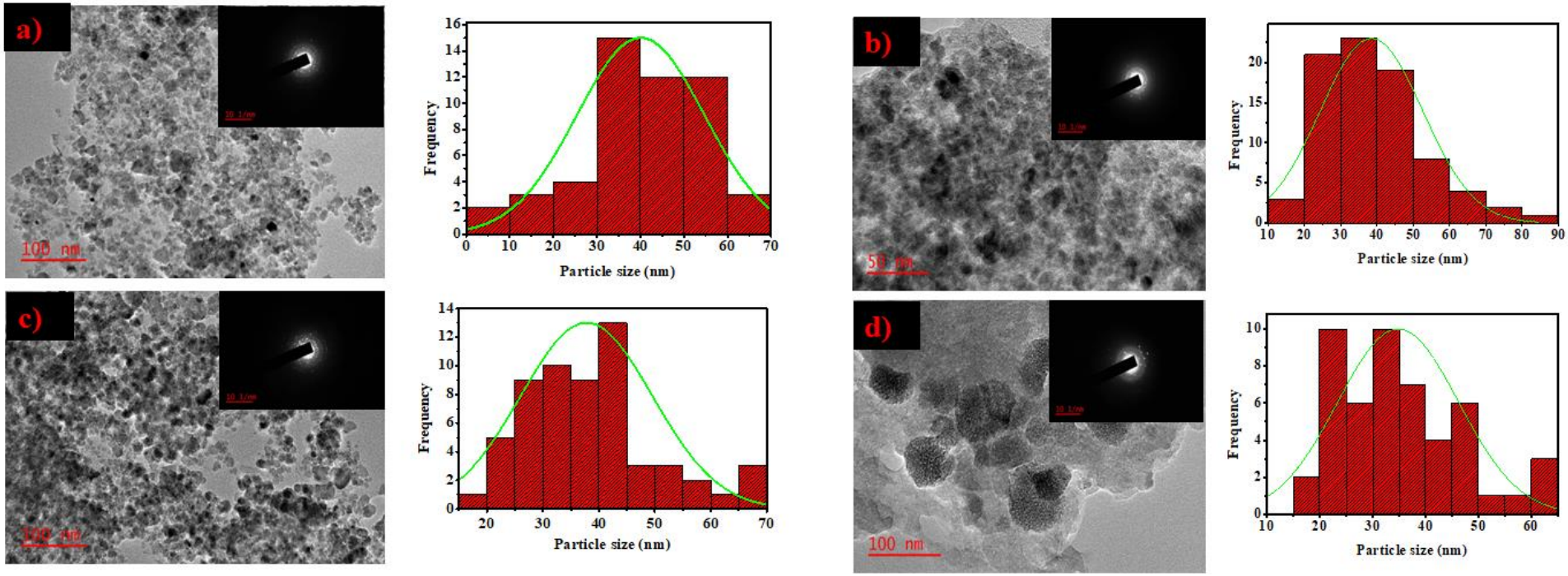

Figure 3.8: TEM images of a) Fe_3O_4@APC, b) Fe_3O_4@ABA, c) Fe_3O_4@ACF and d) Fe_3O_4@AFA.

3.4. Conclusion

In summary, mesoporous magnetic adsorbents; Fe_3O_4@APC, Fe_3O_4@ACFA, Fe_3O_4@AFA and Fe_3O_4@ABA were successfully prepared from petroleum coke, coal fly ash, fly ash and bottom ash by NaOH activation and subsequent Fe_3O_4 nanoparticle coating. They were successful characterized by SEM-EDS, FTIR, TEM and Uv-Vis to confirm the successful preparation of magnetic mesoporous adsorbent. The adsorbents show large surface area and microporosity and they were further applied as adsorbents in the removal of lead (**Chapter 4**) and efavirenz (**Chapter 5**) from water.

REFERENCE

[1] X. Huang, H. Zhao, X. Hu, F. Liu, L. Wang, X. Zhao, P. Gao, P. Ji, Optimization of preparation technology for modified coal fly ash and its adsorption properties for Cd2+, (2020) 122461. https://doi.org/10.1016/j.jhazmat.2020.122461.

[2] G. Buema, N. Lupu, H. Chiriac, D.D. Herea, L. Favier, G. Ciobanu, L. Forminte Litu, M. Harja, Fly Ash Magnetic Adsorbent for Cadmium Ion Removal From an Aqueous Solution, (2021) 42–50. https://doi.org/10.46909/journalalse-2021-004.

[3] M. Wu, Y. Wang, D. Wang, M. Tan, P. Li, W. Wu, N. Tsubaki, SO3H-modified petroleum coke derived porous carbon as an efficient solid acid catalyst for esterification of oleic acid, (2016) 263–271. https://doi.org/10.1007/s10934-015-0078-7.

[4] A. Zaeni, S. Bandyopadhyay, A. Yu, J. Rider, C.S. Sorrell, S. Dain, D. Blackburn, C. White, Colour control in fly ash as a combined function of particle size and chemical composition, (2010) 399–404. https://doi.org/10.1016/j.fuel.2009.07.006.

[5] V.K. Yadav, A. Amari, A. Gacem, N. Elboughdiri, L.B. Eltayeb, M.H. Fulekar, Treatment of Fly-Ash-Contaminated Wastewater Loaded with Heavy Metals by Using Fly-Ash-Synthesized Iron Oxide Nanoparticles, (2023). https://doi.org/10.3390/w15050908.

[6] N. Nadeem, M. Yaseen, Z.A. Rehan, M. Zahid, R.A. Shakoor, A. Jilani, J. Iqbal, S. Rasul, I. Shahid, Coal fly ash supported CoFe2O4 nanocomposites: Synergetic Fenton-like and photocatalytic degradation of methylene blue, (2022) 112280. https://doi.org/10.1016/j.envres.2021.112280.

[7] A. Sciubidło, W. Nowak, Novel sorbents for flue gas purification, Journal of Power Technologies 92 (2012) 115–126.

[8] Siahaan, Removal of Pb2+ from Aqueous Solutions Using K-Type Zeolite Synthesized from Coal Fly Ash, (2019).

[9] V.A. Niraimathee, V. Subha, R.S. Ernest Ravindran, S. Renganathan, Green synthesis of iron oxide nanoparticles from Mimosa pudica root extract, International Journal of (2016) 227–240. https://doi.org/10.1504/IJESD.2016.077370.

[10] S. Boycheva, Á. Szegedi, K. Lázár, C. Popov, M. Popova, Advanced high-iron coal fly ash zeolites for low-carbon emission catalytic combustion of VOCs, (2023). https://doi.org/10.1016/j.cattod.2023.114109.

[11] D. Das, P.K. Rout, Synthesis, Characterization and Properties of Fly Ash Based Geopolymer Materials, (2021) 3213–3231. https://doi.org/10.1007/s11665-021-05647-x.

[12] S. Madan, U. Thapa, S. Tiwari, S.K. Tiwari, S.K. Jakka, M.J. Soares, Designing of a nanoscale zerovalent iron@fly ash composite as efficient and sustainable adsorbents for hexavalent chromium (Cr(VI)) from water, (2021) 22474–22487. https://doi.org/10.1007/s11356-020-11692-1.

CHAPTER 4:

Adsorptive removal of Pb(II) ions from aqueous solutions using magnetic mesoporous pet coke and coal fly ash-based adsorbents

ABSTRACT

Coal fly ash (CFA) is a highly versatile and effective adsorbent due to its mesoporous nature, which is composed of minerals containing oxides in crystalline phase, such as quartz and mullite, as well as unburned carbon. This unique composition enables CFA to act as an adsorbent, making it an essential material in various industrial and environmental applications. Petcoke (PC) is a by-product of the petroleum refining process, created from various types of oils (light/heavy crudes) during refining. PC comes in two forms: green PC, used as fuel, and calcined PC, employed by manufacturers as a feedstock for products like aluminum, paints, coatings, and colorants. PC is a non-porous solid, typically activated before use in different applications. The removal of lead (II) ions from aqueous solutions was carried out using Fe_3O_4@ACFA, Fe_3O_4@AFA, Fe_3O_4@ABA, and Fe_3O_4@APC prepared from coal fly ash, fly ash, bottom ash, and petroleum coke, respectively. The effects of parameters such as sample pH, contact time, initial concentration of lead (II) ions, and extraction temperature on the adsorption process of lead were investigated using the multivariate optimization tool. The optimum conditions obtained were pH value: 5.5, contact time: 10 min, extraction temperature: 60 ˚C, initial concentration: 3 mg/L, and adsorbent mass: 60 mg. The Langmuir, Temkin, and Freundlich isotherm models were applied to analyse the equilibrium data. The maximum adsorption capacity of the adsorbents obtained were 48.8 mg/g, 15.625 mg/g, 12.155 mg/g, and 270.270 mg/g for Fe_3O_4@ACFA, Fe_3O_4@AFA, Fe_3O_4@ABA and Fe_3O_4@APC, respectively. The kinetic data was evaluated, and the pseudo-second-order equation provided the best correlation. Thermodynamic parameters suggest that the adsorption process is endothermic and spontaneous. The findings demonstrate that coal fly ash and pet coke possess the potential to effectively eliminate Pb from aqueous solutions.

Keywords: Lead; coal fly ash; petroleum coke; magnetic mesoporous adsorbents; aqueous solutions.

4.1. Introduction

Reports on the potential toxicity of heavy metal ions in various water bodies now predominate the literature studies, and this is because of the known harmful effects of these metal ions on humans, animals, and environmental health [1]. Lead (Pb) is one of the heavy metals that are persistent and difficult for biological organisms to eliminate as it easily accumulates in vital organs. Once lead enters the body, it is distributed to various organs, including the brain, kidneys, liver, and bones. It accumulates over time, particularly in teeth and bones, and can remain stored in bones for years, continuously releasing into the bloodstream [2]. Unfortunately, aqueous solutions are among the simplest ways for heavy metals such as lead get into the environment [3]. As a result of heavy metal ions entering the aquatic environment, there is a greater chance in exposure to adverse health problems associated with Pb such as brain, nervous system damage, hypertension, and kidney damage. Furthermore, Disruption to the world's need for provision of safe water for consumption and safe environment for aquatic plants and species. Aforementioned reasons, the issues related with water pollution are becoming more and more prevalent every day, particularly when considering how important water is for consumption, irrigation, agriculture, home and industrial uses, aquaculture, and the existence of living things [4,5].

The beneficial roles of water can deeply be limited by the presence of heavy metal contaminants and can progress further to initiate toxic impacts ranging from mild health effects to severe and even resulting in death in certain incidents. Much has been reported on the short, medium, and long-term toxicity impacts of lead [6]. According to the Agency for Toxic Substances and Disease Registry, lead has been ranked second in terms of toxicity among all the compounds under consideration [7,8]. Although the United States Environmental Protection Agency (USEPA) set a maximum limit of 15 mg/L, the World Health Organization (WHO) said that the maximum acceptable level of total Pb is 0.05 mg/L [9].

To maintain concentration levels below the maximum acceptable limit, various procedures must be implemented including chemical precipitation [10], ion exchange [11], and electrochemical processes [12], are used to remove heavy metals from various water bodies. Adsorption of metal ions on a solid adsorbent is an alternative to the aforementioned methods, because it has several advantages such as low-cost process, simplicity of use, batch application potential, process continuity, use at low concentrations, and adsorbent regeneration and reuse [13,14]. Activated carbon [15–18], zeolites [19–24], ion exchange resins [25,26], mesoporous

materials made from artificial zeolites [22,27–32], silico-aluminate minerals [30,33–35], and graphene oxides [36–39] are some of the most widely used solid adsorbent materials because of their high removal efficiency. Their high production costs are, however, the principal drawback. The alternative is to apply inexpensive waste adsorbents from industrial processes, such as fly ash, petroleum coke, red mud, coal gangue, fruit and vegetable pomace, or slag, to overcome the high costs associated with some of the conventional adsorbent materials [40–46].

Fly ash is widely utilized as an inexpensive absorbent for the adsorption of organic compounds, heavy metal ions, dyes in water, SO_x, NO_x, and mercury in air. However, chemical treatment of fly ash is an important step to functionalize fly ash to be a more effective absorbent for gas and water remediation/ purification [47]. In some literature studies, various authors have carried out experiments to treat fly ash by NaOH, NaOH/NH_4HCO_3, ethylenediamine tetracetic acid (EDTA), and HCl solutions to modify specific surface area and porous structure of fly ash. As a result, in all cases, the specific surface area and pore volume of treated fly ash were greater than those of original fly ash. The porosity of the treated fly ash was 10 times higher than that of the untreated fly ash. The treated fly ash was suitable for application as an adsorption material [48]. When activated, the fly ash has strong electrostatic charges, which results in electrostatic charges that are negative. Oxides of silicates and aluminium (as alumina silicates) are the dominant minerals on fly ash's surface. These oxides form anions, which have negative charges when they come into contact with water molecules. Anions have an electrostatic feature that draws cations of heavy metal ions which have opposite charges, to their active sites [49].

Petroleum coke, a by-product of the petroleum refining process, is another industrial waste with the potential to be applied as an absorbent for the removal of heavy metals from water. Petroleum coke fly ashes are composed mostly of sulphur (S) and Calcium (Ca) but also include significant amounts of unburned carbon and trace amounts of heavy metals like Nickel (Ni) and Vanadium (V) [50]. Petroleum coke is the perfect source for creating porous carbon due to its high fixed carbon concentration. Chemically it has already been carbonised; hence it is believed that creating porous carbon from this material will be inexpensive [51]. Therefore, it can be potentially used as activated carbon. The pores, channels, and other vacant spaces of activated carbon produced from petroleum coke provide a significant surface area for mechanically or chemically adsorbing pollutants from wastewater [52].

Petroleum coke activated with potassium hydroxide (KOH) was established and resulted in activated carbon which had a high surface area and pore volume [53]. It was also proved that employing petroleum coke containing sulphur as a precursor might yield a sulfo group, which becomes a better adsorption site of heavy metals, onto oxidised activated carbon surface [54]. The efficacy of metal-impregnated petroleum coke-activated carbon for the adsorption of arsenite and arsenate in acidic waters was investigated by Fisher and Vreugdenhil [55]. Petroleum coke was modified with $FeCl_3$–$KMnO^{4-}$ to enhance the adsorption capacity for arsenate. Adsorption was significantly improved by the addition of an iron–manganese-loaded activated carbon, increasing adsorption from 8 to 51%.

The aim of this study was to evaluate the adsorption capacity of the coal fly ash and petroleum coke modified with iron oxide nanoparticles for the removal of Pb^{2+} ions from aqueous solutions under different conditions. The adsorption kinetics, thermodynamic and adsorption isotherms were studied. Furthermore, the purpose was to determine the physiochemical properties of the adsorbent using a variety of analytical methods.

4.2. Experimental procedure

4.2.1. Materials and methods

All reagents used were of analytical grade purity and Milli-Q water obtained from a water purification system (USA) with water conductivity of 18.2 µS/cm, was used for rinsing and making up solutions. Lead ICP-certified reference standard of 1000 mg/L was used in the preparation of synthetic samples and of different concentrations of standard solution (5 – 25 ppm). 70% ACS nitric acid (HNO_3) and 30% suprapur sodium hydroxide solution (NaOH) were also used, all these reagents were purchased from Sigma-Aldrich, South Africa. All other generic procedures and characterization have already been described in **Chapter 3**, section **3.1** and **3.2,** respectively.

4.2.2. Adsorptive removal of Pb(II)

Batch sorption experiments were conducted using, 10 mL of a solution containing various concentrations of Pb were mixed with 60 mg of magnetic mesoporous adsorbent. For 10 min, the mixture was shaken using a shaker to ensure adsorption equilibrium was reached. Following that step, the mixture was filtered using nylon microfilters (0.45 µm), analyzed the samples with ICP – OES. The influence of pH on the heavy metal adsorption process was

examined at various pH values ranging from 3 to 8, which were adjusted either by 1 M HCl or 1 M NaOH using a pH metre to track the changes. Adsorbent mass ranging from 20 – 60 mg was studied for the extraction of Pb. The removal of metal ions was calculated using the following **Equation 4.1**:

$$\% R = \frac{C_0 - C_e}{C_0} \times 100 \qquad \textbf{Equation 4.1}$$

Where C_0 is the initial concentration of Pb ions in solution and C_e is the concentration at equilibrium. The amount of Pb ions adsorbed per gram of adsorbent was calculated using the following **Equation 4.2**:

$$q_e = \frac{(C_0 - C_e)V}{m} \qquad \textbf{Equation 4.2}$$

Where q_e (mg/L) is the amount of adsorbed metal ion at equilibrium conditions, m is the sorbent mass (g), C_0 and C_e are the initial and equilibrium concentrations of metal ions in solution (mg/L).

4.2.3. Instrumentation

The multielement capability and sensitivity of the Inductively Coupled Plasma Optical Emission spectroscopy (ICP-OES) made it to be favourable for trace elements determination in magnetic sold phase extraction (m-SPE) extracts. The operating parameters for the instrument, and wavelengths monitored for each element are presented in **Table 4.1** The Agilent Technologies 700 Series ICP-OES with an axial orientation of the torch was used for analysis lead. Additionally, an Agilent Technologies SPS 3 autosampler was used for sample uptake.

Table 4.1: Operating parameters of ICP-OES for metal analysis.

ICP-OES instrumental parameters	Condition
RF Power	1200 W
Auxiliary gas Flow	1.5 L/min
Plasma gas (Ar) flow rate	15.0 L/min
Pump speed	85 rpm
Peri-pump speed analysis	15 rpm
Sample uptake delay (s)	15 s

Stabilization time (s)	15 s
Nebulizer	0.75L/min
Elemental wavelengths (Pb)	283.30

4.2.4. Optimization

The multivariate optimisation approach was used for the determination of parameters that are significant for the adsorption of Pb ions on to the Fe_3O_4@ACFA, Fe_3O_4@ABA, Fe_3O_4@AFA and Fe_3O_4@APC. Due to the numerous advantages that multivariate optimisation offers over the univariate technique. The design of the experiments and data analysis were done using Minitab 2018 statistical software for both the two-level full factorial and central composite designs.

Full factorial design

To screen the primary variable and interactions, a two-level full factorial (2^n) design was used. The parameters that were optimised were contact time, temperature, adsorbent mass, pH and initial metal ion concentration. The variable was given the lower level (-) and the higher level (+), and the central point was not included. Factors and levels of experimental designs used for the optimization process are presented in **Table 4.2** and a total of 32 experiments were generated.

Table 4.2: Two-level full factorial (2^5) experimental design.

Factors	Minimum (-)	Maximum (+)
pH	3	8
Adsorbent mass (mg)	20	50
Initial concentration (mg/L)	5	25
Contact time (min)	10	60
Temperature (˚C)	25	60

Response surface methodology

For further optimization of the significant parameters at 95% confidence level, response surface methodology (RSM) was used. There are several RSM techniques that are reported in the literature including central composite design (CCD), three-level factorial design, Box–Behnken design (BBD), and Doehlert matrix [56]. In this study CCD was used for further

optimization of the most significant variables. From the results of these experiments, the data was analyzed and the optimum conditions were identified for each variable selected.

4.3. Kinetic and thermodynamic studies

The kinetics of the adsorption process were studied to determine the effect of the initial concentration of metal ions on the q_e with respect to time and the amount of time required to reach equilibrium adsorption [57,58]. The kinetic studies were conducted by considering the quantity of Pb metal ions adsorbed throughout time. Two simple kinetic models, pseudo-first order and pseudo-second order, were used to analyse the rate of sorption. The pseudo-first-order kinetic **Equation 4.3** and the pseudo-second-order kinetic **Equation 4.4** are expressed as:

$$\ln (q_e - q_t) = \ln q_e - K_1 t \qquad \textbf{Equation 4.3}$$

$$q_t = \frac{K_2 q_e^2 t}{1+K_2+q_e t} \qquad \textbf{Equation 4.4}$$

Where q_e and q_t are the metal ions adsorbed in mg g^{-1} on the adsorbent at equilibrium and time t, respectively, K_2 is the rate constant of second-order adsorption in mg^{-1} min^{-1} and K_1 is the constant of first-order adsorption in min^{-1} [59,60].

Temperature dependence of the thermodynamic parameter on the adsorption of metal ions was calculated using equations **Equation 4.5** and **Equation 4.6**:

$$\ln K_c = -\Delta H° RT + \frac{\Delta S°}{R} \qquad \textbf{Equation 4.5}$$

$$\Delta G° = - RT \ln K_c \qquad \textbf{Equation 4.6}$$

The value $\Delta H°$ and $\Delta S°$ were calculated from the slope and intercept of the plot of $\ln K_c$ versus T^{-1}. The negative values of Gibbs free energy change were used to indicate the feasibility and spontaneity of the adsorption process [61].

4.4. Adsorptive isotherms

To understand the nature of the interaction between metal ions and the adsorbent material, adsorption isotherms were conducted. Three adsorption isotherm methods, the Langmuir, Freundlich and Temkin equations were used to examine the adsorption data [58,62].

4.4.1. Langmuir isotherm

According to the Langmuir adsorption model expressed in **Equation 4.7**, intermolecular interactions rapidly decrease away from the sorption surface, and sorption only occurs at certain homogeneous sorption sites inside the sorbent. The model also assumes that sorption occurs on a structurally homogeneous sorbent and that all sorption sites are energetically independent [63].

$$\frac{C_e}{q_e} = \frac{1}{q_m K_L} + \frac{C_e}{q_e}$$ **Equation 4.7**

Where C_e is equilibrium concentration of metal ions in solution (mg/L); qe is the amount of metal ions adsorbed onto adsorbents at equilibrium (mg/g); K_L is the Langmuir equilibrium constant related to sorption energy; and q_m is the maximum sorption capacity (mg/g) [64,65].

4.4.2. Freundlich isotherm

This isotherm illustrates a heterogeneous surface's equilibrium without taking monolayer capacity into account. The isotherm expresses surface heterogeneity, active site exponential distribution, and their energies [66,67]. The Freundlich isotherm is expressed as follows in **Equation 4.8**:

$$\log q_e = \log K_F + \frac{1}{n} \log C_e$$ **Equation 4.8**

Where q_e is the amount of metal ions adsorbed at equilibrium per unit weight of adsorbent (mg/g); C_e is the equilibrium concentration of metal ions in solution (mg/L); and K_F and n are Freundlich constants corresponding to adsorption capacity and intensity, respectively. The adsorption process is favourable if n^{-1} is between 0.1 and 1. If n =1, then adsorption is linear;

if n < 1, then adsorption is a chemical process, if n > 1, then adsorption is a physical process [68].

4.4.3. Temkin isotherm

The Temkin isotherm model describes adsorption as characterized by a homogeneous distribution of binding energies up to a maximum binding energy. This maximum binding energy reduces linearly with coverage due to adsorbent-adsorbate interactions.[66]. The linear equation is given by **Equation 4.9** as follows:

$$q_e = B \ln K_T + B \ln C_e \qquad \textbf{Equation 4.9}$$

Where C_e is molar concentration of the adsorbate at equilibrium (mg/L), q_e is the quantity of adsorbed absorbate at equilibrium (mg/g), B = RT/bT where T is the temperature (K), and R is the ideal gas constant (8.314 J/mol.K) and KT and bT are constants.

4.5. Reusability

The reusability of the adsorbent was tested by repeating the adsorption and desorption studies. Several experiments were first conducted to check the reusability and these experiments were conducted under optimum conditions. Desorption experiments were carried out by adding fresh 10 mL of 0.5% nitric acid after the supernatant from the adsorption studies had been decanted then the adsorption capacity was calculated using **Equation 4.2.** After every experiment, the adsorbent was washed to remove residues and oven-dried at 100 ℃ for 6 hours.

4.6. Results and discussion

4.6.1. Multivariate optimization

Two-level full factorial

A two-level full factorial design (FFD) was used to investigate the effects of various experimental parameters such as contact time, temperature, adsorbent mass, pH and initial metal ion concentration on the adsorption process. The analysis of variance (ANOVA) results were then presented in the form of Pareto charts for the removal of Pb ion as shown in **Figure 4.1**. The results indicated that pH, concentration, and adsorbent mass were statistically significant at 95% confidence level for the high removal efficiency of Pb ions. These parameters were further optimized since they were most significant for the removal of Pb ions.

The vertical line in **Figure 4.1** represents the 95% confidence level, while the bar length is proportional to the absolute value of the estimated effects [69]. The bar length helps in comparing the relative importance of the effects.

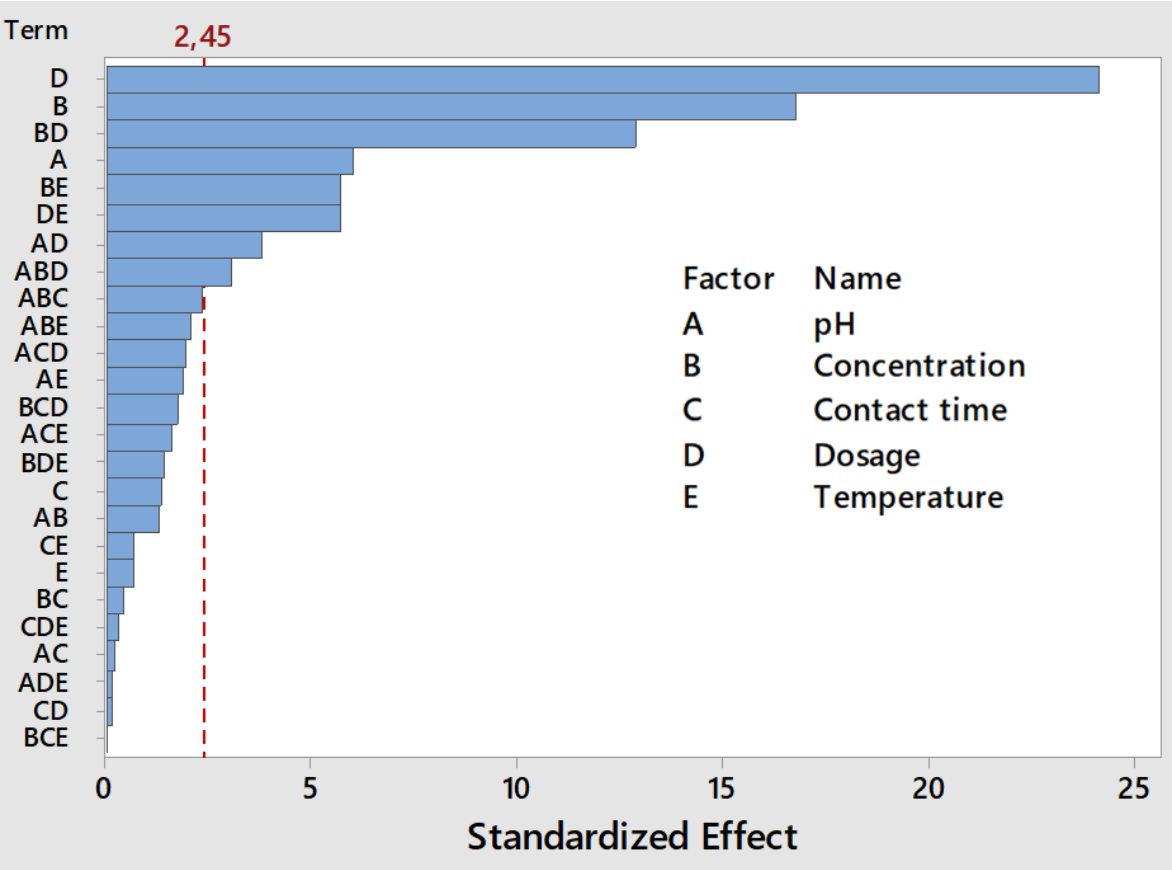

Figure 4.1: Pareto charts for removal of Pb ions from 2-level full fractional factorial full design (2^n) at 95% confidence level for optimization of adsorbent mass (dosage), contact time, pH, concentration and temperature. note: the vertical line indicates 95% confidence level.

Further optimization using Response Surface Methodology based on Central – central-composite design

The central composite design (CCD) was used to further optimize the significant factors which are the sample pH, initial metal concentration, and adsorbent mass. The contact time and temperature were kept constant at 10 min and 60 ˚C, respectively, because they were found to be insignificant for high removal of Pb ions after the screening process.

The contour plot (**Figure 4.2a**) shows that when the sample pH value was approximately 5.5, the percentage removal of Pb ions was dependent on the adsorbent mass. The results show that

at low to medium adsorbent mass, the percentage removal was ranging from 40 – 80 % for concentrations beyond 10 mg/L. However, when the adsorbent mass was high, the percentage removal was increased to a range of 80 – 120% for concentrations beyond 10 mg/L.

The contour plot (**Figure 4.2b**) shows the interaction between concentrations and pH at approximately 60 mg adsorbent mass. It has been observed that a significant amount of approximately 80% of pollutants were removed when the concentration of the solution was between 0 – 5 mg/L, and the pH level was acidic, i.e., between pH 2 to pH 6. On the other hand, high percentage removals were observed above pH 8, which can be attributed to the precipitation of $Pb(OH)_3^{1-}$ in the solution. Based on the FFD and CCD contour plots, the experimental conditions were chosen as sample pH, 5.5; contact time, 10 min; temperature, 60 ˚C; initial concentration, 3 mg/L; and adsorbent mass, 60 mg. These optimum conditions were then applied for the adsorption of Pb ions in water using Fe_3O_4@APC, Fe_3O_4@AFA, and Fe_3O_4@ABA.

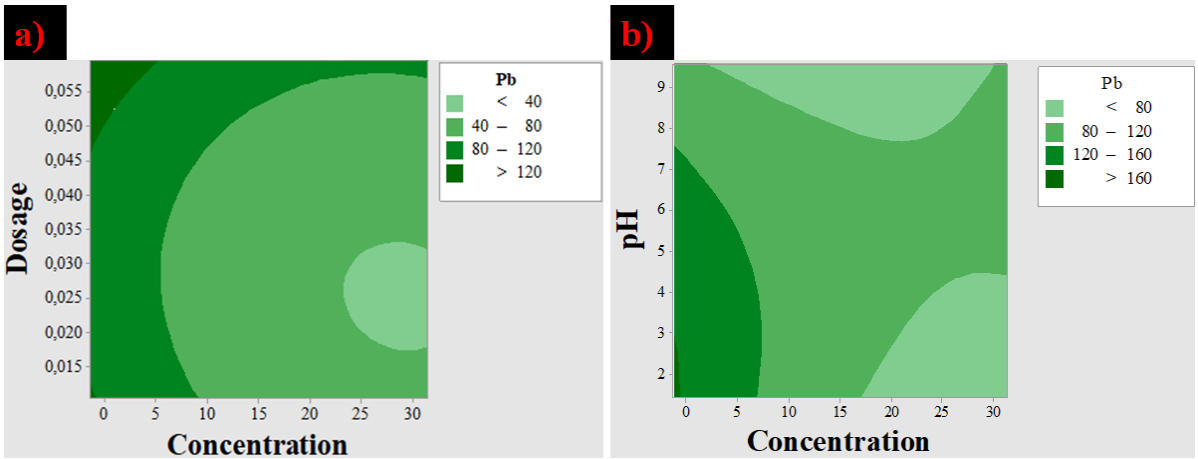

Figure 4.2: Contour plots of the %R of Pb ions a) dosage against concentration and b) pH against concentration.

4.6.2. Kinetic studies

The evaluation of adsorption efficiency depends on the evaluation of the adsorption equilibrium and the identification of the adsorption process and kinetic behaviour [70]. The physical and chemical properties of the adsorbents affect the adsorption mechanism [71]. Adsorption kinetics describes the rate of solute diffusion and adsorption to the surface of the adsorbent, which dictates the amount of time the adsorbate spends at the interface between the adsorbent and sample solution [72]. In this study, two different kinetic models (pseudo first–

order, pseudo–second order) were used to investigate the rate of adsorption of Pb ions onto Fe_3O_4@ACFA, Fe_3O_4@APC, Fe_3O_4@ABA, and Fe_3O_4@AFA.

The results are presented in **Table 4.3** for the experimental. This finding show that the pseudo-second-order model may be the rate-limiting step during the adsorption process of Pb ions onto Fe_3O_4@ACFA, Fe_3O_4@APC, Fe_3O_4@ABA, and Fe_3O_4@AFA. This indicates that the adsorption process is complex and involves multiple steps. Fe_3O_4@APC has a very small K_1, indicating slow adsorption. Fe_3O_4@ABA shows excellent fit (high R^2) and a significant K_2, suggesting strong chemisorption. Fe_3O_4@ACFA and Fe_3O_4@ABA have high R^2 values, supporting pseudo-second-order kinetics. Fe_3O_4@ACFA has the highest q_e, indicating efficient adsorption.

Table 4.3: Kinetic parameters of Pb ion adsorption onto Fe_3O_4@ACFA, Fe_3O_4@APC, Fe_3O_4@ABA and Fe_3O_4@AFA.

Adsorbent	**Pseudo first order**		**Pseudo second order**		
	R^2	**K_1**	**R^2**	**q_e**	**K_2**
Fe_3O_4@ACFA	-0.1156	-8.53E-05	0.9843	2.44	1.276
Fe_3O_4@APC	0.9470	2.62E-06	0.9687	0.006101	-21.82
Fe_3O_4@ABA	0.9115	1.2569	0.9932	0.001597	1657
Fe_3O_4@AFA	0.7049	0.01236	0.9603	0.005027	22.81

4.6.3. Thermodynamic studies

Thermodynamic analyses are essential for determining whether an adsorption process is spontaneous or non-spontaneous. Thermodynamic parameters such as Gibbs free energy change (ΔG°, kJ/mol), enthalpy change (ΔH°, kJ /mol), and entropy change (ΔS°, J/mol/K) at standard state were calculated for Pb ion adsorption on Fe_3O_4@ACFA, Fe_3O_4@APC, Fe_3O_4@ABA and Fe_3O_4@AFA.

As given in **Table 4.4,** negative values of ΔG° were obtained, indicating that Pb ion adsorption on Fe_3O_4@CFA, Fe_3O_4@APC and Fe_3O_4@ABA is a spontaneous process while the opposed was observed for Fe_3O_4@AFA. It was found that the values of G° decreased as the operating temperature was increasing, showing that adsorption was more favourable at higher temperatures for Fe_3O_4@ACFA and Fe_3O_4@APC. The values of G° increased as the operating temperature was rising, showing that the adsorption was more favourable at low temperatures for Fe_3O_4@ABA and Fe_3O_4@AFA. The slope and intercept of the plot of ln K_L against 1/T were used to determine the values of ΔH° and ΔS°. The positive values of ΔH° confirmed the endothermic nature of the adsorption of Pb ions onto Fe_3O_4@ACFA, Fe_3O_4@APC and Fe_3O_4@AFA. While the negative value of ΔH° confirmed the exothermic nature of the adsorption of Pb ions onto Fe_3O_4@ABA. Additionally, the positive values of ΔS° indicated the increased randomness at the solid-solution interface during the fixation of adsorbates on the active sites of the adsorbent onto Fe_3O_4@ACFA, Fe_3O_4@APC and Fe_3O_4@AFA.

Table 4.4: Thermodynamic parameters for the adsorption of Pb(II) onto Fe_3O_4@ACFA, Fe_3O_4@APC, Fe_3O_4@ABA and Fe_3O_4@AFA.

Adsorbent	**ΔG° (kJ/mol)**			**ΔH° (kJ/mol)**	**ΔS°(J/mol/K)**	**R^2**
	25 °C	**45 °C**	**55 °C**			
Fe_3O_4@ACFA	-1.9997	-4.5481	-5.8672	36,3448	128,6539	0,9998
Fe_3O_4@APC	-9.7045	-11.9226	-13.9371	85.8217	305.784	0.9983
Fe_3O_4@ABA	-15.1125	-13.5796	-12.8982	-37.9883	-74.30	0.9994
Fe_3O_4@AFA	3.9875	4.2495	4.527	0.06123	-13.1739	0.8977

4.6.4. Adsorption isotherms

Adsorption isotherms are crucial for describing the interaction between an adsorbent and an adsorbate and are crucial for maximising the use of an adsorbent [59]. Adsorption studies were conducted by varying the initial metal ion concentration from 5 to 35 mg/L at 60 °C to get the Pb ion adsorption isotherms for synthesised materials. To understand the mechanism of adsorption, the experimental data was also fitted to three adsorption models. Three common adsorption isotherms were used to describe the amount of Pb ions adsorbed on the Fe_3O_4@ACFA, Fe_3O_4@APC, Fe_3O_4@ABA, Fe_3O_4@AFA and the concentration of Pb ions at equilibrium: Langmuir, Freundlich and Temkin. The Langmuir, Temkin, and Freundlich isotherm parameters are given in **Table 4.5**.

According to the results, both Fe_3O_4@ACFA and Fe_3O_4@AFA, are best described by the Temkin isotherm while Fe_3O_4@ABA and Fe_3O_4@APC are best described by the Langmuir and Freundlich isotherm, respectively. This was determined by comparison of the R^2 for each isotherm. The maximum adsorption capacities of the adsorbents found using the Langmuir equation were 48.8 mg/g, 15.625 mg/g, 12.155 mg/g, and 270.270 mg/g for Fe_3O_4@ACFA, Fe_3O_4@AFA, Fe_3O_4@ABA, and Fe_3O_4@APC respectively.

The Temkin isotherm was used to investigate the effects of indirect adsorbate/adsorbent interactions on the adsorption system. Additionally, it can be assumed that the heat of adsorption (ΔH_{ads}) of all particles in the layer decreases linearly as increasing the surface coverage [73]. In this study, Temkin isotherm was fitted to confirm that the adsorption of Pb^{2+} onto Fe_3O_4@ABA follow a chemisorption process. Furthermore, based on the obtained b_T value as demonstrated in **Table 4.5**, it can be confirmed that the adsorption was exothermic, suggesting that the sorption process was driven by electrostatic interaction between the adsorbent and Pb^{2+}. From the results, it was also observed that Langmuir dimensionless equilibrium constant (R_L) is less than one and greater than zero, which indicates the favourability of the adsorption. The value of the heterogeneity factor 1/n indicates that the Freundlich isotherm is indeed favourable.

A comparison for Pb ion adsorption capacities with other adsorbents is tabulated in **Table 4.6**. The prepared adsorbents are relatively similar to reported studies using various industrial waste materials. However, the maximum monolayer adsorption capacity of Fe_3O_4@APC from Langmuir isotherms for Pb ions is found to be the highest in comparison with the literature.

Table 4.5: Adsorption isotherms constants for the adsorption of Pb ions onto the Fe_3O_4@ACFA, Fe_3O_4@APC, Fe_3O_4@ABA, Fe_3O_4@AFA at 333.15 K.

Isotherm model	Parameters	Adsorbents			
		Fe_3O_4@ACFA	**Fe_3O_4@AFA**	**Fe_3O_4@ABA**	**Fe_3O_4@APC**
Langmuir					
	q_{max} (mg/g)	48.87	15.62	12.19	270.27
	K_L (L/mg)	0.009371	0.03988	3.9.48	0.0007823
	R_L	0.8773	0.6257	0.0167	0.9884
	R^2	0.9709	0.9567	0.9625	0.9662
Freundlich					
	K_F (L/mg)	0.5859	1.737	6.353	0.4466
	n	22.69	1.848	3.322	1.201
	R^2	0.9327	0.9309	0.9670	0.9861
Temkin					
	B_T	0.6383	6.962	2.084	5.348
	K_T	1.773	0.2123	58.98	0.1496
	R^2	0.9996	0.9336	0.9997	0.9711

Table 4.6: Comparison of the maximum adsorption capacities between reported industrial waste-derived adsorbents for the removal of Pb(II) ions in an aqueous solution.

Adsorbent	Adsorption capacity (mg/g)	Ref
CFA	12.16	[74]
Coal fly ash	99.082	[75]
FA48	55.53	[76]
ANA-AC	125.57	[77]
BFS	30.8	[78]

BFS	43.16	[79]
Modified slag	96.46	[80]
BFS-derived	34.26	[81]
RM/CM	208	[82]
NCRM	218.82	[83]
Fe_3O_4@ACFA	48.8780	Current study
Fe_3O_4@APC	270.270	Current study
Fe_3O_4@ABA	12.1951	Current study
Fe_3O_4@AFA	15.625	Current study

4.7. Comparison studies between raw, activated, and coated industrial waste–based adsorbent for the adsorption of Pb(II) ion in aqueous solutions

Figure 4.8 shows the results obtained from comparing the percentage removal (% R) of the raw material, activated material, and Fe_3O_4 nanoparticles coated material. This was conducted to evaluate the influence of activation and coating of coal fly ash, bottom ash, fly ash and petroleum coke in terms of % R. According to the results, there is a notable increase in the % R of the Pb (II) ions from aqueous solutions from the raw, activated and Fe_3O_4 coated materials. This can be accounted for by the formation of mesopores and the presence of Fe_3O_4 nanoparticles that enhance the negative surface charge of the adsorbents hence facilitating electrostatic interaction between Pb (II) ions and the surface of adsorbents.

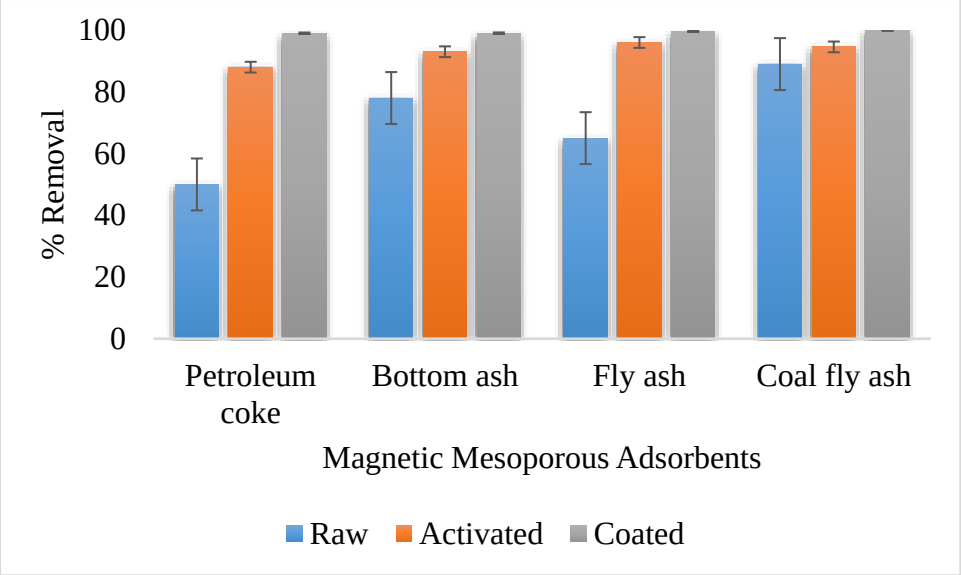

Figure 4.3: Comparison studies between raw, activated, and coated industrial waste–based adsorbent for the adsorption of Pb(II) ion in aqueous solutions.

4.8. Reusability studies

The reusability of the adsorbent plays a crucial role for industrial application considerations. Reusing adsorbents reduces costs requirements for new adsorbent synthesis, waste generation and contributes to a more environmentally friendly approach in water treatment and pollution control. The reusability studies of the magnetic mesoporous adsorbents are shown in **Figure 4.9**. Based on **Figure 4.9,** it was observed that the adsorbents can be used up to 4 adsorption-desorption cycles without a notable decline on the removal efficiencies for Pb^{2+} ions. In this case, the removal efficiencies remained between 92% and 99% upon 4 adsorption-desorption cycles of Pb ions when using the four adsorbents. Therefore, it can be concluded that the adsorbents had long-term reusability towards lead removal in wastewater.

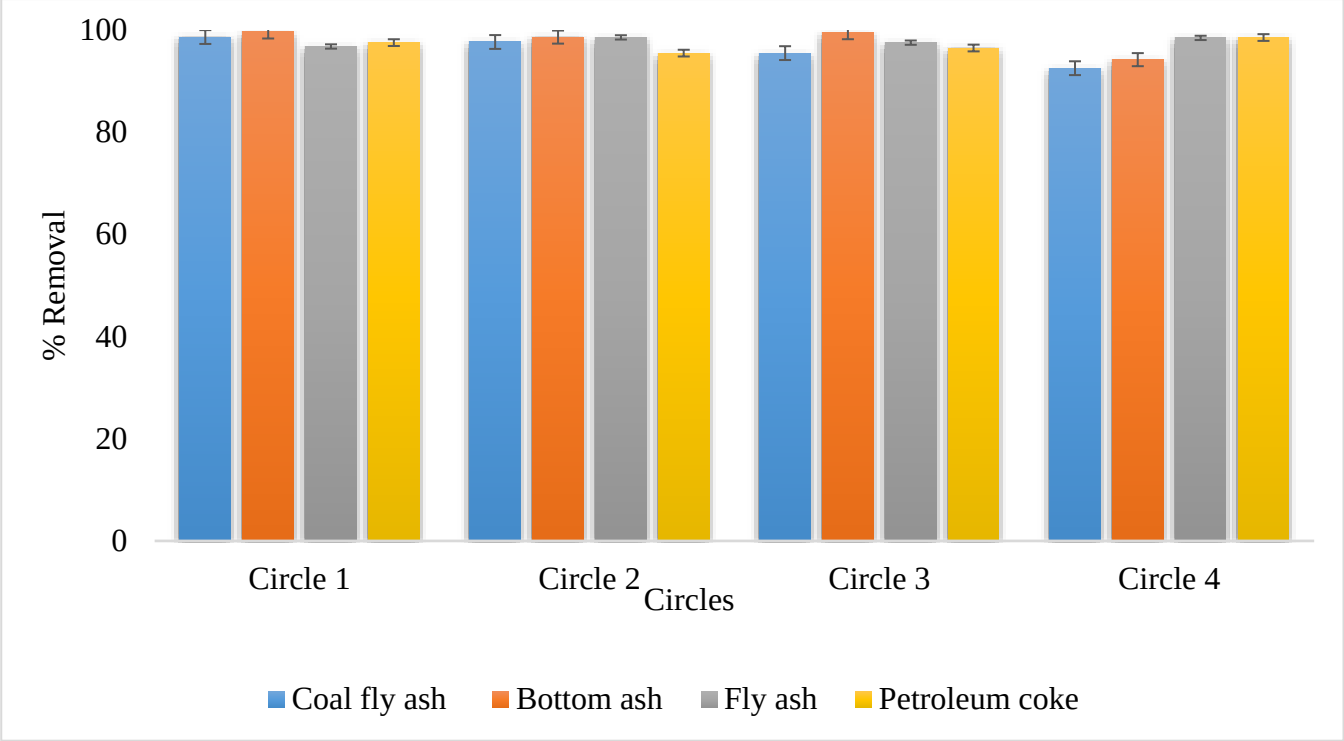

Figure 4.4: Reusability of the Fe_3O_4@ACFA, Fe_3O_4@APC, Fe_3O_4@ABA and Fe_3O_4@AFA for adsorption of Pb^{2+} in aqueous solutions.

4.9. Conclusion

Based on the results of multivariate optimization, the variables that were determined to have a significant impact on the high percentage removal adsorption of lead on coal fly ash were identified as adsorbent mass (dosage), initial metal concentration, and pH, and require further optimization. As shown in **Figure 4.8**, there is a marked rise in the elimination of Pb(II) ions from water-based solutions. This escalation in removal can be credited to the creation of mesopores and the existence of Fe_3O_4 nanoparticles, which amplify the negative surface charge of the adsorbents and enable electrostatic interactions between the Pb(II) ions and the adsorbents' surface. The adsorbents can be reused up to more than four cycles. Fe_3O_4@APC was found to have a higher adsorption capacity for adsorption of Pb(II) compared to Fe_3O_4@ACF, Fe_3O_4@AFA and Fe_3O_4@ABA.

REFERENCE

[1] K.H. Hama Aziz, F.S. Mustafa, K.M. Omer, S. Hama, R.F. Hamarawf, K.O. Rahman, Heavy metal pollution in the aquatic environment: efficient and low-cost removal approaches to eliminate their toxicity: a review, (2023) 17595–17610. https://doi.org/10.1039/D3RA00723E.

[2] R.B. Suami, P. Sivalingam, D.M. Al Salah, D. Grandjean, C.K. Mulaji, P.T. Mpiana, F. Breider, J.P. Otamonga, J. Poté, Heavy metals and persistent organic pollutants contamination in river, estuary, and marine sediments from Atlantic Coast of Democratic Republic of the Congo, (2020) 20000–20013. https://doi.org/10.1007/S11356-020-08179-4/FIGURES/3.

[3] N.D. Nnaji, H. Onyeaka, T. Miri, C. Ugwa, Bioaccumulation for heavy metal removal: a review, (2023) 1–12. https://doi.org/10.1007/S42452-023-05351-6/FIGURES/1.

[4] A. Alengebawy, S.T. Abdelkhalek, S.R. Qureshi, M.Q. Wang, Heavy Metals and Pesticides toxicity in agricultural soil and plants: ecological risks and Human Health Implications, Toxics 9 (2021) 42. https://doi.org/10.3390/toxics9030042.

[5] F.A. Armah, S. Obiri, D.O. Yawson, E.E. Onumah, G.T. Yengoh, E.K.A. Afrifa, J.O. Odoi, Anthropogenic sources and environmentally relevant concentrations of heavy metals in surface water of a mining district in Ghana: a multivariate statistical approach, (2010) 1804–1813. https://doi.org/10.1080/10934529.2010.513296.

[6] S. Raungsomboon, A. Chidthaisong, B. Bunnag, D. Inthorn, N.W. Harvey, Removal of lead (Pb2+) by the Cyanobacterium Gloeocapsa sp., (2008) 5650–5658. https://doi.org/10.1016/J.BIORTECH.2007.10.056.

[7] Toxicological Profile for Lead - NCBI Bookshelf, (n.d.). https://www.ncbi.nlm.nih.gov/books/NBK589538/ (accessed February 26, 2024).

[8] H. Abadin, A. Ashizawa, Y.-W. Stevens, F. Llados, G. Diamond, G. Sage, M. Citra, A. Quinones, S.J. Bosch, S.G. Swarts, Toxicological Profile for Lead, (2020) 582. https://www.ncbi.nlm.nih.gov/books/NBK589538/ (accessed February 26, 2024).

[9] T. Kalak, A. Kłopotek, R. Cierpiszewski, Effective adsorption of lead ions using fly ash obtained in the novel circulating fluidized bed combustion technology, (2019) 1011–1025. https://doi.org/10.1016/J.MICROC.2018.12.005.

[10] N.A.A. Qasem, R.H. Mohammed, D.U. Lawal, Removal of heavy metal ions from wastewater: a comprehensive and critical review, (n.d.). https://doi.org/10.1038/s41545-021-00127-0.

[11] K. Singh, N.A. Renu, M. Agarwal, Methodologies for removal of heavy metal ions from wastewater: an overview, (2017) 124. https://doi.org/10.1504/ier.2017.10008828.

[12] K.H. Hama Aziz, F.S. Mustafa, K.M. Omer, S. Hama, R.F. Hamarawf, K.O. Rahman, Heavy metal pollution in the aquatic environment: efficient and low-cost removal approaches to eliminate their toxicity: a review, (2023) 17595–17610. https://doi.org/10.1039/D3RA00723E.

[13] S.M. and R.M. Athar Hussain, We are IntechOpen , the world ' s leading publisher of Open Access books Built by scientists , for scientists TOP 1 % Removal of Heavy Metals from Wastewater by Adsorption, (2015).

[14] D. Mehta, S. Mazumdar, S.K. Singh, Magnetic adsorbents for the treatment of water/wastewater—A review, (2015) 244–265. https://doi.org/10.1016/J.JWPE.2015.07.001.

[15] Y. Cao, Activated carbon preparation and modification for adsorption, (2017) 111.

[16] D. Zhang, C. Deng, X. Deng, Z. Yu, Application and Development of Activated Carbon Adsorption in Wastewater, (2019) 19–23.

[17] J. Saleem, U. Bin Shahid, M. Hijab, H. Mackey, G. McKay, Production and applications of activated carbons as adsorbents from olive stones, (2019) 775–802. https://doi.org/10.1007/s13399-019-00473-7.

[18] Adsorption of Chromium (VI) Using an Activated CarbonDerived from Petroleum Coke Feedstock.pdf, (n.d.).

[19] D. Barthomeuf, Basic zeolites: Characterization and uses in adsorption and catalysis, (1996) 521–612. https://doi.org/10.1080/01614949608006465.

[20] K. Möller, T. Bein, Mesoporosity – a new dimension for zeolites, (2013) 3689–3707. https://doi.org/10.1039/c3cs35488a.

[21] K. Na, M. Choi, R. Ryoo, Recent advances in the synthesis of hierarchically nanoporous zeolites, (2013) 3–19. https://doi.org/10.1016/j.micromeso.2012.03.054.

[22] C. Perego, R. Bagatin, M. Tagliabue, R. Vignola, Zeolites and related mesoporous materials for multi-talented environmental solutions, (2013) 37–49. https://doi.org/10.1016/j.micromeso.2012.04.048.

[23] M. Popova, S. Boycheva, H. Lazarova, D. Zgureva, K. Lázár, Á. Szegedi, VOC oxidation and CO2 adsorption on dual adsorption/catalytic system based on fly ash zeolites, (2020) 518–525. https://doi.org/10.1016/j.cattod.2019.06.070.

[24] L. Zhou, Y.L. Chen, X.H. Zhang, F.M. Tian, Z.N. Zu, Zeolites developed from mixed alkali modified coal fly ash for adsorption of volatile organic compounds, (2014) 140–142. https://doi.org/10.1016/J.MATLET.2013.12.097.

[25] J. Kammerer, R. Carle, D.R. Kammerer, Adsorption and ion exchange: Basic principles and their application in food processing, (2011) 22–42. https://doi.org/10.1021/jf1032203.

[26] H. Sepehrian, S.J. Ahmadi, S. Waqif-Husain, H. Faghihian, H. Alighanbari, Adsorption Studies of Heavy Metal Ions on Mesoporous Aluminosilicate, Novel Cation Exchanger, (2010) 252–256. https://doi.org/10.1016/j.jhazmat.2009.11.020.

[27] V. Meynen, P. Cool, E.F. Vansant, Verified syntheses of mesoporous materials, 2009) 170–223. https://doi.org/10.1016/j.micromeso.2009.03.046.

[28] J. Liu, X. Feng, G.E. Fryxell, L.Q. Wang, A.Y. Kim, M. Gong, Hybrid mesoporous materials with functionalized monolayers, (1998) 161–165. https://doi.org/10.1002/(SICI)1521-4095(199801)10:2<161::AID-ADMA161>3.0.CO;2-Q.

[29] H.L. Chang, C.M. Chun, I.A. Aksay, W.H. Shih, Conversion of fly ash into mesoporous aluminosilicate, (1999) 973–977. https://doi.org/10.1021/ie980275b.

[30] Z.A. Alothman, A review: Fundamental aspects of silicate mesoporous materials, (2012) 2874–2902. https://doi.org/10.3390/ma5122874.

[31] K.F. Lam, X. Chen, C.M. Fong, K.L. Yeung, Selective mesoporous adsorbents for Ag + / Cu 2 + separation, (2008) 2034–2036. https://doi.org/10.1039/b719961a.

[32] J. V Vaghasiya, Innovations in Engineered Mesoporous Material for Energy Conversion and Storage Applications, 1 (2017) 1–2. https://www.omicsonline.org/open-

access/innovations-in-engineered-mesoporous-material-for-energy-conversion-and-storage-applications.pdf.

[33] M.E. Aphane, F.J. Doucet, R.A. Kruger, L. Petrik, E.M. van der Merwe, Preparation of Sodium Silicate Solutions and Silica Nanoparticles from South African Coal Fly Ash, (2020) 4403–4417. https://doi.org/10.1007/s12649-019-00726-6.

[34] N. Toniolo, A.R. Boccaccini, Fly ash-based geopolymers containing added silicate waste. A review, (2017) 14545–14551. https://doi.org/10.1016/j.ceramint.2017.07.221.

[35] C. Tao, Y. Zhu, Magnetic mesoporous silica nanoparticles for potential delivery of chemotherapeutic drugs and hyperthermia, (2014) 15482–15490. https://doi.org/10.1039/c4dt01984a.

[36] Y.J. Zhang, P.Y. He, Y.X. Zhang, H. Chen, A novel electroconductive graphene/fly ash-based geopolymer composite and its photocatalytic performance, (2018) 2459–2466. https://doi.org/10.1016/j.cej.2017.11.171.

[37] F. Zhou, X. Feng, J. Yu, X. Jiang, High performance of 3D porous graphene/lignin/sodium alginate composite for adsorption of Cd(II) and Pb(II), (2018) 15651–15661. https://doi.org/10.1007/s11356-018-1733-8.

[38] E.C. Umejuru, E. Prabakaran, K. Pillay, Coal Fly Ash Decorated with Graphene Oxide-Tungsten Oxide Nanocomposite for Rapid Removal of Pb2+Ions and Reuse of Spent Adsorbent for Photocatalytic Degradation of Acetaminophen, (2021) 11155–11172. https://doi.org/10.1021/acsomega.0c04194.

[39] N. You, X. Wang, J. Li, H. Fan, H. Shen, Q. Zhang, Journal of Industrial and Engineering Chemistry Synergistic removal of arsanilic acid using adsorption and magnetic separation technique based on Fe 3 O 4 @ graphene nanocomposite, (2019) 346–354. https://doi.org/10.1016/j.jiec.2018.10.035.

[40] U.U. Jadhav, H. Hocheng, A review of recovery of metals from industrial waste, 54 (2012) 159–167.

[41] I. Nhapi, Removal of Heavy Metals from Industrial Wastewater Using Rice Husks, (2011) 170–180. https://doi.org/10.2174/1874829501104010170.

[42] J.H. Jacobs, K.G. Wynnyk, R. Lalani, R. Sui, J. Wu, V. Montes, J.M. Hill, R.A. Marriott, Removal of Sulfur Compounds from Industrial Emission Using Activated Carbon

Derived from Petroleum Coke, (2019) 18896–18900. https://doi.org/10.1021/acs.iecr.9b04443.

[43] L. K, A. Sear, Properties and Use of Coal Fly Ash: A Valuable Industrial By-product, Fly Ash and the Environment (2001) 268.

[44] H.A. Hegazi, Removal of heavy metals from wastewater using agricultural and industrial wastes as adsorbents, (2013) 276–282. https://doi.org/10.1016/j.hbrcj.2013.08.004.

[45] M. Harja, G. Buema, D. Bucur, Recent advances in removal of Congo Red dye by adsorption using an industrial waste, (2022) 1–18. https://doi.org/10.1038/s41598-022-10093-3.

[46] M.J.K. Ahmed, M. Ahmaruzzaman, A review on potential usage of industrial waste materials for binding heavy metal ions from aqueous solutions, (2016) 39–47. https://doi.org/10.1016/j.jwpe.2016.01.014 .

[47] T.C. Nguyen, T.D.M. Tran, V.B. Dao, Q.T. Vu, T.D. Nguyen, H. Thai, Using Modified Fly Ash for Removal of Heavy Metal Ions from Aqueous Solution, (2020). https://doi.org/10.1155/2020/8428473.

[48] Z. Sarbak, M. Kramer-Wachowiak, Porous structure of waste fly ashes and their chemical modifications, Powder Technol 123 (n.d.) 2002–53. www.elsevier.comrlocaterpowtec (accessed February 27, 2024).

[49] E.O. Orakwue, V. Asokbunyarat, E.R. Rene, P.N.L. Lens, A. Annachhatre, Adsorption of Iron(II) from Acid Mine Drainage Contaminated Groundwater Using Coal Fly Ash, Coal Bottom Ash, and Bentonite Clay, (2016). https://doi.org/10.1007/s11270-016-2772-8.

[50] A. González, R. Navia, N. Moreno, Fly ashes from coal and petroleum coke combustion: Current and innovative potential applications, (2009) 976–987. https://doi.org/10.1177/0734242X09103190.

[51] M. Yuan, S. Tong, S. Zhao, C.Q. Jia, Adsorption of polycyclic aromatic hydrocarbons from water using petroleum coke-derived porous carbon, (2010) 1115–1120. https://doi.org/10.1016/j.jhazmat.2010.05.130.

[52] Z. Heidarinejad, M.H. Dehghani, M. Heidari, G. Javedan, I. Ali, M. Sillanpää, Methods for preparation and activation of activated carbon: a review, (2020) 18:2 18 (2020) 393–415. https://doi.org/10.1007/S10311-019-00955-0.

[53] Z. Sun, A. Ma, S. Zhao, H. Luo, X. Xie, Y. Liao, X. Liang, Research progress on petroleum coke for mercury removal from coal-fired flue gas, (2022) 122084. https://doi.org/10.1016/j.fuel.2021.122084.

[54] K. Sato, K. Hagiwara, K. Watanabe, M. Kato, Y. Amano, M. Machida, Adsorption of Cd(II) by petroleum coke treated with KOH activation and oxidation, (2018) 128–131. https://doi.org/10.7209/tanso.2018.128.

[55] K.S. Fisher, A.J. Vreugdenhil, Metal-Impregnated Petroleum Coke-Derived Activated Carbon for the Adsorption of Arsenic in Acidic Waters, (2023) 29083–29100. https://doi.org/10.1021/acsomega.3c02078.

[56] M.S. Manzar, G. Khan, P.V. dos Santos Lins, M. Zubair, S.U. Khan, R. Selvasembian, L. Meili, N.I. Blaisi, M. Nawaz, H. Abdul Aziz, T.S. Kayed, RSM-CCD optimization approach for the adsorptive removal of Eriochrome Black T from aqueous system using steel slag-based adsorbent: Characterization, Isotherm, Kinetic modeling and thermodynamic analysis, (2021) 116714. https://doi.org/10.1016/j.molliq.2021.116714.

[57] S. Mpelane, N. Mketo, N. Bingwa, P.N. Nomngongo, Synthesis of mesoporous iron oxide nanoparticles for adsorptive removal of levofloxacin from aqueous solutions: Kinetics, isotherms, thermodynamics and mechanism, (2022) 8457–8468. https://doi.org/10.1016/j.aej.2022.02.014.

[58] S. Mpelane, N. Mketo, N. Bingwa, P.N. Nomngongo, Synthesis of mesoporous iron oxide nanoparticles for adsorptive removal of levofloxacin from aqueous solutions: Kinetics, isotherms, thermodynamics and mechanism, (2022) 8457–8468. https://doi.org/10.1016/j.aej.2022.02.014.

[59] M. Kapur, M.K. Mondal, Competitive sorption of Cu(II) and Ni(II) ions from aqueous solutions: Kinetics, thermodynamics and desorption studies, (2014) 1803–1813. https://doi.org/10.1016/j.jtice.2014.02.022.

[60] S. Kaur, S. Rani, R.K. Mahajan, M. Asif, V.K. Gupta, Synthesis and adsorption properties of mesoporous material for the removal of dye safranin: Kinetics, equilibrium, and thermodynamics, (2015) 19–27. https://doi.org/10.1016/j.jiec.2014.06.019.

[61] K. Al-zboon, M.S. Al-harahsheh, F. Bani, Fly ash-based geopolymer for Pb removal from aqueous solution, (2011) 414–421. https://doi.org/10.1016/j.jhazmat.2011.01.133.

[62] H. Xiyili, S. Çetintaş, D. Bingöl, Removal of some heavy metals onto mechanically activated fly ash: Modeling approach for optimization, isotherms, kinetics and thermodynamics, (2017) 288–300. https://doi.org/10.1016/j.psep.2017.04.012.

[63] F.A. Olabemiwo, B.S. Tawabini, F. Patel, T.A. Oyehan, M. Khaled, T. Laoui, Cadmium Removal from Contaminated Water Using Polyelectrolyte-Coated Industrial Waste Fly Ash, 2017). https://doi.org/10.1155/2017/7298351.

[64] K.Y. Foo, B.H. Hameed, Insights into the modeling of adsorption isotherm systems, (2010) 2–10. https://doi.org/10.1016/j.cej.2009.09.013.

[65] M. Brdar, M. Šćiban, A. Takači, T. Došenović, Comparison of two and three parameters adsorption isotherm for Cr(VI) onto Kraft lignin, (2012) 108–111. https://doi.org/10.1016/j.cej.2011.12.036.

[66] L. Darmayanti, S. Notodarmodjo, E. Damanhuri, R.R. Mukti, Removal of Copper (II) Ions in Aqueous Solutions by Sorption onto Alkali Activated Fly Ash, (2018) 1–6. https://doi.org/10.1051/matecconf/201814704007.

[67] R. Yousef, H. Qiblawey, M.H. El-Naas, Adsorption as a process for produced water treatment: A review, (2020) 1–22. https://doi.org/10.3390/pr8121657.

[68] T.A. Khan, S.A. Chaudhry, I. Ali, Equilibrium uptake, isotherm and kinetic studies of Cd(II) adsorption onto iron oxide activated red mud from aqueous solution, J Mol Liq 202 (2015) 165–175. https://doi.org/10.1016/j.molliq.2014.12.021.

[69] N.S. Mdluli, C.D. Knottenbelt, P.N. Nomngongo, N. Mketo, Microwave-assisted hydrogen peroxide digestion followed by ICP-OES for determination of metals in selected fuel oils, Scientific Reports | 14 (123AD) 2362. https://doi.org/10.1038/s41598-024-52898-4.

[70] A. Awwad, N. Salem, M. Amer, M. Shammout, Adsorptive removal of Pb (II) and Cd (II) ions from aqueous solution onto modified Hiswa iron-kaolin clay: Equilibrium and thermodynamic aspects, (2021) 139–144.

[71] H. Javadian, F. Ghorbani, H. allah Tayebi, S.M.H. Asl, Study of the adsorption of Cd (II) from aqueous solution using zeolite-based geopolymer, synthesized from coal fly ash; kinetic, isotherm and thermodynamic studies, (2015) 837–849. https://doi.org/10.1016/j.arabjc.2013.02.018.

[72] P. Tiwari, M.C. Vishwakarma, S.K. Joshi, H. Sharma, N.S. Bhandari, Adsorption of Pb (II), Cu (II), and Zn (II) Ions onto Urtica dioica Leaves (UDL) as a Low Cost Adsorbent : Equilibrium and Thermodynamic Studies, (2017) 11–18. https://doi.org/10.11648/j.mc.20170501.13.

[73] T.A. Saleh, Isotherm models of adsorption processes on adsorbents and nanoadsorbents, (2022) 99–126. https://doi.org/10.1016/B978-0-12-849876-7.00009-9.

[74] Z. Hussain, H. Zhang, N. Chang, H. Wang, Synthesis of porous materials by the modification of coal fly ash and its environmentally friendly use for the removal of heavy metals from wastewater, (2022) 1–13. https://doi.org/10.3389/fenvs.2022.1085326.

[75] W. Wang, Z. Zheng, C. Feng, X. Gao, Y. Qiao, M. Xu, Application of zeolite synthesized from coal fly ash via wet milling as a sustainable resource on lead(II) removal, (2023) 1246–1254. https://doi.org/10.1177/0734242X231160077.

[76] Siahaan, Removal of Pb2+ from Aqueous Solutions Using K-Type Zeolite Synthesized from Coal Fly Ash, (2019).

[77] Q. Li, L. Lv, X. Zhao, Y. Wang, Y. Wang, Cost-effective microwave-assisted hydrothermal rapid synthesis of analcime-activated carbon composite from coal gangue used for Pb2+ adsorption, (2022) 77788–77799. https://doi.org/10.1007/s11356-022-20942-3.

[78] S.M. Abdelbasir, M.A.A. Khalek, From waste to waste: iron blast furnace slag for heavy metal ions removal from aqueous system, (2022) 57964–57979. https://doi.org/10.1007/s11356-022-19834-3.

[79] T. Chouchane, O. Khireddine, S. Chibani, A. Boukari, Removal of Cr(III), Pb(II) and Cr-Pb Mixture by Blast Furnace Slag (BFS) in Solution, (2023) 251–268. https://doi.org/10.22036/ABCR.2022.365182.1843.

[80] Y. Wang, H. Li, S. Cui, Q. Wei, Adsorption behavior of lead ions from wastewater on pristine and aminopropyl-modified blast furnace slag, (2021). https://doi.org/10.3390/w13192735.

[81] Q.T.N. Le, E.L. Vivas, K. Cho, Calcium oxalate/calcium silicate hydrate (Ca-Ox/C-S-H) from blast furnace slag for the highly efficient removal of Pb2+ and Cd2+ from water, (2021) 106287. https://doi.org/10.1016/j.jece.2021.106287.

[82] T.T. Luu, V.P. Dinh, Q.H. Nguyen, N.Q. Tran, D.K. Nguyen, T.H. Ho, V.D. Nguyen, D.X. Tran, H.A.T. Kiet, Pb(II) adsorption mechanism and capability from aqueous solution using red mud modified by chitosan, (2022) 132279. https://doi.org/10.1016/j.chemosphere.2021.132279.

[83] H. Mi, L. Yi, Q. Wu, J. Xia, B. Zhang, Preparation and optimization of a low-cost adsorbent for heavy metal ions from red mud using fraction factorial design and Box-Behnken response methodology, (2021) 127198. https://doi.org/10.1016/j.colsurfa.2021.127198.

CHAPTER 5:

Adsorptive removal of efavirenz from aqueous solutions using magnetic mesoporous pet coke and coal fly ash-based adsorbents

ABSTRACT

In recent years, there has been a growing concern among various stakeholders, academics, and researchers regarding the pollution of aquatic environments with synthetic organic chemicals. One specific area of concern is the presence of emerging contaminants like pharmaceutical drugs such as antiretroviral drugs, including efavirenz which is used in the treatment of HIV. These drug compounds have proven to be environmentally persistent and pose a potential health risk to humans, animals and aquatic species, while also posing a risk to the safety of drinking water supplies and aquatic environments. Sources of pharmaceutical drugs include effluents from Wastewater Treatment Plants (WWTPs), hospital effluent and waste from pharmaceutical production facilities, and the incorrect disposal of unused and expired medicines. However, it is worth noting that there are currently no proper monitoring programs or legislative guidelines for regulating these drugs in Africa. Therefore, there is a need for policymakers and regulators to act and develop appropriate guidelines to ensure the safety of drinking water supplies and protect the environment from the harmful effects of emerging contaminants.

The removal of efavirenz from aqueous solutions was carried out using Fe_3O_4@ACFA, Fe_3O_4@AFA, Fe_3O_4@ABA, and Fe_3O_4@APC prepared from coal fly ash, fly ash, bottom ash, and petroleum coke, respectively. The effects of parameters such as sample pH, contact time, initial concentration of efavirenz, and temperature on the adsorption process were investigated using the multivariate optimization tool. The optimum conditions obtained were pH: 2, contact time: 28 min, temperature: 35˚C, initial concentration: 5 mg/L, and adsorbent mass: 20 mg.

The kinetic studies indicated that the adsorption process was best described by the pseudo-second-order model. The study evaluates the adsorption of efavirenz on various adsorbents, revealing non-spontaneous adsorption. The adsorption process is endothermic on Fe_3O_4@APC and Fe_3O_4@ACFA adsorbents, while exothermic on Fe_3O_4@ABA and Fe_3O_4@AFA adsorbents. Positive values of $\Delta S°$ indicate increased randomness at the solid-solution interface, suitable for increased adsorption molecules. The Fe_3O_4@AFA shows decreased

randomness, making it suitable for precise adsorption. The best correlation for efavirenz was however observed for the Langmuir model, confirming that the adsorption took place in the monolayer homogeneous surface. The maximum adsorption capacity for Fe_3O_4@ACFA, Fe_3O_4@APC, Fe_3O_4@ABA, Fe_3O_4@AFA obtained to be 25.3807, 37.6364, 13.07 and 76.5376 mg/g respectively.

Keywords: Efavirenz; coal fly ash; petroleum coke; magnetic mesoporous adsorbents; aqueous solutions.

5.1. Introduction

Efavirenz is an antiretroviral drug developed for the treatment of human immunodeficiency virus (HIV-1) infection in combination with other antiretroviral drugs. Efavirenz is a non-nucleoside reverse transcriptase inhibitor that blocks the reverse transcriptase enzyme HIV to replicate [1,2]. Its chemical structure contains a group of nonpolar aromatic rings and a hydroxyl group that makes it hydrophobic and increases its absorption in the gut [3]. Efavirenz is metabolized by the liver into inactive compounds that are excreted via urine [4]. It has been detected in several South African water bodies such as rivers, dams, wastewater and estuaries. According to previous reports, efavirenz is the most common pharmaceutical found in South African waters. Higher amounts of up to 140 μg/L have been found in WWTP influent in the city of Durban, South Africa [5]. Abafe *et al*. [6] found efavirenz at concentrations as high as 34 μg/L in all samples (influent and effluent) from the WWTP of KwaZulu-Natal Province.

The primary cause of efavirenz's presence in aquatic systems is the discharge of effluent from wastewater treatment plant. The presence of efavirenz in different water systems is strongly associated to a greater prevalence of HIV drugs prescription in South Africa for individuals who are HIV positive. Research has shown that efavirenz can accumulate in aquatic organisms, causing adverse effects on their health and ecosystems by disrupting their endocrine and reproductive systems [7,8]. Ncube *et al*. [9] revealed that efavirenz significantly reduced the hatching success of African Sharptooth catfish eggs. Furthermore, the toxicity of efavirenz affects other aquatic organisms, such as algae and plant species. Although there is limited information on the long-term effects of efavirenz on aquatic biodiversity in South Africa, it is crucial to monitor and regulate its presence in aquatic systems to prevent irreversible ecological degradation and loss of biodiversity. Current wastewater treatment plants (WWTP) are not designed to effectively remove contaminants such as ARVs. They are mainly designed to

remove solids, dissolved organic matter and nutrients. Thus far, some conventional treatment methods reported in the literature for the removal of ARVs and related drugs, have achieved removal efficiencies of 6 – 84 % for nevirapine using trickling filters and anaerobic pond treatment [10].

The objective of the current work is mainly focused on the application of the magnetic mesoporous adsorbent from coal fly ash, petroleum coke, fly ash and bottom ash for the removal of efavirenz from water systems. To our knowledge, there is no reported work on the removal of efavirenz drugs using industrial waste materials. This is the first comprehensive report on the removal of efavirenz from wastewater.

5.2. Experimental procedures

5.2.1. Materials and methods

All the reagents used were analytical grade with high purity (≥ 96%). Efavirenz, Calcium chloride ($CaCl_2$) and NaN_3 were purchased from Sigma-Aldrich (Steinheim, Germany), while acetonitrile was purchased from Merck (Massachusetts, United States of America). 99 % formic acid were purchased from Sigma-Aldrich (St Louis, United States of America). All solutions were prepared using ultra- high purity water (18.2MΩ) obtained from a Millipore Milli-Q water purification system (Massachusetts, United States of America). The physicochemical properties of efavirenz are shown in **Table 5.1**.

Table 5.1: The physicochemical properties of efavirenz.

	Structure	**Molecular weight (g/mol)**	**Log Kow (µg/mL)**	**Pka**	**Ref**
Efavirenz	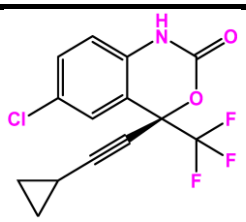	315.68	0.093	12.52	[11]

5.2.2. Instrumentation and chromatographic conditions

A Hewlett-Packard 1090 II liquid chromatograph equipped with a DAD Agilent 1260 Infinity high-pressure liquid chromatography (HPLC) system procured from Agilent Technologies (Waldbronn, Germany) was used for analysis of efavirenz. The chromatographic system consisted of a degasser unit, binary pump, autosampler, auto-injector and thermostatic column compartment. The chromatographic column, a Waters Xterra® C18 3.5 µm 4.6 × 150 mm column from Waters Corporation, was maintained at 30 °C (Milford, MA, United States). The chromatographic analysis was achieved under isocratic elution. The chromatograms were recorded at 254 m. Mobile phase composition consisted of 60% (0.1% formic acid in water): 40% acetonitrile an elution system at a flow rate of 1.0 mL/min and injection volume of 10 µL. The retention time was at 3.26 min at 60% A: 40% B. Solid-Phase-Extraction was the main technique used for sample preparation of real wastewater sample. In this case, Oasis HLB 6cc/150 mg cartridges procured from Waters Corporations (Milford, MA, United States) were used as a sorbent bed to trap analytes during the extraction process.

5.2.3. Preparation of standards

Efavirenz reference standards were prepared by accurately weighing 10 mg of the compound and diluting to the mark in a 10 mL to make a final concentration of 1000 mg/L. The mixture solutions were then sonicated for 15 min to enable complete dissolution. Working standards were prepared by serial dilution of appropriate volumes of the stock solution into volumetric flasks and using the same diluent.

5.2.4. Adsorption and desorption experiment

The adsorption capacity of the Fe_3O_4@APC, Fe_3O_4@ABA, Fe_3O_4@ACFA and Fe_3O_4@AFA was evaluated using a simple batch adsorption method. To determine the equilibrium and rate of interaction, different parameters were optimised such as temperature, adsorbent dosage, adsorbate concentration and contact time. The adsorption isotherms of the efavirenz were achieved in the concentration range of 1 – 5 mg/L. A known amount of (20 – 60 mg) Fe_3O_4@APC, Fe_3O_4@ABA, Fe_3O_4@ACFA and Fe_3O_4@AFA 20 – 60 mg was added to each flask, followed by agitation for a specified time 10 – 120 min at different temperatures ranging from 25 – 60 °C. The solutions were then filtered and the concentration of efavirenz in the filtrate was analysed using HPLC-DAD. The percentage removal and adsorption capacity for

efavirenz was calculated using **Equation 4.1**. Desorption experiments were carried out by adding fresh 10 mL of background electrolyte after the supernatant from the adsorption studies had been decanted then the adsorption capacity was calculated using **Equation 4.2**.

5.2.5. Optimization

The multivariate optimization approach was used for the determination of parameters that are significant for the adsorption of efavirenz onto the Fe_3O_4@ACFA, Fe_3O_4@ABA, Fe_3O_4@AFA and Fe_3O_4@APC. This is because there are numerous advantages that multivariate optimization offers over the univariate technique. The design of the experiments and data analysis were done using Minitab 2018 statistical software for both the two-level full factorial and central composite designs.

Two-level half factorial

To screen the primary variable and interactions, a two-level half factorial (2^{n-1}) design was used. The optimized parameters included contact time, temperature, adsorbent mass, pH, and initial metal ion concentration. The variable was assigned lower (-) and higher levels (+), with the central point omitted. The experimental designs' factors and levels for the optimization process are detailed in **Table 5.2**, and a total of 16 experiments were conducted.

Table 5.2: Two-level half factorial (2^4) experimental design.

Factors	Minimum (-)	Maximum (+)
pH	2	12
Adsorbent mass (mg)	20	60
Initial concentration (mg/L)	1	5
Contact time (min)	10	60
Temperature (˚C)	25	60

Box-Behnken Design

In this study Box-Behnken design (BBD) was employed for further optimization of the most significant variables. These factors were also assigned two levels (minimum and maximum), using literature reports as our guide. These levels resulted in 31 experiments. From the results of these experiments, optimum conditions for each variable were deduced.

5.2.6. Adsorptive isotherms, kinetics and thermodynamic studies

To understand the nature of the interaction between efavirenz and the adsorbent, adsorption isotherms were evaluated. The adsorption data was analyzed using three different methods: the Langmuir, Freundlich, and Temkin equations, represented by **Equations 4.3, 4.4**, and **4.5**. Additionally, studies were carried out to assess the rate-limiting steps (**Equations 4.6-4.7**) and determine the thermodynamic parameters (**Equations 4.8-4.9**).

5.3. Results and discussions

5.3.1. Multivariate optimization

Two-level half factorial

Two-level half factorial design was used to investigate the influence of experimental conditions contact time, temperature, adsorbent mass, pH and initial metal ion concentration. The ANOVA (**APPENDIX B 2**) results were then presented in form of Pareto charts for % R of efavirenz ion as shown in **Figure 5.1**. The results indicated that pH, concentration, contact time and adsorbent mass (dosage) were statistically significant at 95% confidence level for the high removal efficiency of efavirenz. pH has a significant influence on the surface charge of the adsorbent and the ionization state of its functional groups. When the pH is optimal, it allows for favorable electrostatic interactions between efavirenz and the adsorbent, which is crucial for efficient adsorption. The initial concentration of efavirenz also plays a significant role in determining the driving force for adsorption. A higher initial concentration means more molecules are available for binding, which affects both the equilibrium capacity and removal efficiency.

The duration of contact time between efavirenz and the adsorbent is another critical parameter, as it determines the length of the interaction. Longer contact times provide sufficient binding between the two, influencing the kinetics of adsorption. The mass of the adsorbent is also a significant factor, as more mass translates to a greater surface area. Consequently, more binding sites become available, directly impacting the overall adsorption capacity. By optimizing these parameters, efficient adsorption of efavirenz can be ensured. These parameters were further optimization since they were most significant for the removal of efavirenz. The vertical line represents the 95% confidence level, while the bar length is proportional to the absolute value

of the estimated effects[12]. The bar length helps in comparing the relative importance of the effects.

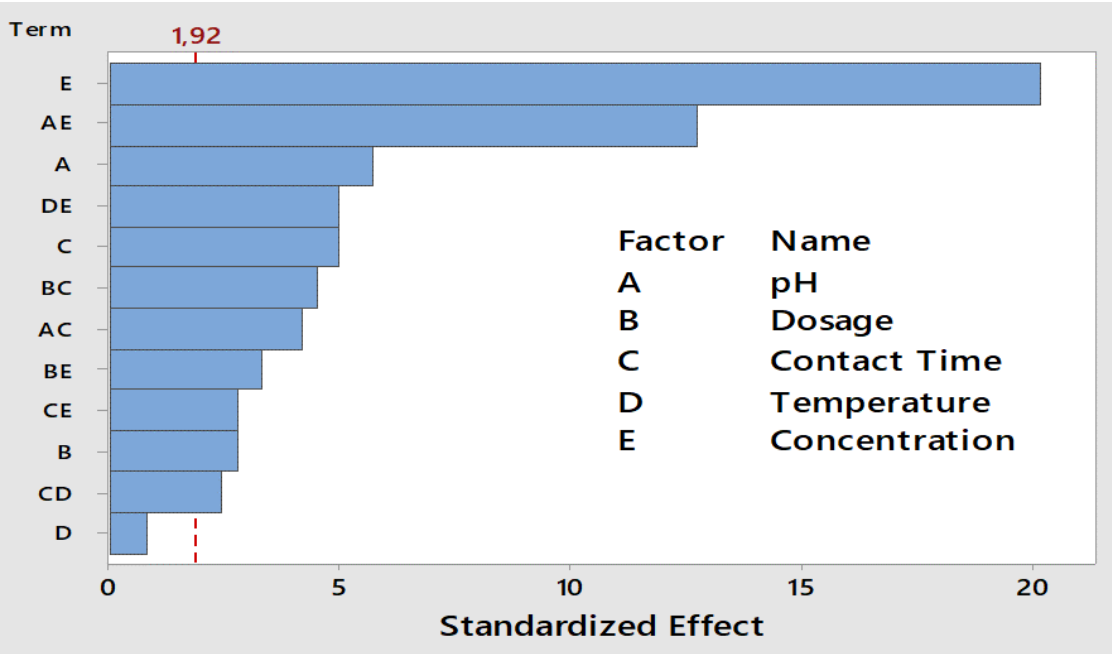

Figure 5.1: Pareto charts for % R of efavirenz from 2-level half fractional factorial full design (2^{n-1}) at 95 % confidence level for optimization of adsorbent mass (dosage), contact time, pH, concentration and temperature. note: the vertical line indicates 95 % confidence.

Further optimization using Response Surface Methodology based on Box-Behnken Design (BBD).

The Box-Behnken design (BBD) was used to further optimize the significant factors such as pH, initial efavirenz concentration, contact time and adsorbent mass. The Box-Bohnken design matrix and the values of analytical response are shown in **APPENDIX B 3.** Temperature was kept constant at 35 ˚C, because it was found to be insignificant for high % removal of efavirenz after screening. The ANOVA results indicated that the design model was suitable for optimization of the removal of efavirenz since it lead to coefficient of determination (R^2) and adjusted R^2 values of 0.7368 and 0.5066, respectively. *F*-value for the lack of fit was 3 indicating that it is not significant relative to pure error.

The relationship between two variables in order to attain maximum adsorption capacity is depicted in **Figure 5.3a – d**. The impact of contact time on the percentage removal of efavirenz from the 3D plots, which pertain to (adsorbent mass – contact time and concentration – contact

time), is illustrated in **Figure 5.3a** and **c**. It is evident that contact time is a crucial factor that significantly affects the efficiency of removal. His is because contact time provides information about the rate of adsorption. It should be noted that the contact time was examined within the range of 10 to 60 min. The results in **Figure 5.3a** and **c** indicate that the removal efficiency of efavirenz was greatly enhanced with an increase in contact time from 10 to 30 min. However, with further increases in contact time up to 40 min, the removal efficiency did not show any significant improvement. This is because of the less availability of abundant adsorption sites [13–15] ; the reactions occur rapidly and reach equilibrium within the first 30 min, and then a slowdown as these sites are gradually filled up. Therefore, 30 min was considered the optimum value.

Based on the outcomes of the research on the impact of pH on efavirenz adsorption efficiency (**Figure 5.3b, d**), it is evident that solution pH is another significant factor that greatly affects the efficiency of removal. The surface of the adsorbent's functional groups is a crucial factor in the adsorption of process, and it can be adjusted by different NaOH or HCl [16,17]. At low pH (acidic Conditions), the surface of CFA becomes protonated. This protonation enhances the adsorption due to electrostatic attraction. CFA's functional groups can form stronger bonds under acidic conditions. The modification of the surface properties of Fe_3O_4@ACFA can be examined by the zeta potential curve, which is displayed in **Figure 5.2**.

As demonstrated in **Figure. 5.2**, in acidic media, the Fe_3O_4@ACFA surface is negatively charged, and when the pH is increased to 10, the negatively charged sites on the sorbent surface are increased. Given the aforementioned findings, the adsorption efficiency of efavirenz at a solution pH of 2 is more desirable. At low pH (acidic conditions), efavirenz will be positively charged due to its pKa value. There will be electrostatic interactions between efavirenz and Fe_3O_4@ACFA. These interactions enhance the adsorption efficiency of efavirenz onto Fe_3O_4@ACFA.

The adsorbent mass used was in the range of 20 – 60 mg. In **Figure 5.2a** and **b**, adsorption efficiencies increased with an increase in the amount of sorbent, which is related to the availability of higher binding sites and however, at higher adsorbent mass the active sites get blocked due to agglomeration [18–20]. As sorbent mass increases, agglomeration (clumping) of particles can occur. Agglomerated particles may block some active sites on the sorbent surface. This can reduce overall adsorption efficiency, especially if the agglomerates hinder

access to critical binding sites. Therefore, the optimum adsorbent mass with maximum removal efficiency was 20 mg. Therefore, 20 mg was considered as the optimum value.

Based on the response optimizer **Figure 5. 4** and BBD surface plots experimental conditions were chosen sample pH, 2; contact time, 28 min; temperature, 35 ˚C; initial concentration, 5 mg/L; and adsorbent mass, 20 mg. These optimum conditions were then applied to Fe_3O_4@APC, Fe_3O_4@AFA and Fe_3O_4@ABA. Compared to literature reports on adsorption of ARVs these materials show a different trend. The different trends in the adsorption of ARVs may be due to various factors such as the specific properties of the materials being used, and differences in experimental conditions employed in the literature reports. These differences could lead to varying outcomes in the adsorption behaviour of ARVs.

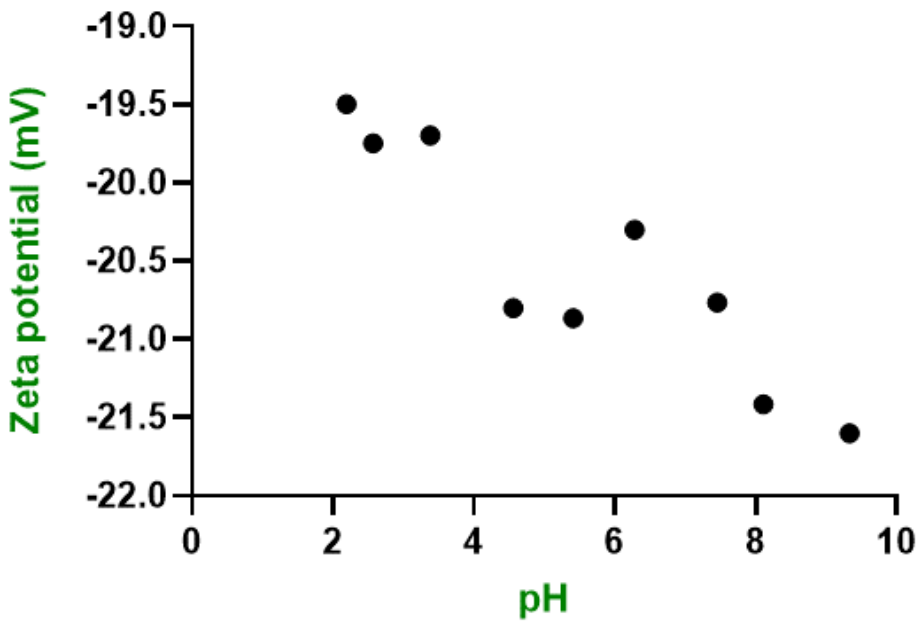

Figure 5.2: Zeta potential of Fe_3O_4@ACFA.

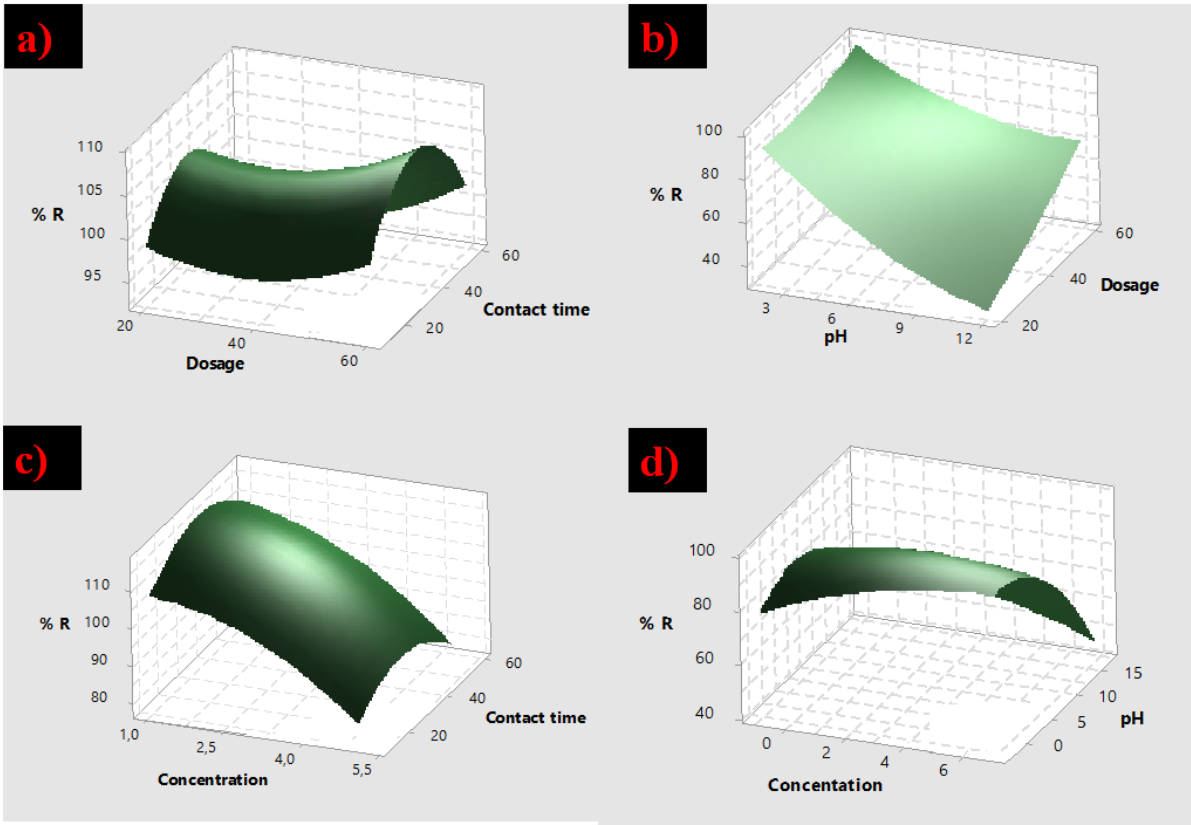

Figure 5. 3: Response surface methodology 3D surface plots.

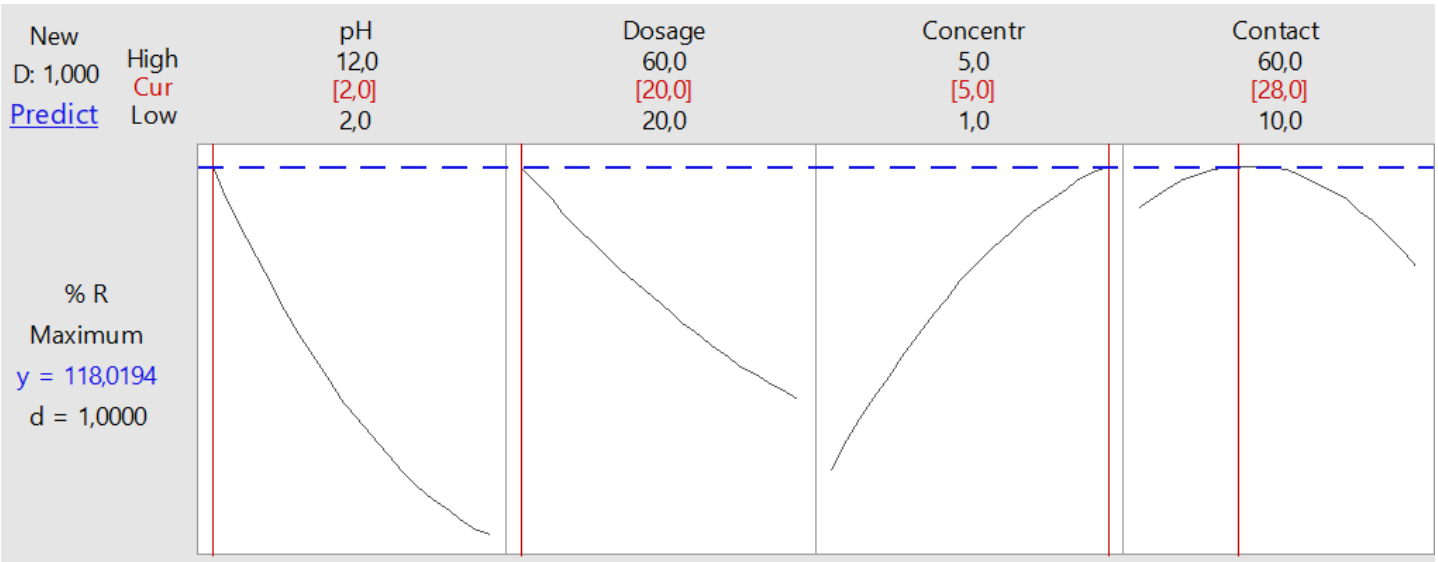

Figure 5.4: Response optimizer

5.3.2. Kinetic studies

In this research, two distinct kinetic models (pseudo-first-order, pseudo-second order) were applied to illustrate the kinetics of efavirenz adsorption on Fe_3O_4@ACFA, Fe_3O_4@APC,

Fe_3O_4@ABA, and Fe_3O_4@AFA. The results of the pseudo-first-order kinetics model for Fe3O4@ACFA revealed an R^2 value of 0.246, indicating moderate agreement with the model. In contrast, the pseudo-second-order kinetics model demonstrated an excellent R^2 value of 1.0, indicating strong agreement with the model. The analysis of Fe_3O_4@APC showed a low R^2 value of 0.037 for the pseudo-first-order kinetics model, indicating poor agreement with the model, while the pseudo-second-order kinetics model exhibited a high R^2 value of 0.999, suggesting a good fit. For Fe_3O_4@ABA, the R^2 value of 0.192 for the pseudo-first-order kinetics model indicated moderate agreement with the model, and the pseudo-second-order kinetics model resulted in an R^2 value of 0.999, suggesting a strong fit. Finally, the results for Fe_3O_4@AFA showed a low R^2 value of 0.044 for the pseudo-first-order kinetics model, indicating poor agreement with the model, while the pseudo-second-order kinetics model displayed a high R^2 value of 0.9996, suggesting a good fit.

The results indicated that the adsorption process was best described by the pseudo-second-order model, as evidenced by the linear regression coefficients presented in **APPENDIX B 5 – 6**. Furthermore, the calculated results in **Table 5.3** showed a higher degree of similarity, which suggests that the pseudo-second-order model may be the rate-limiting step in the process. The adsorbents' surface properties, functional groups, and charge distribution play a crucial role in their interaction with efavirenz. Fe_3O_4@ACFA shows the strongest agreement with both kinetic models, likely due to its favourable surface characteristics. These results are consistent with reported literature on adsorption of AVRs [15]

Table 5.3: Kinetic parameters of efavirenz adsorption onto Fe_3O_4@ACFA, Fe_3O_4@APC, Fe_3O_4@ABA and Fe_3O_4@AFA.

Adsorbent	Pseudo first order		Pseudo second order		
	R^2	K_1	R^2	q_e	K_2
Fe_3O_4@ACFA	0.246	-119.754	1.0	2.2784	288.408
Fe_3O_4@APC	0.037	-119.993	0.999	2.2737	64.2305
Fe_3O_4@ABA	0.192	-120.037	0.9998	2.2748	20.8506
Fe_3O_4@AFA	0.044	-119.98	0.9996	2.2732	18.215

5.3.3. Thermodynamic studies

Thermodynamic analyses play a crucial role in determining the spontaneity of adsorption processes. These analyses allow for the evaluation of important thermodynamic parameters such as Gibbs free energy change (ΔG°, kJ/mol), enthalpy change (ΔH°, kJ/mol), and entropy change (ΔS°, J/mol/K) at standard state [21]. In this study, these parameters were calculated for the adsorption of efavirenz on Fe_3O_4@ACFA, Fe_3O_4@APC, Fe_3O_4@ABA, and Fe_3O_4@AFA. The results indicated that the adsorption of efavirenz on these adsorbents is non-spontaneous due to the positive values of ΔG° obtained. To determine the values of ΔH° and ΔS°, the slope and intercept of the plot of ln K_L against 1/T were utilized. The positive values of ΔH° indicated that the adsorption process of efavirenz onto Fe_3O_4@APC and Fe_3O_4@ACFA was endothermic, while the negative value of ΔH° confirmed that the adsorption process of efavirenz onto Fe_3O_4@ABA and Fe_3O_4@AFA was exothermic. Fe_3O_4@APC and Fe_3O_4@ACFA are suitable for applications where an increase in temperature is desired. Fe_3O_4@ABA and Fe_3O_4@AFA are ideal for applications where a decrease in temperature is beneficial.

The positive values of ΔS° indicated an increase in randomness at the solid-solution interface for Fe_3O_4@ACFA, Fe_3O_4@APC, and Fe_3O_4@ABA while adsorbing adsorbates onto the active sites of the adsorbent. This increased randomness is favourable for adsorption applications that require an increase in the number of adsorbed molecules [22–24]. However, the negative values of Fe_3O_4@AFA indicated a decrease in randomness, making it an excellent adsorbent for applications that require the adsorption of a precise number of molecules.

Table 5.4: Thermodynamic parameters for the adsorption efavirenz onto Fe_3O_4@ACFA, Fe_3O_4@APC, Fe_3O_4@ABA and Fe_3O_4@AFA.

Adsorbent	ΔG° (kJ/mol)			ΔH° (kJ/mol)	ΔS° (J/mol/K)	R^2
	25 °C	45 °C	55 °C			
Fe_3O_4@ACFA	1.8727	2.00956	2.1667	4.18119	8.0944	0.9736
Fe_3O_4@APC	2.1063	1.9834	2.0289	7.03507	15.1647	0.9806
Fe_3O_4@ABA	1.8484	2.01664	5.3609	- 4.7362	8.0015	0.9457
Fe_3O_4@AFA	1.8702	2.1146	2.9857	-0.01987	-8677.99	0.8479

5.3.4. Adsorption isotherms

Adsorption studies were conducted by varying the initial concentration from 1 to 5 mg/L at 35 °C. To understand the mechanism of adsorption, the experimental data was fitted to three adsorption models. The Langmuir, Temkin and Freundlich isotherms.

The Langmuir and Temkin equilibrium constants and other parameters of the isotherm models are shown in **Table 5.5**. From the results, it was observed that Langmuir dimensionless equilibrium constant (R_L) is less than one and greater than zero [25], which indicates the favourability of the adsorption. The value of the heterogeneity factor 1/n indicates that the Freundlich isotherm is indeed favourable [26–29]. The value of (1/n) can range from 0 to 1. When (1/n = 0), adsorption is independent of concentration. When (1/n = 1), adsorption is directly proportional to concentration. Therefore, if (1/n) is close to 1, it indicates favourable adsorption behaviour. Based on the R^2 values the experimental data can be satisfactorily explained by three adsorption models. The best correlation for efavirenz was however observed for the Langmuir model, confirming that the adsorption took place in the monolayer homogeneous surface [30–32]. The maximum adsorption capacity for Fe_3O_4@ACFA, Fe_3O_4@APC, Fe_3O_4@ABA, Fe_3O_4@AFA obtained to be 25.3807, 37.6364, 13.07 and 76.5376 mg/g respectively.

Table 5.5: Adsorption isotherms constants for the adsorption of efavirenz onto the Fe_3O_4@ACFA, Fe_3O_4@APC, Fe_3O_4@ABA, Fe_3O_4@AFA at 308.15 K.

Isotherm model	Parameters	Adsorbents			
		Fe_3O_4@ACFA	**Fe_3O_4@AFA**	**Fe_3O_4@ABA**	**Fe_3O_4@APC**
Langmuir					
	q_{max} (mg/g)	25.38	76.54	13.01	37.64
	K_L (L/mg)	0.04369	0,0584	0.0600	0.0166
	R_L	0.8304	0.7855	0.7819	0.9525
	R^2	0.9989	0.9953	0.9948	0.9910
Freundlich					
	K_F (L/mg)	9.2	1.27	3,82	2.042
	n	0.01566	0.0124	0.0289	0.003
	R^2	0.9733	0.9902	0.9969	0.9559
Temkin					
	B_T	0.4999	0.8714	0.2128	1.639
	K_T	14.09	1.398	19.95	3.904
	R^2	0.9856	0.9892	0.09794	0.9651

5.3.5. Comparison studies between raw, activated and coated industrial waste – based adsorbents

The primary objective of this comprehensive research study was to evaluate the efficacy of activating and coating coal fly ash, bottom ash, fly ash, and petroleum coke in enhancing the removal of efavirenz ions from aqueous solutions. The researchers conducted a thorough comparison of the removal percentages for the untreated raw materials, activated materials, and materials coated with Fe_3O_4 nanoparticles, as depicted in **Figure 5.8**. The results of the study were conclusive, demonstrating a substantial and noteworthy increase in the removal percentage, which was attributed to the formation of mesoporous materials and the incorporation of Fe_3O_4 nanoparticles. These modifications resulted in a stronger negative charge on the adsorbent surface, thereby enhancing the electrostatic interaction with efavirenz ions.

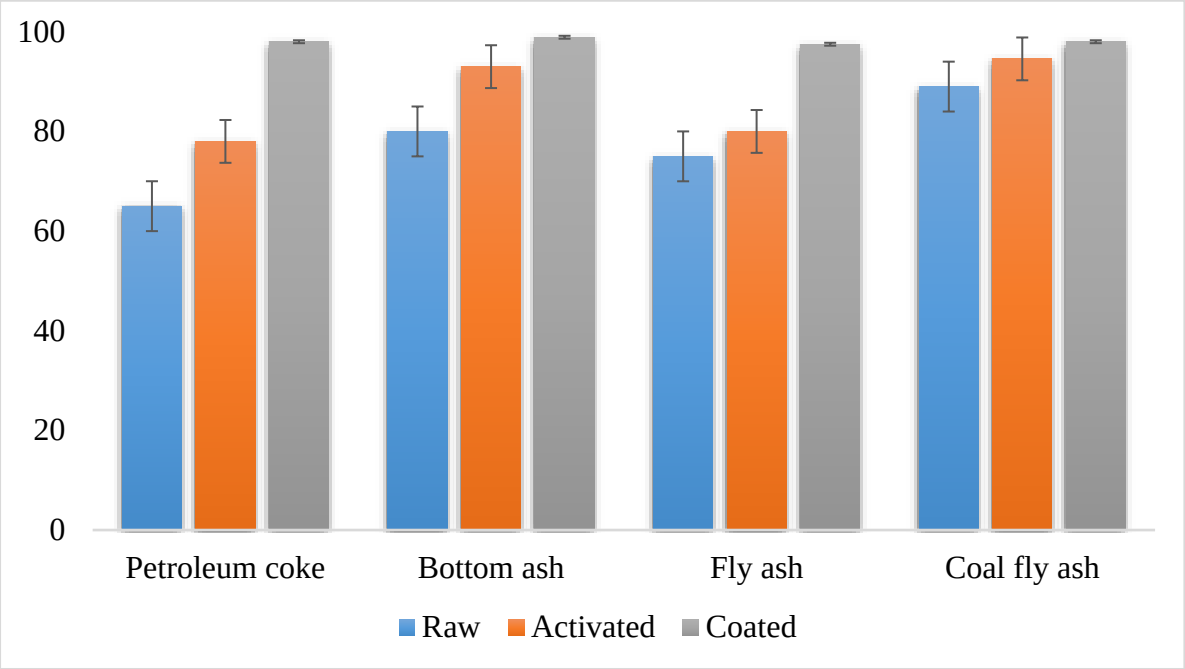

Figure 5.5: Comparison studies between raw, activated, and coated industrial waste–based adsorbent for the adsorption of efavirenz in aqueous solutions.

5.3.6. Reusability studies

The ability to reuse adsorbents is essential for industry, as it minimizes waste and supports environmentally friendly water treatment and pollution control. In **Figure 5.9**, studies on magnetic mesoporous adsorbents demonstrate that they remain effective for up to three cycles

when removing efavirenz. Even after multiple adsorption-desorption cycles, the removal efficiencies consistently range from 92% to 98%. This confirms the long-term reusability of these adsorbents for efavirenz removal.

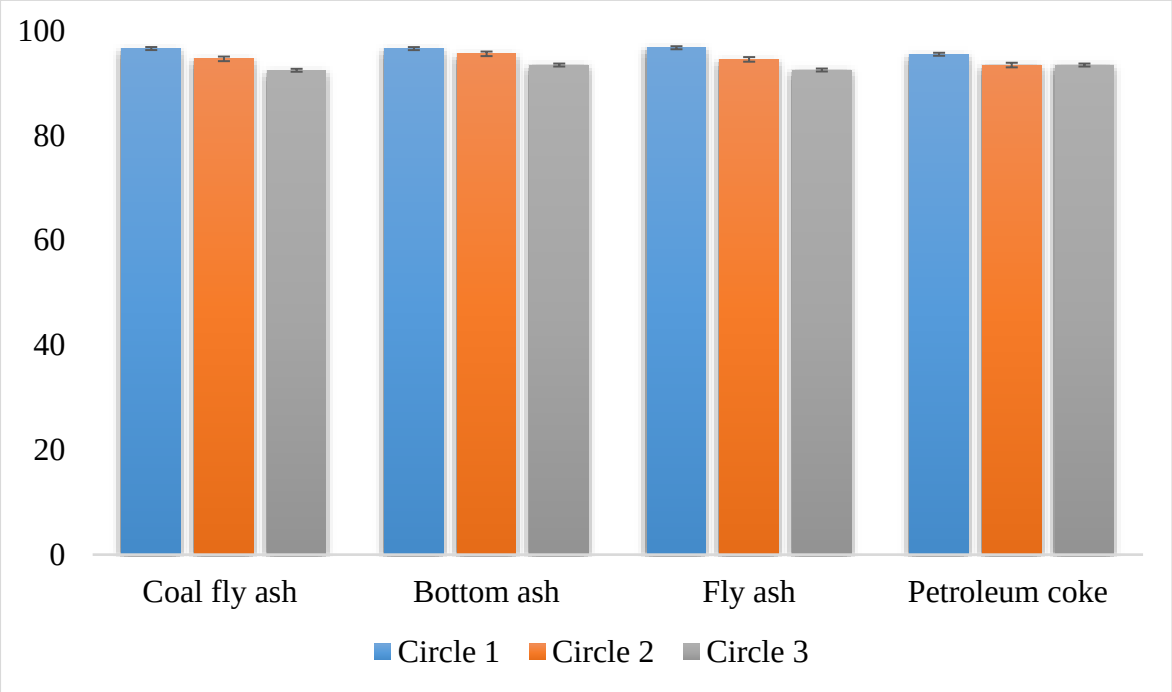

Figure 5.6: Reusability of the Fe_3O_4@ACFA, Fe_3O_4@APC, Fe_3O_4@ABA and Fe_3O_4@AFA for adsorption of efavirenz in aqueous solutions.

5.4. Conclusion

Based on the multivariate optimization results, key factors influencing the efficient removal of efavirenz using coal fly ash adsorbents were identified: adsorbent mass, initial solution concentration, contact time, and pH. These factors warrant further fine-tuning. Comparative studies revealed that the mesoporous nature of the materials, along with the incorporation of Fe_3O_4 nanoparticles, enhanced the negative surface charge. This facilitated strong electrostatic interactions between efavirenz and the adsorbents, resulting in high adsorption capacity. The adsorbents demonstrated reusability for up to three cycles. Notably, Fe_3O_4@AFA exhibited a superior adsorption capacity compared to Fe_3O_4@ACFA, Fe_3O_4@ABA, and Fe_3O_4@APC-based adsorbents.

REFERENCE

[1] N. Zareifopoulos, M. Lagadinou, A. Karela, F. Pouliasi, I. Economou, A. Tsigkou, D. Velissaris, Efavirenz as a psychotropic drug, 24 (2020) 10729–10735. https://doi.org/10.26355/EURREV_202010_23433.

[2] N. Apostolova, A. Blas-Garcia, M.J. Galindo, J. V. Esplugues, Efavirenz: What is known about the cellular mechanisms responsible for its adverse effects, (2017) 163–173. https://doi.org/10.1016/J.EJPHAR.2017.07.016.

[3] E.L. Schymanski, C. Ruttkies, M. Krauss, C. Brouard, T. Kind, K. Dührkop, F. Allen, A. Vaniya, D. Verdegem, S. Böcker, J. Rousu, H. Shen, H. Tsugawa, T. Sajed, O. Fiehn, B. Ghesquière, S. Neumann, Critical Assessment of Small Molecule Identification 2016: automated methods, (2017). https://doi.org/10.1186/S13321-017-0207-1.

[4] S. Oswald, H.E. Meyer Zu Schwabedissen, A. Nassif, C. Modess, Z. Desta, E.T. Ogburn, J. Mostertz, M. Keiser, J. Jia, A. Hubeny, A. Ulrich, D. Runge, M. Marinova, D. Lütjohann, H.K. Kroemer, W. Siegmund, Impact of efavirenz on intestinal metabolism and transport: Insights from an interaction study with ezetimibe in healthy volunteers, (2012) 506–513. https://doi.org/10.1038/clpt.2011.255.

[5] L.M. Madikizela, S. Ncube, L. Chimuka, Analysis, occurrence and removal of pharmaceuticals in African water resources: A current status, (2020) 109741. https://doi.org/10.1016/j.jenvman.2019.109741.

[6] O.A. Abafe, J. Späth, J. Fick, S. Jansson, C. Buckley, A. Stark, B. Pietruschka, B.S. Martincigh, LC-MS/MS determination of antiretroviral drugs in influents and effluents from wastewater treatment plants in KwaZulu-Natal, South Africa, (2018) 660–670. https://doi.org/10.1016/j.chemosphere.2018.02.105.

[7] P. Arnab, R. Croxford, J. Scott, S. Perumal, Z. Mohammed, L. Wiesner, K. Cohen, S. Wasserman, Severe efavirenz associated neurotoxicity: A retrospective cohort study, (2023). https://doi.org/10.4102/SAJID.V38I1.522.

[8] S. Oswald, H.E. Meyer Zu Schwabedissen, A. Nassif, C. Modess, Z. Desta, E.T. Ogburn, J. Mostertz, M. Keiser, J. Jia, A. Hubeny, A. Ulrich, D. Runge, M. Marinova, D. Lütjohann, H.K. Kroemer, W. Siegmund, Impact of efavirenz on intestinal metabolism

and transport: insights from an interaction study with ezetimibe in healthy volunteers, (2012) 506–513. https://doi.org/10.1038/CLPT.2011.255.

[9] L.M. Madikizela, S. Ncube, L. Chimuka, Uptake of pharmaceuticals by plants grown under hydroponic conditions and natural occurring plant species: A review, (2018) 477–486. https://doi.org/10.1016/j.scitotenv.2018.04.297.

[10] V. Mhuka, S. Dube, M.M. Nindi, Occurrence of pharmaceutical and personal care products (PPCPs) in wastewater and receiving waters in South Africa using LC-Orbitrap™ MS, (2020) 250–258. https://doi.org/10.1016/j.emcon.2020.07.002.

[11] B. Costa, N. Vale, Efavirenz: History, Development and Future, (2023). https://doi.org/10.3390/BIOM13010088.

[12] M.S. Manzar, G. Khan, P.V. dos Santos Lins, M. Zubair, S.U. Khan, R. Selvasembian, L. Meili, N.I. Blaisi, M. Nawaz, H. Abdul Aziz, T.S. Kayed, RSM-CCD optimization approach for the adsorptive removal of Eriochrome Black T from aqueous system using steel slag-based adsorbent: Characterization, Isotherm, Kinetic modeling and thermodynamic analysis, (2021) 116714. https://doi.org/10.1016/j.molliq.2021.116714.

[13] D.H.K. Reddy, S.M. Lee, Application of magnetic chitosan composites for the removal of toxic metal and dyes from aqueous solutions, (2013) 68–93. https://doi.org/10.1016/J.CIS.2013.10.002.

[14] M. Vakili, M. Rafatullah, B. Salamatinia, A.Z. Abdullah, M.H. Ibrahim, K.B. Tan, Z. Gholami, P. Amouzgar, Application of chitosan and its derivatives as adsorbents for dye removal from water and wastewater: A review, (2014) 115–130. https://doi.org/10.1016/J.CARBPOL.2014.07.007.

[15] A. Gupta, V. Sharma, K. Sharma, V. Kumar, S. Choudhary, P. Mankotia, B. Kumar, H. Mishra, A. Moulick, A. Ekielski, P.K. Mishra, A Review of Adsorbents for Heavy Metal Decontamination: Growing Approach to Wastewater Treatment, (2021). https://doi.org/10.3390/MA14164702.

[16] B. Thomas, E.P. Shilpa, L.K. Alexander, Role of functional groups and morphology on the pH-dependent adsorption of a cationic dye using banana peel, orange peel, and neem leaf bio-adsorbents, (2021) 1479–1487. https://doi.org/10.1007/S42247-021-00237-Y/FIGURES/11.

[17] T.G. Ambaye, · M Vaccari, · E D Van Hullebusch, · A Amrane, · S Rtimi, Mechanisms and adsorption capacities of biochar for the removal of organic and inorganic pollutants from industrial wastewater, (2021) 3273–3294. https://doi.org/10.1007/s13762-020-03060-w.

[18] J.O. Eniola, B. Sizirici, Y. Fseha, J.F. Shaheen, A.M. Aboulella, Application of conventional and emerging low-cost adsorbents as sustainable materials for removal of contaminants from water, (2023) 88245–88271. https://doi.org/10.1007/S11356-023-28399-8.

[19] M.F. Cheira, H.I. Mira, A.K. Sakr, S.A. Mohamed, Adsorption of U(VI) from acid solution on a low-cost sorbent: equilibrium, kinetic, and thermodynamic assessments, (2019) 1–18. https://doi.org/10.1007/S41365-019-0674-3/TABLES/8.

[20] O.P. Murphy, M. Vashishtha, P. Palanisamy, K.V. Kumar, A Review on the Adsorption Isotherms and Design Calculations for the Optimization of Adsorbent Mass and Contact Time, (2023) 17407–17430. https://doi.org/10.1021/ACSOMEGA.2C08155/SUPPL_FILE/AO2C08155_SI_003.XLSX.

[21] Z. Hasan, S.H. Jhung, Removal of hazardous organics from water using metal-organic frameworks (MOFs): Plausible mechanisms for selective adsorptions, (2015) 329–339. https://doi.org/10.1016/J.JHAZMAT.2014.09.046.

[22] N. Ozcan, B. Saygi Yalcin, E. Bilgin Simsek, D. Saloglu, Removal of naproxen from wastewater using chitosan–aerogel–activated carbon biocomposites: Theory, equilibrium, kinetics, thermodynamics, and process optimization, (2022) 1–16. https://doi.org/10.1002/wer.10699.

[23] M. Kapur, M.K. Mondal, Competitive sorption of Cu(II) and Ni(II) ions from aqueous solutions: Kinetics, thermodynamics and desorption studies, (2014) 1803–1813. https://doi.org/10.1016/j.jtice.2014.02.022.

[24] Y. Li, Q. Du, T. Liu, J. Sun, Y. Jiao, Y. Xia, L. Xia, Z. Wang, W. Zhang, K. Wang, H. Zhu, D. Wu, Equilibrium, kinetic and thermodynamic studies on the adsorption of phenol onto graphene, (n.d.). https://doi.org/10.1016/j.materresbull.2012.04.021.

[25] T.G. Kebede, S. Dube, M.M. Nindi, Application of mesoporous nanofibers as sorbent for removal of veterinary drugs from water systems, (2020) 140282. https://doi.org/10.1016/j.scitotenv.2020.140282.

[26] T. Ahamad, M. Naushad, T. Al-Shahrani, N. Al-hokbany, S.M. Alshehri, Preparation of chitosan based magnetic nanocomposite for tetracycline adsorption: Kinetic and thermodynamic studies, (2020) 258–267. https://doi.org/10.1016/j.ijbiomac.2020.01.025.

[27] X. Guo, S. Zhang, X. quan Shan, Adsorption of metal ions on lignin, (2008) 134–142. https://doi.org/10.1016/j.jhazmat.2007.05.065.

[28] Y. Cao, Activated carbon preparation and modification for adsorption, (2017) 111.

[29] R. Arora, Adsorption of heavy metals-a review, (2019) 4745–4750. https://doi.org/10.1016/j.matpr.2019.07.462.

[30] O.P. Murphy, M. Vashishtha, P. Palanisamy, K.V. Kumar, A Review on the Adsorption Isotherms and Design Calculations for the Optimization of Adsorbent Mass and Contact Time, (2023) 17407–17430. https://doi.org/10.1021/ACSOMEGA.2C08155.

[31] H. Swenson, N.P. Stadie, Langmuir's Theory of Adsorption: A Centennial Review, Langmuir (2019). https://doi.org/10.1021/ACS.LANGMUIR.9B00154/ASSET/IMAGES/LARGE/LA-2019-00154A_0009.JPEG.

[32] I. Langmuir, The constitution and fundamental properties of solids and liquids. II. Liquids, (1917) 1848–1906. https://doi.org/10.1021/JA02254A006.

CHAPTER 6: OVERALL CONCLUSION & FUTURE RECOMMENDATIONS

6.1. Overall Conclusion

In conclusion, successful synthesis and characterization of magnetic mesoporous adsorbents was achieved for the purpose of removing lead and efavirenz from aqueous solutions. The study has highlighted the impact of various factors on the adsorption process for each substance. For efavirenz removal, the results indicate that pH, initial solution concentration, adsorbent mass, and contact time play a pivotal role. While for lead; pH, initial metal concentration, and adsorbent mass were found to be the main contributing factors for its adsorption removal. It was also determined that these adsorbents can be reused for multiple cycles, with efavirenz having a lifespan of 3> cycles and lead having a lifespan of 4> cycles. Fe_3O_4@AFA exhibited better performance for efavirenz while Fe_3O_4@APC showed good performance for lead in comparison to other reported industrial waste-derived adsorbents for the removal of lead and efavirenz. They can be classified as better adsorbents.

The comparative studies conducted have shown that the mesoporous nature of the adsorbents, along with the functionalization with Fe_3O_4 nanoparticles, improves the removal percentage of both lead and efavirenz in aqueous solutions. Moreover, the study identified that Fe_3O_4@APC has a higher maximum adsorption capacity than other adsorbents for lead removal, while Fe_3O_4@AFA is more effective for adsorbing efavirenz. These findings hold great significance in the development of efficient and cost-effective adsorbents for the removal of heavy metals and pharmaceuticals from aqueous solutions.

6.2. Future work and recommendation

The results of the energy-dispersive X-ray spectroscopy (EDS) analysis were inconclusive in determining the successful incorporation of Fe_3O_4 nanoparticles onto AFA, ACFA, and ABA. This uncertainty was due to the presence of Fe in the form of hematite present in these waste materials. Therefore, it is necessary to conduct further analysis using Powder X-ray diffraction (PXRD) and X-ray Fluorescence (XRF) in the future. This technique would provide a more accurate and comprehensive evaluation of the incorporation of Fe_3O_4 nanoparticles onto AFA, ACFA, and ABA.

After conducting several tests, it was found that the High-Performance Liquid Chromatography with Diode Array Detection (HPLC-DAD) method was not effective in detecting even trace

amounts of efavirenz in real samples. Due to this limitation, it is essential to use a more sensitive and accurate method for detecting the efavirenz. Therefore, Liquid Chromatography-Mass spectrometry (LC-MS) analysis is recommended as it can identify even minute quantities of the drug, making it a more reliable method for detecting efavirenz. More analysis is needed to understand how competitive ions in solution impact adsorption. This will help to better understand the behaviour of adsorbents and the interactions of ions, and their overall impact on the adsorption process.

APPENDIX

PREAMBLE

This section highlights the figures and tables that were previously omitted in **Chapter 4** and **Chapter 5**. These graphical and tabular representations provide additional insights and a better understanding of the research findings.

APPENDIX A (Manuscript one)

APPENDIX A 1: The parameters, number of experiments, experimental conditions and results from the full factorial design for the removal of Pb^{2+} ions from aqueous solution.

StdOrder	pH	Initial Concentration (mg/L)	Contact time (min)	Dosage (mg)	Temperature (˚C)	% Removal of Pb (II)
1	3	5	10	20	25	65
2	8	5	10	20	25	95
3	3	25	10	20	25	28
4	8	25	10	20	25	36
5	3	5	60	20	25	80
6	8	5	60	20	25	95
7	3	25	60	20	25	20
8	8	25	60	20	25	40
9	3	5	10	50	25	94
10	8	5	10	50	25	95
11	3	25	10	50	25	74
12	8	25	10	50	25	74
13	3	5	60	50	25	95
14	8	5	60	50	25	94
15	3	25	60	50	25	68
16	8	25	60	50	25	94
17	3	5	10	20	60	54
18	8	5	10	20	60	81
19	3	25	10	20	60	26
20	8	25	10	20	60	34
21	3	5	60	20	60	62
22	8	5	60	20	60	80
23	3	25	60	20	60	31
24	8	25	60	20	60	29
25	3	5	10	50	60	92
26	8	5	10	50	60	94
27	3	25	10	50	60	99
28	8	25	10	50	60	97
29	3	5	60	50	60	93

30	8	5	60	50	60	94
31	3	25	60	50	60	99
32	8	25	60	50	60	99

APPENDIX A 2: ANOVA for the full factorial design.

Source	DF	Adj SS	Adj MS	F-Value	P-Value
Model	25	22836,0	913,4	47,51	0,000
Linear	5	17392,6	3478,5	180,93	0,000
pH	1	706,0	706,0	36,72	0,001
Concentration	1	5396,8	5396,8	280,71	0,000
Contact time	1	36,3	36,3	1,89	0,219
Dosage	1	11244,8	11244,8	584,90	0,000
Temperature	1	8,8	8,8	0,46	0,523
2-Way Interactions	10	4852,6	485,3	25,24	0,000
pH*Concentration	1	32,3	32,3	1,68	0,242
pH*Contact time	1	0,8	0,8	0,04	0,848
pH*Dosage	1	279,6	279,6	14,54	0,009
pH*Temperature	1	65,7	65,7	3,42	0,114
Concentration*Contact time	1	3,1	3,1	0,16	0,701
Concentration*Dosage	1	3207,4	3207,4	166,83	0,000
Concentration*Temperature	1	629,5	629,5	32,75	0,001
Contact time*Dosage	1	0,6	0,6	0,03	0,862
Contact time*Temperature	1	9,3	9,3	0,49	0,512
Dosage*Temperature	1	624,1	624,1	32,46	0,001
3-Way Interactions	10	590,8	59,1	3,07	0,091
pH*Concentration*Contact time	1	102,7	102,7	5,34	0,060
pH*Concentration*Dosage	1	180,9	180,9	9,41	0,022
pH*Concentration*Temperature	1	84,3	84,3	4,39	0,081
pH*Contact time*Dosage	1	71,7	71,7	3,73	0,102
pH*Contact time*Temperature	1	51,5	51,5	2,68	0,153
pH*Dosage*Temperature	1	0,7	0,7	0,04	0,855
Concentration*Contact time*Dosage	1	58,2	58,2	3,03	0,133
Concentration*Contact time*Temperature	1	0,0	0,0	0,00	0,988
Concentration*Dosage*Temperature	1	39,4	39,4	2,05	0,202
Contact time*Dosage*Temperature	1	1,5	1,5	0,08	0,791

Error	6	115,4	19,2
Total	31	22951,4	

APPENDIX A 3: The parameters, number of experiments, experimental conditions and results from the central composite design (CCD) for the removal of Pb^{2+} ions from aqueous solution

StdOrder	pH	Concentration (mg/L)	Dosage (g)	Contact time (min)	Temperature (˚C)	% Removal of Pb
1	3,0000	5,00	0,020000	10	60	91
2	8,0000	25,00	0,020000	10	60	99
3	8,0000	5,00	0,050000	10	60	94
4	3,0000	25,00	0,050000	10	60	59
5	5,5000	15,00	0,035000	10	60	43
6	5,5000	15,00	0,035000	10	60	50
7	8,0000	5,00	0,020000	10	60	94
8	3,0000	25,00	0,020000	10	60	12
9	3,0000	5,00	0,050000	10	60	88
10	8,0000	25,00	0,050000	10	60	62
11	5,5000	15,00	0,035000	10	60	80
12	5,5000	15,00	0,035000	10	60	51
13	1,4175	15,00	0,035000	10	60	10
14	9,5825	15,00	0,035000	10	60	26
15	5,5000	1,33	0,035000	10	60	100
16	5,5000	31,33	0,035000	10	60	15
17	5,5000	15,00	0,010505	10	60	24
18	5,5000	15,00	0,059495	10	60	98
19	5,5000	15,00	0,035000	10	60	65
20	5,5000	15,00	0,035000	10	60	43

APPENDIX A 4: Pseudo-first-order kinetic plot for the adsorption of Pb(II) onto a) Fe_3O_4@APC, b) Fe_3O_4@ABA, c) Fe_3O_4@ACFA and d) Fe_3O_4@AFA.

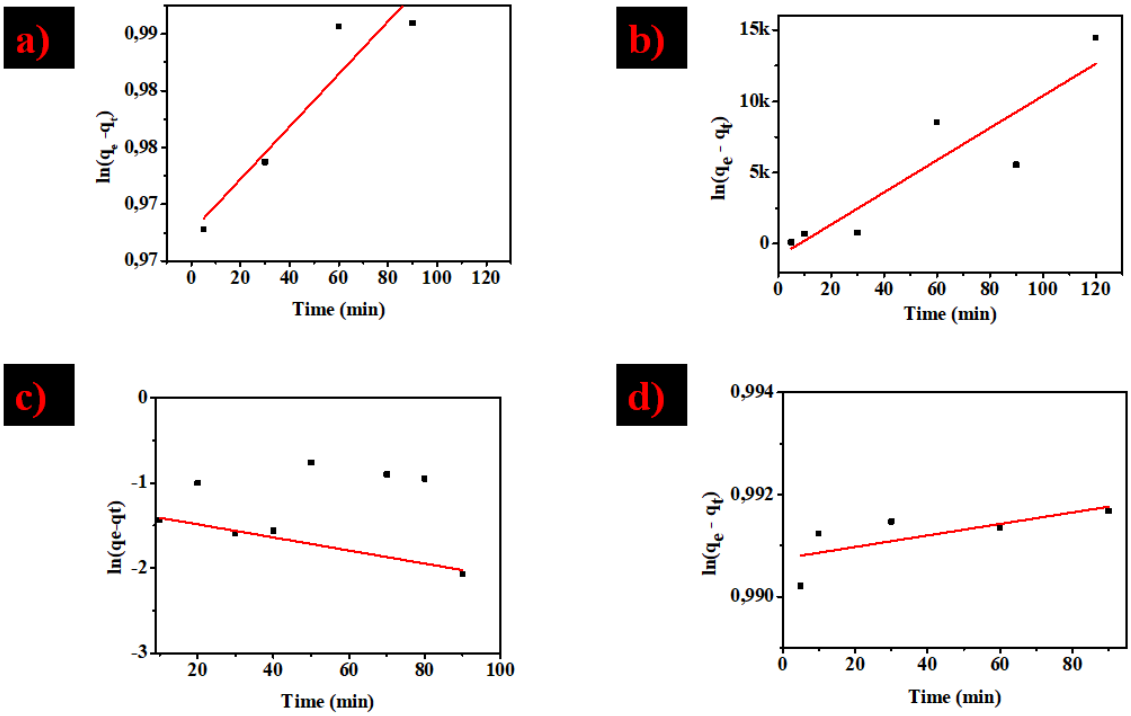

APPENDIX A 5: Pseudo-second-order kinetic plot for the adsorption of Pb(II) onto a) Fe_3O_4@APC, b) Fe_3O_4@ABA, c) Fe_3O_4@ACFA and d) Fe_3O_4@AFA

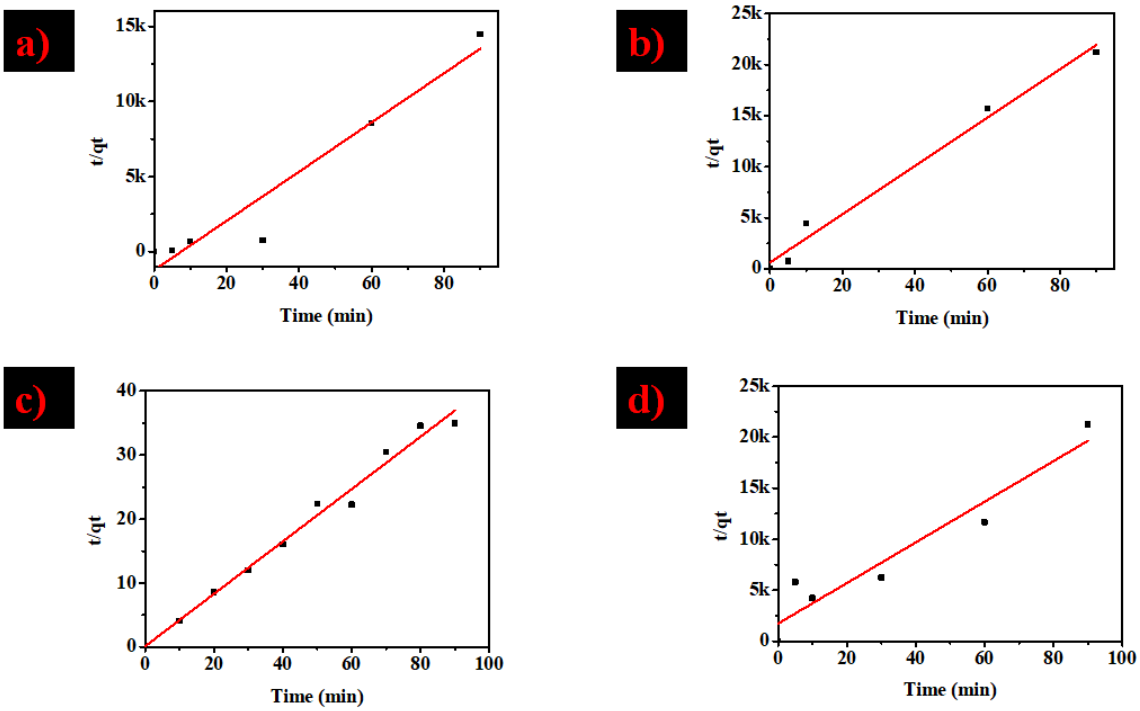

.

APPENDIX A 6: Thermodynamic plots for the adsorption of Pb(II) onto a) Fe_3O_4@APC, b) Fe_3O_4@ABA, c) Fe_3O_4@ACFA and d) Fe_3O_4@AFA.

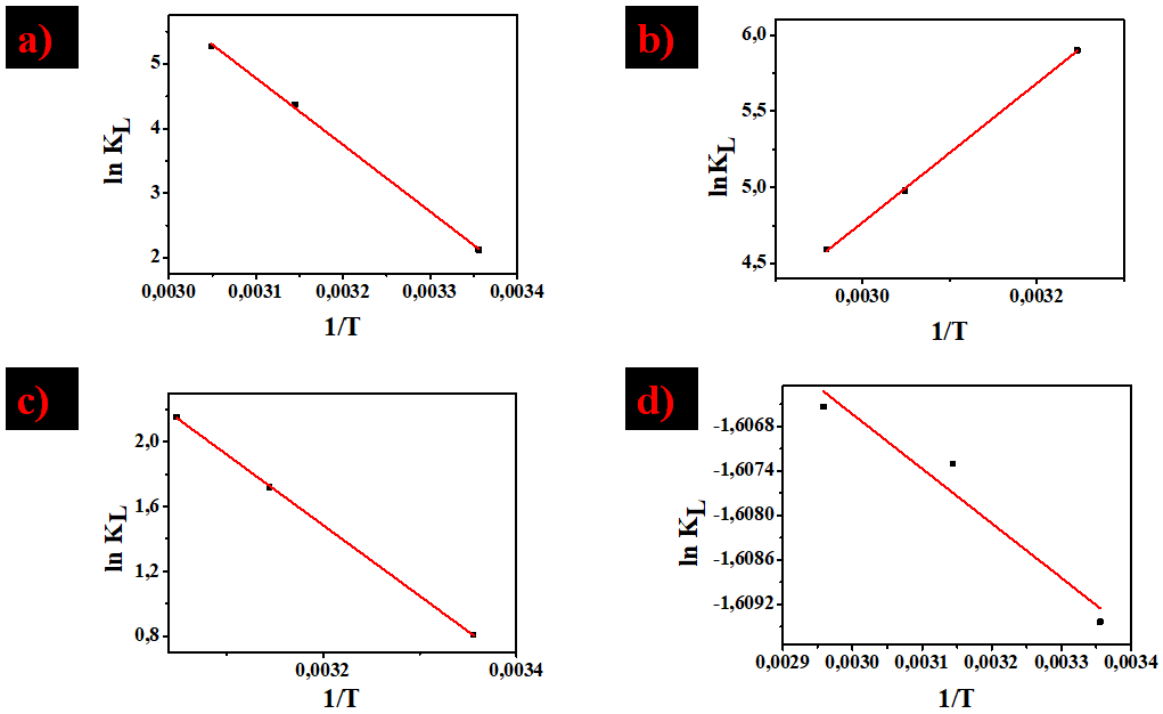

APPENDIX A 7: Freundlich plot for the adsorption of Pb(II) ions onto a) Fe_3O_4@APC, b) Fe_3O_4@ABA, c) Fe_3O_4@ACFA and d) Fe_3O_4@AFA.

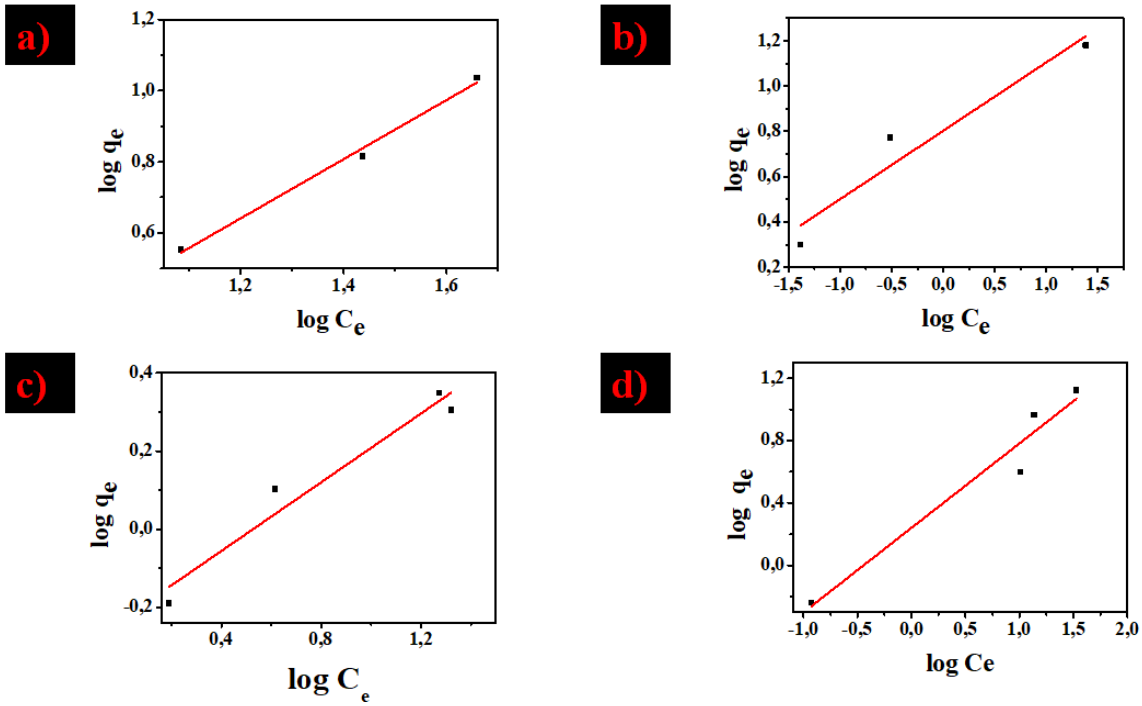

APPENDIX A 8: Langmuir plot for the adsorption of Pb(II) ions onto a) Fe_3O_4@APC, b) Fe_3O_4@ABA, c) Fe_3O_4@ACFA and d) Fe_3O_4@AFA.

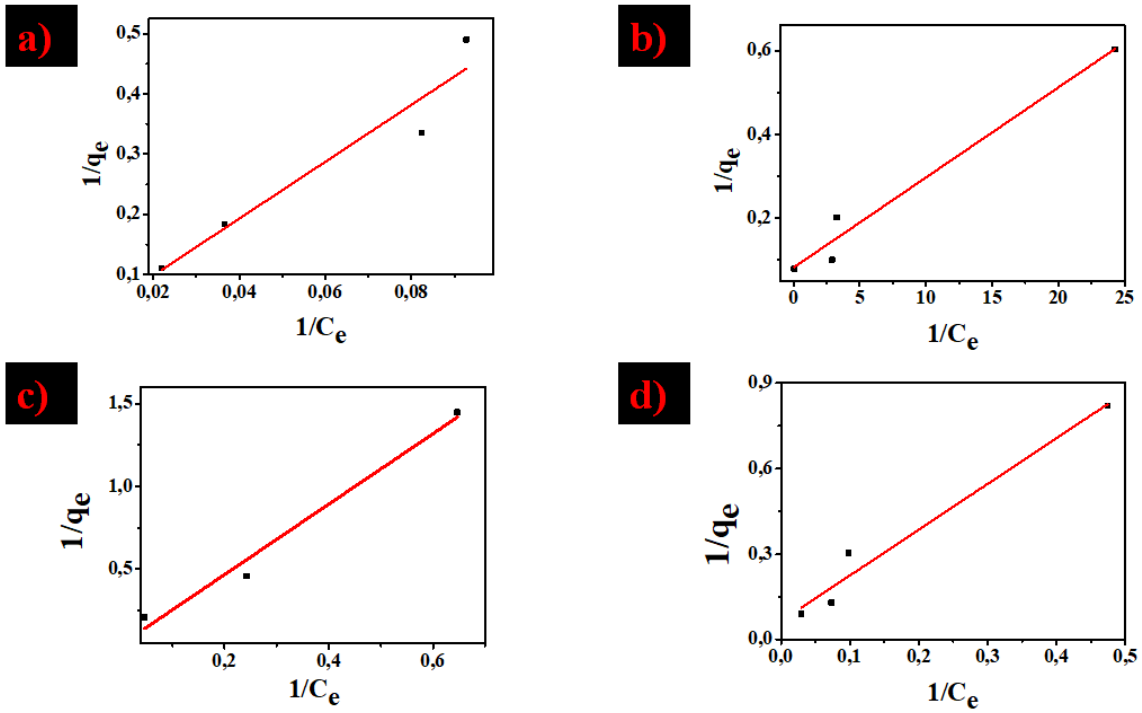

APPENDIX B (Manuscript two)

APPENDIX B 1: The parameters, number of experiments, experimental conditions and results from the full factorial design for the removal of efavirenz from aqueous solution

StdOrder	pH	Dosage (mg)	Contact Time (min)	Temperature (˚C)	Concentration (mg/L)	% Removal of efavirenz
1	2	20	10	25	5	93,5022
2	12	20	10	25	1	97,5890
3	2	60	10	25	1	11,2276
4	12	60	10	25	5	72,1532
5	2	20	60	25	1	11,8445
6	12	20	60	25	5	54,6106
7	2	60	60	25	5	93,0206
8	12	60	60	25	1	39,9541
9	2	20	10	60	1	13,6952
10	12	20	10	60	5	89,9397
11	2	60	10	60	5	89,7837
12	12	60	10	60	1	47,9908
13	2	20	60	60	5	93,4733
14	12	20	60	60	1	38,8313
15	2	60	60	60	1	1,5267

16	12	60	60	60	5	82,1448

APPENDIX B 2: Analysis of Variance

Source	DF	Adj SS	Adj MS	F-Value	P-Value
Model	12	18324,1	1527,0	60,11	0,003
Linear	5	11971,0	2394,2	94,24	0,002
pH	1	828,6	828,6	32,62	0,011
Dosage	1	193,8	193,8	7,63	0,070
Contact Time	1	631,0	631,0	24,84	0,016
Temperature	1	17,0	17,0	0,67	0,473
Concentration	1	10300,7	10300,7	405,47	0,000
2-Way Interactions	7	6353,1	907,6	35,73	0,007
pH*Contact Time	1	438,8	438,8	17,27	0,025
pH*Concentration	1	4128,1	4128,1	162,50	0,001
Dosage*Contact Time	1	522,8	522,8	20,58	0,020
Dosage*Concentration	1	279,2	279,2	10,99	0,045
Contact Time*Temperature	1	153,8	153,8	6,05	0,091
Contact Time*Concentration	1	197,5	197,5	7,77	0,069
Temperature*Concentration	1	632,9	632,9	24,91	0,015
Error	3	76,2	25,4		
Total	15	18400,3			

APPENDIX B 3: The parameters, number of experiments, experimental conditions and results from the box-behnken design for the removal of efavirenz from aqueous solution.

StdOrder	pH	Dosage (mg)	Contact time (min)	Concentration (mg/L)	% Removal of efavirenz
1	2	20	10	1	88,4872
2	12	20	10	1	73,3803
3	2	50	10	1	90,3608
4	12	50	10	1	88,5324
5	2	20	60	1	88,5566
6	12	20	60	1	37,6281
7	2	50	60	1	88,2790
8	12	50	60	1	86,5029
9	2	20	10	5	93,8496
10	12	20	10	5	46,7985
11	2	50	10	5	93,7732
12	12	50	10	5	65,2988
13	2	20	60	5	93,4674
14	12	20	60	5	64,1042
15	2	50	60	5	94,1173
16	12	50	60	5	95,0954
17	-3	35	35	3	90,4119
18	17	35	35	3	69,7497
19	7	5	35	3	87,9995
20	7	65	35	3	89,7720
21	7	35	-15	3	88,6052
22	7	35	85	3	94,1869

23	7	35	35	-1	86,5584
24	7	35	35	7	92,1697
25	7	35	35	3	93,6316
26	7	35	35	3	81,3380
27	7	35	35	3	91,8447
28	7	35	35	3	98,2919
29	7	35	35	3	83,7682
30	7	35	35	3	85,4121
31	7	35	35	3	96,7192

APPENDIX B 4: Pseudo-second-order kinetic plot for the adsorption of efavirenz onto a) Fe_3O_4@APC, b) Fe_3O_4@ABA, c) Fe_3O_4@ACFA and d) Fe_3O_4@AFA.

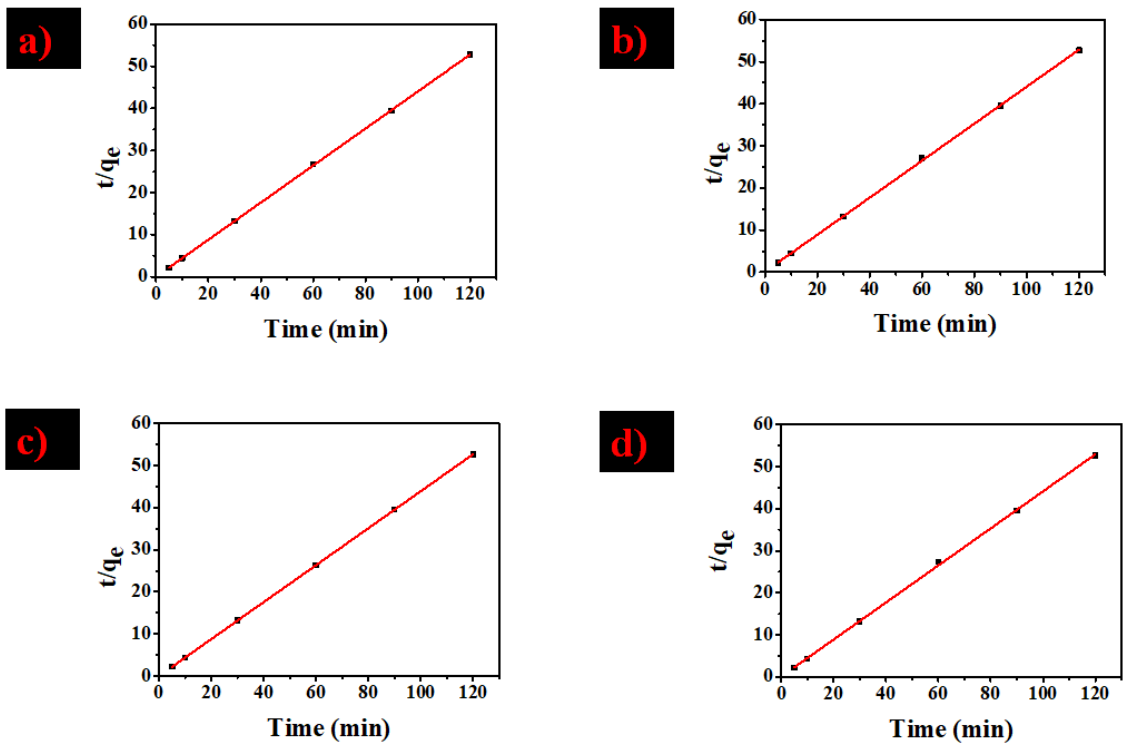

APPENDIX B 5: Pseudo-first-order kinetic plot for the adsorption of efavirenz onto a) Fe_3O_4@APC, b) Fe_3O_4@ABA, c) Fe_3O_4@ACFA and d) Fe_3O_4@AFA

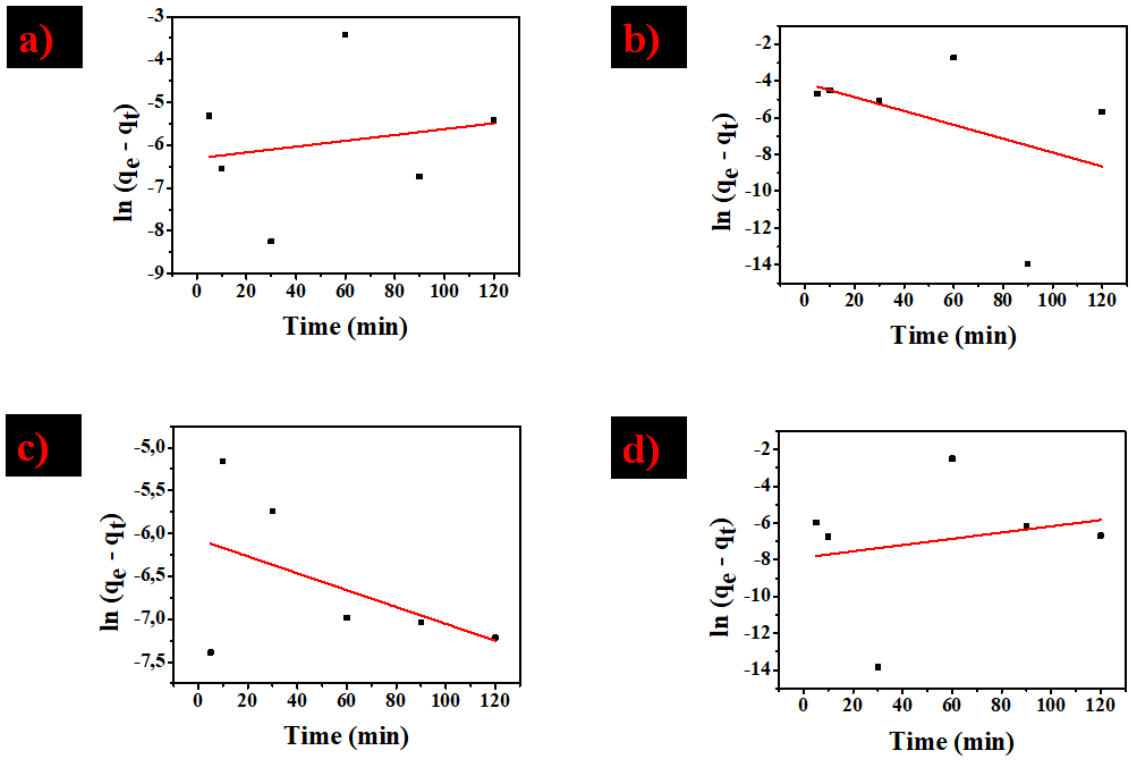

.

APPENDIX B 6: Pseudo-first-order kinetic plot for the adsorption of efavirenz onto a) Fe_3O_4@APC, b) Fe_3O_4@ABA, c) Fe_3O_4@ACFA and d) Fe_3O_4@AFA

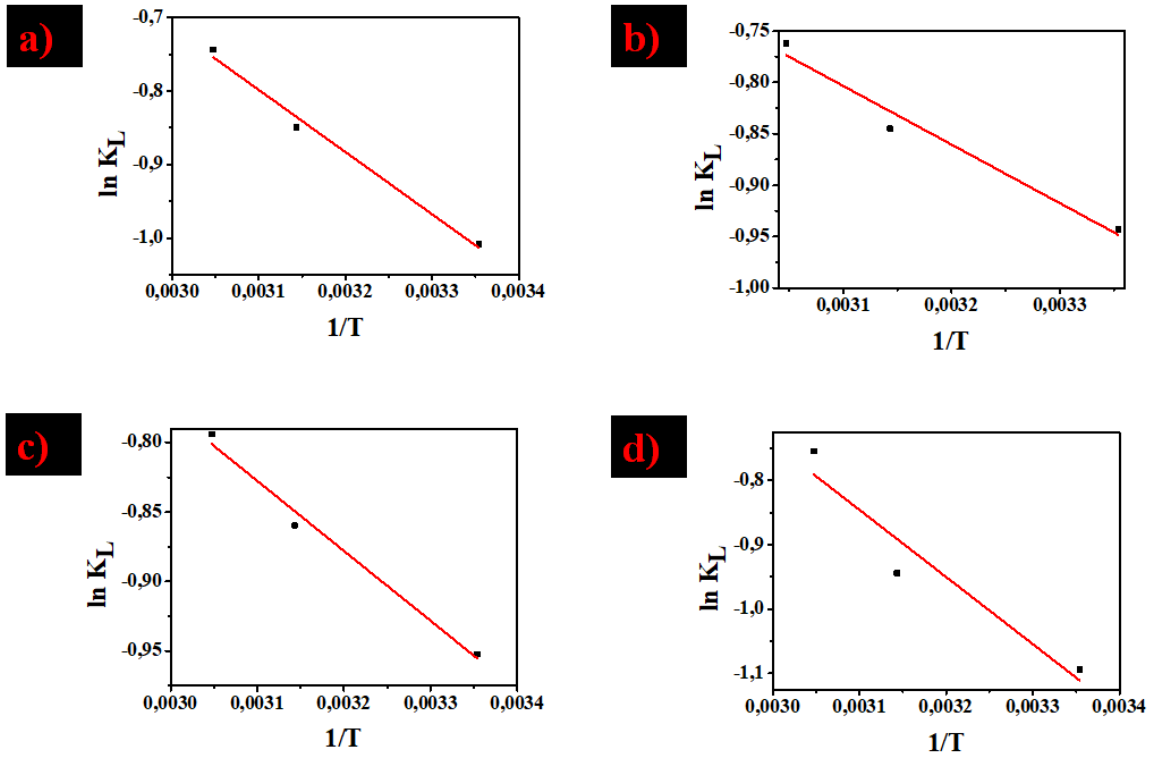

APPENDIX B 7: Temkin plot for the adsorption of efavirenz onto a) Fe3O4@APC, b) Fe_3O_4@ABA, c) Fe_3O_4@ACFA and d) Fe_3O_4@AFA.

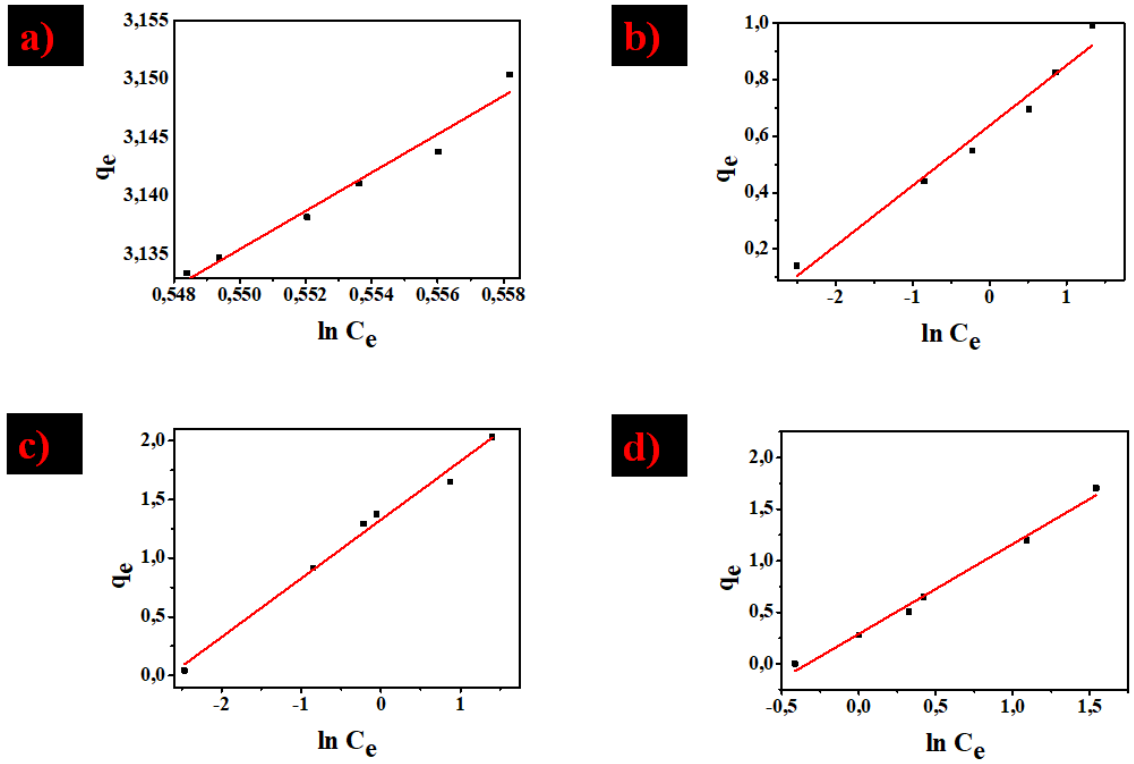

APPENDIX B 8: Freundlich plot for the adsorption of efavirenz onto a) Fe_3O_4@APC, b) Fe_3O_4@ABA, c) Fe_3O_4@ACFA and d) Fe_3O_4@AFA.

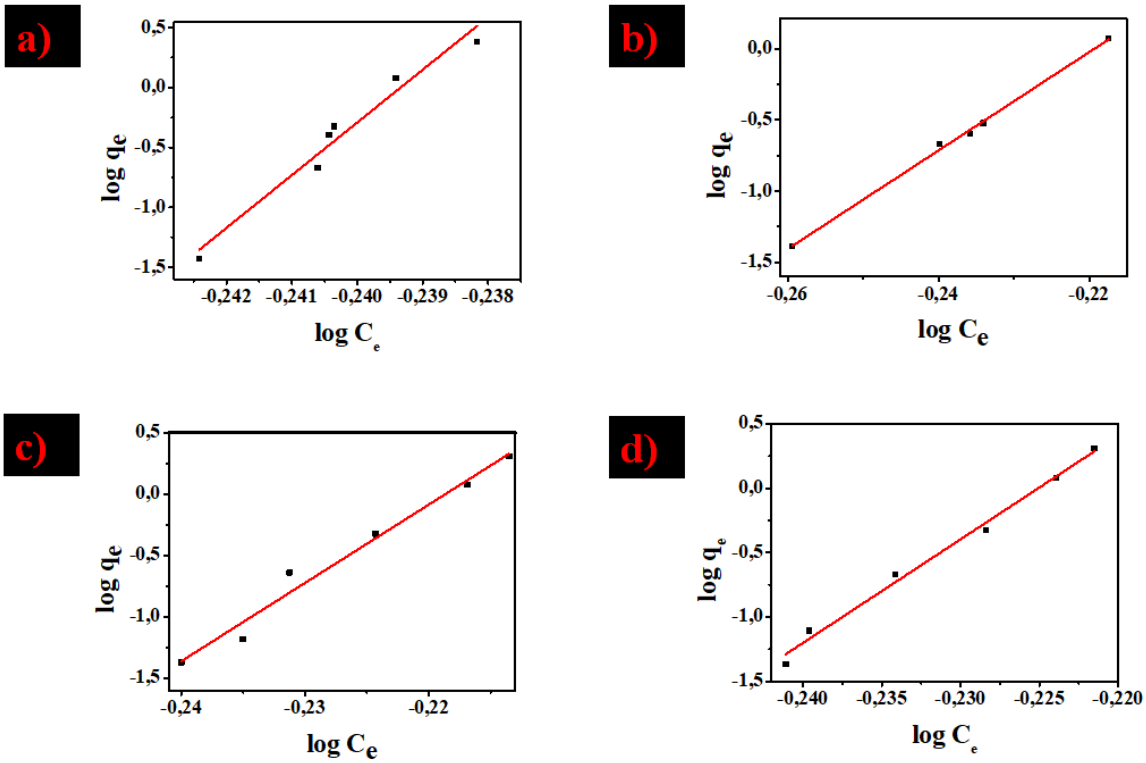

APPENDIX B 9: Langmuir plot for the adsorption of efavirenz onto a) Fe_3O_4@APC, b) Fe_3O_4@ABA, c) Fe_3O_4@ACFA and d) Fe_3O_4@AFA